NACA RM A9K01

NACA

RESEARCH MEMORANDUM

AN ANALYSIS OF THE FORCES AND PRESSURE DISTRIBUTION ON A WING WITH THE LEADING EDGE SWEPT BACK 37.25°

By George G. Edwards and Frederick W. Boltz

Ames Aeronautical Laboratory
Moffett Field, Calif.

NATIONAL ADVISORY COMMITTEE
FOR AERONAUTICS

WASHINGTON

March 30, 1950

NATIONAL ADVISORY COMMITTEE FOR AERONAUTICS

RESEARCH MEMORANDUM

AN ANALYSIS OF THE FORCES AND PRESSURE DISTRIBUTION ON A WING WITH THE LEADING EDGE SWEPT BACK 37.25°

By George G. Edwards and Frederick W. Boltz

SUMMARY

A semispan model of a wing with the leading edge swept back 37.25°, an aspect ratio of 6.04, and a taper ratio of 0.5 was tested to ascertain the compressibility effects on the forces, the moments, and the surface pressures. The wing had no twist and the profiles normal to the quarter-chord line were the NACA 64_1-212.

Lift, drag, and pitching-moment data together with the chordwise distribution of static pressure at five spanwise stations are presented for Mach numbers from 0.18 to 0.94 at a constant Reynolds number of 2,000,000. Force data are presented also for this Mach number range at a constant Reynolds number of 1,100,000, and for Mach numbers up to 0.90 at a Reynolds number of 3,000,000.

An analysis of the data is made to correlate the changes in the pressure distribution over the wing with the changes in the total forces. In this analysis a critical flow condition is considered to exist when the component of local velocity normal to the isobar equals the local speed of sound. It is indicated that, at angles of attack between 0° and 4°, the abrupt drag increase began at Mach numbers slightly higher than that at which the critical flow condition had occurred at the crest line of the entire wing (the crest line being defined as the locus of points on the wing surface at which the surface is tangent to the direction of the undisturbed air stream). For this wing, having moderate sweepback, the critical flow condition was attained at the crest of the various spanwise stations within a narrow range of Mach numbers.

An approximate procedure for calculating the drag-divergence Mach number from low-speed data is investigated.

INTRODUCTION

The use of the swept-wing plan form for delaying the onset of serious compressibility effects to higher Mach numbers has received considerable theoretical and experimental study. A knowledge of the degree

to which these compressibility effects can be delayed and alleviated by wing sweep is of value in the proper design and application of swept wings. It is important to know the Mach number above which the rapid drag increase, the loss of lift, and the sudden changes in load distribution and longitudinal stability occur. The basic theory of the swept wing was developed from consideration of the flow over a yawed airfoil of infinite span and has served as a very useful guide for qualitative estimates of the benefits of wing sweep. The simple sweep theory does not, however, take account of many of the variables in the flow over a swept wing of finite span. Pressure measurements at high Mach numbers correlated with measurements of forces and moments are important to the extension of present swept-wing theory and to a better understanding of the flow phenomena involved.

In this report, the results of such an investigation are presented for a wing having moderate sweepback. The tests were conducted in the Ames 12-foot pressure wind tunnel at Mach numbers from 0.18 to 0.94 and a constant Reynolds number of 2,000,000. In the analysis of the data, an effort has been made to correlate the changes in local wing pressures with the resulting changes in total forces, particularly in the range of Mach numbers for which supercritical flow is developing on the wing.

NOTATION

C_D drag coefficient $\left(\frac{\text{drag}}{q_o S}\right)$

C_L lift coefficient $\left(\frac{\text{lift}}{q_o S}\right)$

C_m pitching-moment coefficient about the quarter point of the wing mean aerodynamic chord $\left(\frac{\text{pitching moment}}{q_o S \bar{c}}\right)$

C_N normal-force coefficient $\left(\frac{1}{S}\int_o^{b/2} c_n c \, dy\right)$

c_c section chord-force coefficient $\left(\frac{\text{section chord force}}{q_o c}\right)$

c_n section normal-force coefficient $\left(\frac{\text{section normal force}}{q_o c}\right)$

L/D ratio of lift to drag

M local Mach number $\left(\frac{V}{a}\right)$

M_D drag-divergence Mach number (the free-stream Mach number at which $(\partial C_D/\partial M_o)_\alpha = 0.10$)

M_L lift-divergence Mach number (the free-stream Mach number at which the absolute value of the lift coefficient at constant angle of attack reaches a maximum)

M_o free-stream Mach number $\left(\frac{V_o}{a_o}\right)$

$M_\perp$ component of local Mach number normal to the isobar (See fig. 1.)

M_φ the free-stream Mach number at which $M_\perp = 1$ at a specific point on the wing

P local pressure coefficient $\left(\frac{p-p_o}{q_o}\right)$

P_φ local critical pressure coefficient (the pressure coefficient corresponding to the critical flow condition wherein the component of local velocity normal to the isobar inclined at the angle φ equals the local speed of sound)

P_i local pressure coefficient for incompressible flow

R Reynolds number $\left(\frac{\rho_o V_o \bar{c}}{\mu}\right)$

S semispan wing area, square feet

V local air velocity, feet per second

V_o free-stream velocity, feet per second

$V_\perp$ component of local velocity normal to the isobar, feet per second

a local speed of sound, feet per second

a_o speed of sound in free stream, feet per second

$b/2$ wing semispan normal to plane of symmetry, feet

c local wing chord parallel to plane of symmetry, feet

c_{av} average wing chord parallel to plane of symmetry, feet

$\bar{c}$ mean aerodynamic wing chord $\left(\frac{\int_0^{b/2} c^2\,dy}{\int_0^{b/2} c\,dy}\right)$, feet

p local static pressure, pounds per square foot

p_o free-stream static pressure, pounds per square foot

q_o free-stream dynamic pressure $\left(\frac{1}{2}\rho_o V_o^2\right)$, pounds per square foot

x distance from leading edge along chord line, feet

y perpendicular distance from plane of symmetry along semispan, feet

α angle of attack, degrees

α_u uncorrected angle of attack, degrees

γ ratio of specific heat of air at constant pressure to specific heat of air at constant volume $\left(\frac{c_p}{c_v} = 1.4\right)$

ϵ angle of twist with respect to root chord (positive for washin), degrees

η fraction of semispan $\left(\frac{y}{b/2}\right)$

θ angle of inclination of local velocity vector from free-stream direction, degrees

μ coefficient of viscosity of air, slugs per foot-second

ρ_o free-stream mass density of air, slugs per cubic foot

φ local angle of sweep of isobars, degrees (See fig. 1.)

DEFINITIONS

An attempt is made in this report to correlate the changes in local flow conditions on a wing having 37.25° sweep of the leading edge and an aspect ratio of 6.04 with the abrupt changes in total forces occurring at high, subsonic, free-stream Mach numbers. It is convenient to have at hand certain definitions relating to critical changes in the local flow and in the total lift and drag on the wing.

Critical Flow Conditions on a Swept Wing

The effect of sweepback in delaying the onset of the adverse compressibility effects on a yawed airfoil of infinite span has been discussed in reference 1. The component of free-stream velocity parallel to the leading edge of such a wing is assumed to have no effect on the induced velocities resulting from translation of the yawed airfoil in a frictionless fluid. As may be seen in figure 1(a), the local velocity vector V is the vector sum of the free-stream velocity V_o and the additional velocity $\Delta V_\perp$ induced by the airfoil thickness. This resultant vector V is inclined at an angle θ to the free stream, which fact implies a lateral displacement of the stream lines. Lines of constant velocity, and therefore lines of constant pressure (isobars), on a yawed airfoil of infinite span are parallel to the leading edge.

In contrast to the case of the unyawed airfoil, the attainment of sonic velocities on the yawed airfoil does not necessarily signify any immediate change in the flow characteristics. Critical flow conditions analogous to those on an unyawed airfoil will not exist until the component of local velocity normal to the leading edge of the wing equals the local speed of sound. These critical flow conditions will occur along a line of constant pressure parallel to the leading edge and inclined at the sweep angle φ with the normal to the free-stream direction. The shock wave, when it forms, will also be inclined at this angle. In the appendix, the following expression is developed for the critical pressure coefficient based on the attainment of critical flow conditions along a line of constant pressure inclined at the angle φ with the normal to the free-stream direction:

$$P_\varphi = \frac{2}{\gamma M_o^2} \left\{ \left[\frac{2}{\gamma+1} \left(1 + \frac{\gamma-1}{2} M_o^2 \cos^2 \varphi \right) \right]^{\frac{\gamma}{\gamma-1}} - 1 \right\} \qquad (1)$$

When the reference sweep angle φ equals zero, as for an unswept airfoil, equation (1) reduces to that for critical pressure coefficient given in reference 2. Equation (1) has been evaluated for a range of sweep angles in figure 2.

The application of this equation in the analysis of pressures on a swept wing requires additional considerations. When two airfoils are joined as shown in figure 1(b), a swept wing of infinite span is formed. As pointed out in reference 1, the flow at and near the plane of symmetry is quite different from that some distance away inasmuch as there can be no lateral displacement of the streamlines at the plane of symmetry. Kuchemann has computed the pressures at zero angle of attack near the plane of symmetry of a swept wing of infinite span having biconvex profiles (reference 3), and has found that the isobars are normal to the free-stream direction at the plane of symmetry and curved

in a manner to approach the sweep angle of the wing at points some distance from the plane of symmetry. If it is assumed that such pressure conditions exist for the idealized wing under consideration, it is evident that critical conditions will first be attained at the plane of symmetry where the effective sweep is zero. At some higher free-stream Mach number, a shock wave will form at the plane of symmetry and with further increase of Mach number will extend outward.

It was concluded in reference 4 that the position of the shock wave is determined by the velocity normal to the isobars, that is, that the shock wave is located at that point where the component of local velocity normal to the isobars equals the local speed of sound. Consider the system of curved isobars for the swept wing shown in figure 1(b). A free-stream Mach number of 0.8 was assumed and the local critical pressure coefficient was computed from equation (1), the reference sweep angle φ having been evaluated by measuring the local sweep angle of the isobars. It is to be noted that the line through points at which the component of local velocity normal to the isobars equals the local speed of sound crosses the isobars, a result which could be anticipated from the fact that the critical pressure coefficient has been assumed to be a function of the sweep of the isobars. This procedure presumably gives the correct position and the angle of the shock wave at two points, namely, at the plane of symmetry and at some distance away, and these points are connected by a line which is free from discontinuities or abrupt changes of curvature.

For the purpose of analyzing the pressure data of this report, the critical flow condition will be assumed to exist when the component of local velocity normal to the isobar equals the local speed of sound. Equation (1) and the sweep of the isobars will be used to compute the local critical pressure coefficient corresponding to this critical flow condition. The free-stream Mach number at which the critical flow condition is attained at a specified point on the wing will be denoted by the symbol M_{φ}.

Drag and Lift-Divergence Mach Numbers

In general, critical flow conditions do not occur simultaneously at all spanwise stations on a swept wing of finite span, and the effect of the growing region of supercritical flow on the lift and drag forces increases progressively with Mach number.

The drag-divergence Mach number will be defined in this report as that free-stream Mach number at which the rate of change of drag coefficient with Mach number at a constant angle of attack equals 0.10. This definition is advantageous in that the drag-divergence Mach number can be determined with fair accuracy from plots of C_D against M_0, and in that it is not greatly affected by minor variations in the drag

curve caused by changes in wind-tunnel air-stream turbulence or by experimental scatter in the data. For similar reasons, the lift-divergence Mach number will be defined as that subsonic free-stream Mach number at which the absolute value of the lift coefficient at a constant angle of attack reaches a maximum.

Crest Line

In reference 5 supercritical flow phenomena on unswept airfoils have been analyzed relative to the drag increase at high subsonic Mach numbers. The analysis of experimental pressure distributions for a number of airfoil sections indicated that, for an airfoil at a fixed angle of attack, the local region of supersonic flow increased in chordwise extent as the free-stream Mach number was increased beyond the critical Mach number. It was noted that the abrupt supercritical drag increase did not begin until the supersonic region enveloped the airfoil crest (the crest being defined as the point on the airfoil section at which the surface is tangent to the direction of the undisturbed air stream). With further increase in the free-stream Mach number, the surface pressures ahead of the crest tended to increase while those to the rear continued to decrease, the latter as a result of rearward growth of the local region of supersonic flow. These pressure changes entailed an increase in the pressure drag and, thus, for an unswept airfoil, it appears that the attainment of sonic velocity at the airfoil crest presages the rapid drag increase with further increase in the free-stream Mach number.

Although the analysis of the flow over a swept wing of finite span involves more factors than does that for an unswept airfoil, it is reasonable to expect the crest concept to be of value in correlating the pressure changes with the drag increase at high Mach numbers. The crest line will be defined as the locus of points on the wing at which the surface is tangent to the direction of the undisturbed air stream. The crest-line location has been noted on the pressure plots for the upper range of Mach numbers.

Local Mach Number and Local Pressure Coefficient

The local Mach number is related to the local pressure coefficient and to the free-stream Mach number by the relation

$$P = \frac{2}{\gamma M_o^2}\left[\left(\frac{1 + \frac{\gamma-1}{2} M_o^2}{1 + \frac{\gamma-1}{2} M^2}\right)^{\frac{\gamma}{\gamma-1}} - 1\right] \qquad (2)$$

For convenience in calculating the local Mach number from the pressure data, a graphical solution of equation (2) has been shown in figure 3.

MODEL AND APPARATUS

The semispan model used in these tests represented a wing having the leading edge swept back 37.25°, an aspect ratio of 6.04, and a taper ratio of 0.5. The wing had no twist and the profiles normal to the quarter-chord line were the NACA 64_1-212. Coordinates for the NACA 64_1-212 airfoil are presented in table I; coordinates of sections parallel to the free-stream direction are presented in table II.

The model, which had a semispan of 5 feet, was constructed of laminated mahogany secured to a steel spar. Pressure orifices were installed at five spanwise stations on the wing and distributed from the leading edge to the 85-percent-chord points. Additional orifices were installed at 40 percent of the chord at intervals of about 4 inches from the root to the tip of the wing. A sketch of the plan form of the model showing pertinent dimensions and the location of pressure orifices is shown in figure 4.

A photograph of the model installation is presented in figure 5. The semispan model was mounted vertically in the wind tunnel with the floor of the tunnel serving as a reflection plane. The turntable upon which the model was mounted was directly connected to the force-measuring apparatus. Pressures were evaluated from photographic records of multiple-tube manometers.

Static load tests were conducted in order to furnish an indication of the effects of the elastic properties of the model on the test results. The model was clamped in a horizontal position and loaded with lead shot as illustrated in figure 6. The load was proportioned both spanwise and chordwise to simulate the aerodynamic load on the model, for two specific test conditions, as determined from pressure-distribution measurements on the wing. Templates were utilized to insure an accurate representation of the load. Deflections at the leading and the trailing edges at five spanwise stations were measured with a height gage. It was established that for duplicated loadings the twist measurements could be repeated within 10 percent. In figure 6, the upper photograph shows the model loaded to produce the deflections occurring at a Mach number of 0.75, a Reynolds number of 2,000,000, and an uncorrected angle of attack α_u of 4°. The loading corresponding to a Mach number of 0.90 at the same Reynolds number and angle of attack is shown in the lower portion of figure 6.

CORRECTIONS TO DATA

The force and moment data have been corrected for the effects of tunnel–wall interference, including constriction due to the tunnel walls, and of turntable tares. The pressure data have been corrected only for the effects of constriction due to the tunnel walls.

Corrections to the data for tunnel–wall interference were evaluated by the method of reference 6, modified to take into account the effects of sweep. The following corrections were used:

$$\Delta\alpha = 0.489\ C_L$$

$$\Delta C_D = 0.00754\ C_L^2$$

No correction was applied to the pitching–moment data.

The constriction effects due to the presence of the tunnel walls were evaluated by the method of reference 7. Although this method is strictly applicable only to full–span models located centrally in the tunnel and does not allow for large angles of sweep, it has been used as a reasonable estimate of the constriction effects. The magnitude of the corrections applied to the Mach number and dynamic pressure is illustrated in the following table:

Corrected Mach number	Uncorrected Mach number	$\frac{\text{Corrected } q_o}{\text{Uncorrected } q_o}$
0.30	0.300	1.002
.40	.400	1.002
.50	.499	1.003
.60	.599	1.003
.70	.698	1.004
.80	.796	1.006
.85	.844	1.008
.90	.890	1.012
.94	.922	1.019

Tare corrections for the air forces exerted on the exposed surface of the turntable were applied to the drag data. The tare–drag coefficient, obtained from turntable drag measurements with the model removed from the tunnel, decreased slightly with increasing Reynolds number, but was not influenced by compressibility. The tare–drag coefficient varied from 0.0038 at a Reynolds number of 1,100,000 to 0.0035 at a Reynolds number of 3,000,000. Interference between the model and the turntable was not investigated, but is believed to have been small.

TESTS

The chordwise distribution of static pressure on the wing at five spanwise stations and the total lift, drag, and pitching moment were measured at Mach numbers in the range from 0.18 to 0.94 at a constant Reynolds number of 2,000,000. Lift, drag, and pitching moment were also measured in this Mach number range at a constant Reynolds number of 1,100,000 and for Mach numbers up to 0.90 at a Reynolds number of 3,000,000. With roughness applied to the upper and the lower surfaces of the wing at 10 percent of the chord, lift, drag, and pitching moment were measured at Mach numbers from 0.18 to 0.94 at a Reynolds number of 2,000,000.

At a Mach number of 0.18 the angle of attack was varied from -8° to 19°. At higher Mach numbers the angle-of-attack range was limited by model strength, model vibration, and tunnel power.

RESULTS AND DISCUSSION

Force and Moment Characteristics

Effects of Mach number.- The lift, drag, and pitching-moment characteristics of the wing at Mach numbers from 0.18 to 0.94 for a constant Reynolds number of 2,000,000 are presented in figure 7. These data are summarized in figures 8 and 9 wherein the coefficients are plotted as functions of Mach number. The effect of Mach number on the lift-curve slope, the aerodynamic center at zero lift, the maximum lift-drag ratio, the lift coefficient for maximum lift-drag ratio, and the minimum drag coefficient are illustrated in figures 10 and 11.

As indicated from the lift data presented in figure 8, the Mach number for lift divergence was 0.88 at an angle of attack of 0° and decreased to 0.84 at an angle of attack of 6°. The lift-curve slope, shown in figure 10, increased with increasing Mach number approximately to the Mach number of lift divergence and decreased with further increase in Mach number. Also shown in figure 10 is the theoretical lift-curve slope obtained from a chart of reference 8 and corrected for compressibility by the method of reference 9. The agreement between the theoretical values of lift-curve slope at zero lift coefficient and the experimental values is excellent up to the Mach number for lift divergence.

The pitching-moment coefficients for constant lift coefficients between 0 and 0.4 became more negative with increasing Mach number as shown in figure 8. As illustrated in figure 10, the aerodynamic center at zero lift coefficient remained at about 28.5 percent of the mean aerodynamic chord in the range of Mach numbers from 0.18 to 0.78 and then moved aft with further increase in Mach number to 44 percent at a Mach

number of 0.94. With reference to figure 7(b), it is to be noted that the location of the aerodynamic center was a function of the lift coefficient as inferred from the nonlinearity of the pitching-moment curves, particularly at the higher Mach numbers.

The effect of Mach number on the drag coefficient corresponding to constant angles of attack is shown in figure 9. A small, nearly linear, increase in drag coefficient with increasing Mach number preceded the abrupt increase in drag. The drag-divergence Mach number for which $(\partial C_D/\partial M_o)_\alpha$ is equal to 0.10 is noted on each drag curve of figure 9. The drag-divergence Mach number was 0.88 at 0° angle of attack and gradually decreased with increasing angle of attack to approximately 0.81 at 4° angle of attack. The variation of minimum drag coefficient with Mach number is presented in figure 11. Also shown in this figure are the maximum lift-drag ratio and the lift coefficient for maximum lift-drag ratio as functions of Mach number. Since the model could not be maintained aerodynamically smooth, the minimum drag was probably higher and the maximum lift-drag ratio was probably lower than for an aerodynamically smooth wing.

From the results of the force tests, it is concluded that the effects of compressibility on the force and moment characteristics of this wing at low and moderate lift coefficients were small up to the Mach numbers for which the abrupt drag increase occurred. Deterioration of the lifting characteristics of the wing at high Mach numbers generally did not occur until the drag had increased by a considerable amount.

Effects of Reynolds number and of surface roughness.- In figure 12, lift, drag, and pitching-moment data for constant Reynolds numbers of 1,100,000, 2,000,000, and 3,000,000 are presented for Mach numbers from 0.18 to 0.94. Low-speed scale effects on a model of a wing of this design investigated in the Langley 19-foot pressure wind tunnel have been reported in reference 10. Portions of the lift and the pitching-moment curves from that reference for a Reynolds number of 3,000,000 are shown in figure 12(a) for comparison with data from the present tests. At the same Reynolds number the maximum lift coefficient obtained for the present tests was higher than that obtained in the referenced tests, probably due either to differences in model surface conditions or in airstream turbulence. At a Mach number of 0.18, the maximum lift coefficient increased with increasing Reynolds number, as did the lift coefficient at which the abrupt decrease in static longitudinal stability occurred. At Mach numbers from 0.90 to 0.94, a decrease in Reynolds number from 2,000,000 to 1,100,000 resulted in perceptible changes in lift-curve slope and marked changes in pitching-moment characteristics.

An inspection of the drag data of figure 12(b) reveals that there was a decrease in drag coefficient with increasing Reynolds number in the range of Mach numbers between 0.80 and 0.90. The inconsistencies in the effects of Reynolds number at Mach numbers of 0.18, 0.92, and 0.94 are believed to be the result of differences in model surface conditions.

It was found that the condition of the model surfaces tended to deteriorate during the tests, necessitating frequent refinishing of the model. An example of the effects of surface conditions at high lift coefficients is furnished by the data shown in figure 7. The data identified by the flagged symbols in figure 7 were obtained immediately after resurfacing the model. It is evident from the lift data of figure 7(a) and the pitching-moment data of figure 7(b) that the flow over the wing at large angles of attack was greatly influenced by surface roughness. Improvement of the wing surface resulted in an increase in the lift-curve slope at the higher angles of attack and a delay to higher lift coefficients of the abrupt forward movement of the aerodynamic center.

In an effort to circumvent the difficulties associated with uncontrolled variation of model surface conditions, 1/2-inch-wide roughness strips were placed along the entire length of the upper and lower surfaces of the wing. The leading edge of the strips was at 10 percent of the chord. The roughness was created by sprinkling number 60 carborundum particles on an adhesive agent until the particles covered approximately 80 percent of the area of the strips. The test results for the wing with roughness are compared with those for the wing without roughness at a Reynolds number of 2,000,000 in figure 13. The roughness strips apparently had a severe effect on the flow at supercritical Mach numbers, reducing the lift-curve slope and causing changes in the pitching moment.

Pressure Distribution

The chordwise distributions of static pressure on the wing at five spanwise stations are presented in figures 14 through 22 for a constant Reynolds number of 2,000,000. The figures are arranged in sequence to show the distribution of pressure at the Mach numbers and the angles of attack indicated in the following table:

Figure	Angle of attack	Mach number
14	0° to 18°	0.18
15	4° to 10°	0.60
16	-2°	0.18 to 0.94
17	-1°	
18	0°	
19	1°	
20	2°	
21	3°	
22	4°	

All pressure data except those for a Mach number of 0.18 were obtained simultaneously with the force and moment data shown in figure 7.

With reference to figures 14(d) and 14(e), it is noted that, at a Mach number of 0.18, stall occurred on the outer portion of the wing at an angle of attack between 14° and 16° and progressed toward the root, causing the unstable trend of the pitching moment noted from figure 7. A similar stall characteristic may be observed in figure 15 for a Mach number of 0.60, the stall occurring in this case at an angle of attack between 8° and 10°.

Reference will be made to the data of figures 18 through 22 in discussing the distribution of normal force and chord force obtained by integration of the data and also in correlating local pressure changes with the increase in total drag at high Mach numbers. In order to integrate the pressure data, it was necessary to extrapolate the pressure-distribution curves to the trailing edge of the wing. At Mach numbers below 0.85, the load on the forward 70 percent of the wing, obtained by integration of the pressure data, amounted to over 80 percent of the normal force computed from the lift and drag data. This suggests that accurate extrapolation of the pressure data is not required to obtain relatively accurate results. Above a Mach number of 0.88, the percentage of load carried by the rear portion of the wing increased as the shock wave moved aft, and the steep pressure gradients in this region precluded extrapolation of the pressure data.

For convenience in ascertaining the extent of supercritical flow on the wing at any particular Mach number, the local critical pressure coefficient is indicated in figures 18 through 22 for the higher Mach numbers. Also indicated are the crest location and the approximate sweep angle of the isobars, to be discussed later.

Normal-force characteristics.- The spanwise distributions of section normal-force coefficient for angles of attack from 0° to 16° at a Mach number of 0.18 are shown in figure 23. The effect of compressibility on the spanwise distribution of section normal-force coefficient is illustrated in figure 24 for angles of attack of 0°, 2°, and 4°. For all angles of attack and Mach numbers at which data were obtained, the section normal-force coefficient near the root of the wing was less than it was farther out on the wing semispan. Examination of figure 24 reveals that in the angle-of-attack range from 0° to 4° the section normal-force coefficients increased with increasing Mach number up to 0.80 Mach number. Further increase of the Mach number to 0.88 resulted in reduced section normal-force coefficients on the outer portion of the wing while those on the inner portion continued to increase. This indicates that the spanwise center of pressure shifted toward the wing root at the higher Mach numbers.

A comparison of the spanwise distribution of normal loading coefficient $c_n c/C_N c_{av}$ at a Mach number of 0.18 with the theoretical distribution from the charts of reference 8 is presented in figure 25. Although the theory used takes account of only the additional loading due to angle

of attack, the theoretical distribution agrees fairly well with the experimental data except at 0° angle of attack and at angles of attack near that at which stall occurred at the tip. At 0° angle of attack, good agreement cannot be expected since the loading is predominately the result of the camber of the wing.

The spanwise distribution of normal loading coefficient at several Mach numbers is presented in figure 26 for angles of attack of 0°, 2°, and 4°. Also shown are the theoretical additional loading distributions for Mach numbers of 0.18 and 0.85. Up to the Mach number at which the abrupt drag increase occurred, the experimental results confirm the theoretical prediction that the effect of compressibility on the distribution of the normal loading coefficient is small.

Aeroelastic characteristics.- The results of the static load tests to evaluate the elastic properties of the model are shown in figure 27. The test method has been described previously in the section Model and Apparatus and has been illustrated in figure 6. In figure 27, the spanwise distribution of twist ϵ is shown for the wing at 4° angle of attack and a Reynolds number of 2,000,000 for Mach numbers of 0.75 and 0.90. The symbols represent the measured angles of twist due to the combined effects of wing bending and torsion. To evaluate the separate effects of bending and torsion on the angle of twist, the elastic axis was assumed to be a straight line at 40 percent of the chord. This axis corresponded closely to the center line of the steel spar in the model.

Inspection of figure 27 reveals that the wing twist was only about -0.5° near the tip. The effect of this amount of washout on the measured pressures, forces, and moments is apparently small. It is noted that twist due to torsion partially offset the twist due to bending. At a Mach number of 0.90, this effect was slightly less as a result of rearward movement of the chordwise center of pressure.

Compressibility effect on section chord force.- To explore the effect of compressibility on pressure drag, some of the pressure data were integrated to obtain section chord-force coefficients at 0° angle of attack for various Mach numbers. The results must be considered of qualitative value only, since it was necessary to extrapolate the pressure data to 100 percent of the chord. In order to better indicate the variation in chord force along the semispan, the section chord-force coefficients were weighted according to the local chord to obtain the section chord-force parameter $c_c(c/c_{av})$. The spanwise distribution of section chord-force parameter at several Mach numbers is illustrated in the upper portion of figure 28. In the lower part of the figure, the section chord-force parameters at five spanwise stations are shown as functions of Mach number.

It is noted from figure 28 that the root sections of the wing had positive pressure drag, while the tip sections had negative pressure drag.

This result is in qualitative agreement with the theoretical prediction given in reference 11. With increasing Mach number, the region of positive pressure drag increased both in magnitude and spanwise extent.

The reason for this distribution of pressure drag is evident from the pressure data of figure 29 in which the upper- and the lower-surface pressures at three spanwise stations are compared for Mach numbers of 0.18, 0.80, and 0.88 for the wing at 0° angle of attack. The crest line on the upper surface of the wing, as previously defined, is at 40 percent of the chord for this angle of attack. Near the wing root, the surface pressures ahead of the crest were higher and behind the crest they were lower than at sections near the wing tip. The integrated effects of these pressure differences were such as to cause the section chord force at the root to be higher than at the tip.

With further reference to figure 28, it is noted that the effect of compressibility on the section chord-force parameter varied along the semispan. At stations 0.15 b/2 and 0.31 b/2, the section chord-force parameter at 0° angle of attack continually increased with increasing Mach number. On the remainder of the wing, the section chord-force parameter decreased up to a Mach number of about 0.80, thus tending to offset the increase occurring in the vicinity of the wing root. For Mach numbers above about 0.80, the section chord-force parameter increased with Mach number at all except the outermost station. The source of these changes in section chord-force parameter can be traced to the manner in which pressures ahead of and behind the crest varied with Mach number. Examination of figure 18 reveals that, after the critical flow condition was attained near the root sections, pressures to the rear of the crest decreased greatly and those ahead of the crest increased slightly. At the tip sections where minimum pressure occurred well forward of the crest, the rearward growth of the supercritical region resulted in decreasing pressures ahead of the crest until the critical flow condition was attained at the crest.

Critical Flow and Drag Increase at High Subsonic Mach Numbers

To determine the critical pressure coefficients at various points on the wing, the isobar diagrams of figure 30 were prepared from the pressure data of figures 18 through 22. These isobar diagrams show the pressure coefficients on the upper surface of the wing for angles of attack from 0° to 4° and for selected Mach numbers in the range where critical flow conditions were expected to appear on the wing. The angle of sweep of the isobars was measured at a number of stations along the wing semispan and used to determine the local critical pressure coefficient from equation (1) (fig. 2). At stations near the wing root, the appropriate isobar sweep angle was not well defined because of the spanwise pressure gradient. In this instance, the sweep angle of the line of minimum pressure was used to determine the local critical pressure coefficient. The crest line was

chosen as a reference from which to gauge the probable effect of pressure changes on the drag on the assumption that the pressure drag at any section will increase soon after the attainment of the critical pressure at the crest. The location of the crest and the local critical pressure coefficient are noted on the pressure diagrams of figures 18 through 22 for the higher Mach numbers.

With reference to figure 30(a), it is noted that at 0° angle of attack the critical flow condition was first attained near the wing root at a free-stream Mach number of about 0.83. With increasing free-stream Mach number, the line through points for which the component of local Mach number normal to the isobars was unity moved rearward and extended outward to the wing tip as indicated by the heavy lines in figure 30(a).

Figure 31 is a graphical illustration of the relation of the occurrence of critical flow conditions at the crest point of several stations along the wing semispan to the total drag variation with increasing Mach number. In this figure, the experimental curves showing the variation with Mach number of pressure coefficient at the crest line are intersected by theoretical curves representing the variation of local critical pressure coefficient P_{φ} with Mach number. The intersection of these curves defines the Mach number M_{φ} at which the critical flow condition was attained at the crest of each spanwise section. Also indicated in this figure is the drag-divergence Mach number which has been defined as the Mach number at which $(\partial C_D/\partial M_o)_{\alpha}$ is equal to 0.10.

The correlation between the occurrence of critical flow conditions at the crest line of the wing and the abrupt drag increase is good throughout the angle-of-attack range from 0° to 4°, drag divergence having occurred at a Mach number slightly above that at which the critical flow condition was attained at the crest of the entire wing. It is interesting to note that had the minimum pressure line been used as a reference instead of the crest line, the correlation would not have been as satisfactory at angles of attack of 3° and 4° because of the forward position of minimum pressure at the outer stations. For instance, it is indicated in figure 22(a) that at 4° angle of attack supercritical flow prevailed near the leading edge of the outer half of the wing at a Mach number of 0.70, yet from figure 31(e) the drag-divergence Mach number is indicated to be 0.81. The critical flow condition at the crest of the outer portion of the wing was attained at a Mach number of about 0.78.

Since the rate of drag increase is dependent upon the rate of development of the supercritical flow regions, it should be noted that this wing had the special property of attaining the critical flow condition at the crest of the various spanwise stations within a narrow range of Mach numbers. This range of Mach numbers is probably larger for more highly swept wings.

Pressure Changes with Increasing Mach Number

The variation of pressure coefficient with free-stream Mach number at several positions on the upper surface of the wing is illustrated in figure 32 for 0°, 2°, and 4° angle of attack. Data are presented for stations 0.15 b/2, 0.55 b/2, and 0.917 b/2. Also shown in this figure are the lift-divergence and drag-divergence Mach numbers for the wing at various angles of attack. It is apparent from the data that the effects of compressibility on the surface pressures were different at the various spanwise and chordwise stations.

At chordwise stations near the crest, there was a fairly uniform decrease in pressure coefficient with increasing Mach number up to the Mach number of drag divergence, but, at points near the leading edge and near the trailing edge of the wing, the pressure coefficients showed no consistent variation with Mach number. While this fact discourages attempts to predict from the low-speed data the chordwise and spanwise distribution of pressure at high subsonic Mach numbers, it does suggest that a theoretical compressibility correction might be useful in predicting the upper-surface pressures in the vicinity of the wing crest line and thus might provide a means for estimating the drag-divergence Mach number.

Estimates of crest pressure changes with increasing Mach number.- There are available several approximate expressions derived on the basis of linearized theory for estimating the effects of compressibility on the pressures over a yawed airfoil. These expressions generally involve the assumption of two-dimensional nonviscous flow in the subcritical Mach number range.

In the absence of more general expressions applicable to the three-dimensional flow over a swept wing of finite span, several such expressions have been investigated with regard to their usefulness in predicting the pressures at the crest line of the swept wing of this report. These expressions are:

1. Prandtl-Glauert expression modified for sweep effect

$$\frac{P}{P_i} = \frac{1}{\sqrt{1 - M_o^2 \cos^2 \varphi}} \tag{3}$$

2. Kármán-Tsien expression modified for sweep effect

$$\frac{P}{P_i} = \frac{1}{\sqrt{1 - M_o^2 \cos^2 \varphi} + \frac{P_i}{2 \cos^2 \varphi}\left(1 - \sqrt{1 - M_o^2 \cos^2 \varphi}\right)} \tag{4}$$

3. Weber expression from reference 12

$$\frac{P}{P_i} = \frac{1}{\sqrt{1 - M_o^2 (\cos^2 \varphi - P_i)}} \qquad (5)$$

It should be mentioned that equation (5) involves an additional assumption based on experimental results of tests of a wing of finite span having 45° sweepback of the leading edge. Since all these relationships are based on two-dimensional flow, it is to be expected that their application would give the best results at the midsemispan of the wing where the flow is the least influenced by end effects.

In figure 33, the effect of compressibility on the experimentally determined pressure coefficient on the upper surface at the crest point of station 0.55 b/2 is compared with those which would be predicted by the use of equations (3), (4), and (5). The comparison is shown for 0°, 2°, and 4° angle of attack. In each of the theoretical expressions, the sweep angle φ was taken as the sweep angle of the crest line, varying from approximately 33.7° at 0° angle of attack to 34.9° at 4° angle of attack. Also indicated in figure 33 are the experimentally determined Mach numbers for the attainment of the critical flow condition (denoted by M_φ) at the crest of station 0.55 b/2 for the three angles of attack. While the pressure coefficients calculated by use of the Prandtl-Glauert expression, equation (3), appear to compare more favorably with the experimental data at the lower Mach numbers, those calculated by use of the Kármán-Tsien expression, equation (4), show the best agreement at Mach numbers near that at which the critical flow condition is attained. In the following section, use is made of equation (4) in estimating M_φ at the crest of station 0.55 b/2 from the low-speed pressure data.

Estimated Mach number for attainment of the critical flow condition.- As has been pointed out, the drag of this wing increased abruptly at a Mach number slightly above that at which the critical flow condition had been attained at the crest of the entire wing. Therefore, it is of interest to compare the Mach number for drag divergence with the estimated values of M_φ at the crest of station 0.55 b/2 based on the low-speed pressure data and equation (4). This comparison is made in figure 34 wherein the experimental drag-divergence Mach number of the wing and the estimated values of M_φ for the crest point of spanwise station 0.55 b/2 are shown as functions of the angle of attack. The estimated values of M_φ were calculated from equations (1) and (4) using the crest pressures obtained from experimental data at a Mach number of 0.18. The sweep of the crest line was used in determining the local critical pressure coefficient. Also shown in figure 34 are the experimental values of M_φ for the crest points of stations 0.15 b/2, 0.55 b/2, and 0.917 b/2 obtained from figure 31.

Good agreement exists between the experimental and estimated values of M_φ at station 0.55 b/2. At 0° angle of attack, M_φ for station 0.15 b/2 was considerably lower than for stations farther from the wing root, but, at about 3° angle of attack, M_φ was approximately the same for all stations. At all angles of attack, the values of M_φ were lower than the drag-divergence Mach number M_D, as might be anticipated in consideration of the arbitrary definition of drag-divergence Mach number (the Mach number at which $(\partial C_D/\partial M_o)_\alpha = 0.10$).

CONCLUSIONS

The aerodynamic characteristics of a wing having 37.25° sweepback of the leading edge and an aspect ratio of 6.04 have been evaluated from wind-tunnel tests of a semispan model at Mach numbers up to 0.94. The results of the tests indicate the following conclusions:

1. The effects of compressibility on the force and moment characteristics of this wing at low and moderate lift coefficients were small up to Mach numbers for which the abrupt drag increase occurred. Deterioration of the lifting characteristics of the wing at high Mach numbers generally did not occur until the drag had increased by a considerable amount.

2. The effect of compressibility on the spanwise distribution of normal loading coefficient was small for angles of attack of 0° to 4° and for Mach numbers up to that at which the abrupt drag increase began. At higher Mach numbers, a reduction in load on the outer portion of the wing caused the spanwise center of pressure to shift toward the wing root.

3. At 0° angle of attack, as the Mach number was increased to that at which the abrupt drag rise began, the section chord-force parameter $c_c(c/c_{av})$ for sections near the wing root increased, while for sections near the wing tip it decreased.

4. At angles of attack between 0° and 4°, the abrupt drag increase began at Mach numbers slightly higher than those at which the critical flow condition had been attained at the crest line of the entire wing (the crest line being defined as the locus of points on the wing surface at which the surface is tangent to the direction of the undisturbed air stream). A critical flow condition was considered to exist when the component of local velocity normal to the isobar equalled the local speed of sound. For this wing, having moderate sweepback, the critical flow condition was attained at the crest of the various spanwise stations within a narrow range of Mach numbers.

5. A useful guide in estimating the drag-divergence Mach number of a moderately swept wing at low angles of attack is provided by calculations of the Mach numbers at which the critical flow condition occurs at the crest of various spanwise sections. For sections near the midsemispan, these calculations may be based on pressure distributions measured at low speeds suitably modified for the effects of compressibility.

Ames Aeronautical Laboratory,
National Advisory Committee for Aeronautics,
Moffett Field, Calif.

APPENDIX

DERIVATION OF THE CRITICAL PRESSURE COEFFICIENT

An expression for local critical pressure coefficient in terms of the local sweep angle of the isobars and the free-stream Mach number can be developed as follows. With reference to figure 1,

$$V^2 = V_o^2 \sin^2 \varphi + V_\perp^2 \quad . \quad . \quad . \quad . \quad . \tag{A1}$$

or when $V_\perp = a$

$$\frac{V^2}{a^2} = \frac{V_o^2 \sin^2 \varphi}{a^2} + 1 \tag{A2}$$

The energy equation for compressible flow may be written in the form

$$\frac{V^2}{2} + \frac{\gamma}{\gamma-1}\frac{p}{\rho} = \frac{V_o^2}{2} + \frac{\gamma}{\gamma-1}\frac{p_o}{\rho_o} \tag{A3}$$

Making use of the isentropic relations $a^2 = \gamma p/\rho$ and $a_o^2 = \gamma p_o/\rho_o$, and combining equations (A2) and (A3)

$$\frac{V_o^2 \sin^2 \varphi}{a_o^2} + \frac{a^2}{a_o^2}\frac{\gamma+1}{\gamma-1} = \frac{V_o^2}{a_o^2} + \frac{2}{\gamma-1} \tag{A4}$$

At the critical flow condition, $p = p_{cr}$ and $a = a_{cr}$. Writing $V_o/a_o = M_o$, and noting that $\frac{p_{cr}}{p_o} = \left(\frac{a_{cr}}{a_o}\right)^2 \frac{\gamma}{\gamma-1}$, it follows that

$$\frac{p_{cr}}{p_o} = \left(\frac{2}{\gamma+1} + \frac{\gamma-1}{\gamma+1} M_o^2 \cos^2 \varphi\right)^{\frac{\gamma}{\gamma-1}} \tag{A5}$$

or since $p_o = \rho_o a_o^2/\gamma$,

$$p_{cr} - p_o = \frac{\rho_o a_o^2}{\gamma} \left[\left(\frac{2}{\gamma+1} + \frac{\gamma-1}{\gamma+1} M_o^2 \cos^2 \varphi \right)^{\frac{\gamma}{\gamma-1}} - 1 \right] \qquad (A6)$$

which can immediately be expressed as in equation (1)

$$P_\varphi = \frac{2}{\gamma M_o^2} \left\{ \left[\frac{2}{\gamma+1} \left(1 + \frac{\gamma-1}{2} M_o^2 \cos^2 \varphi \right) \right]^{\frac{\gamma}{\gamma-1}} - 1 \right\}$$

REFERENCES

1. Jones, Robert T.: Wing Plan Forms for High-Speed Flight. NACA TN 1033, 1946.

2. Robinson, Russell G., and Wright, Ray H.: Estimation of Critical Speeds of Airfoils and Streamline Bodies. NACA ACR, 1940.

3. Kuchemann, D.: Design of Wing Junction, Fuselage, and Nacelles to Obtain the Full Benefit of Sweptback Wings at High Mach Number. Rep. No. Aero. 2219, R.A.E. (British), 1947.

4. Thom, A., and Perring, W. G. A.: The Design and Work of the Farnborough High Speed Tunnel. Jour. Roy. Aero. Soc., vol. 52, no. 448, Apr. 1948, pp. 205-250.

5. Nitzberg, Gerald E., and Crandall, Stewart: A Study of Flow Changes Associated with Airfoil Section Drag Rise at Supercritical Speeds. NACA TN 1813, 1949.

6. Sivells, James C., and Deters, Owen J.: Jet-Boundary and Plan-Form Corrections for Partial-Span Models with Reflection Plane, End Plate, or No End Plate in a Closed Circular Wind Tunnel. NACA Rep. 843, 1946.

7. Herriot, John G.: Blockage Corrections for Three-Dimensional-Flow Closed-Throat Wind Tunnels, with Consideration of the Effect of Compressibility. NACA RM A7B28, 1947.

8. DeYoung, John: Theoretical Additional Span Loading Characteristics of Wings with Arbitrary Sweep, Aspect Ratio, and Taper Ratio. NACA TN 1491, 1947.

9. Dickson, R.: The Relationship Between the Compressible Flow Round a Swept-Back Aerofoil and the Incompressible Flow Round Equivalent Aerofoils. Rep. No. Aero. 2146, R.A.E. (British), 1946.

10. Koven, William, and Graham, Robert R.: Wind-Tunnel Investigation of High-Lift and Stall-Control Devices on a 37° Swept-Back Wing of Aspect Ratio 6 at High Reynolds Numbers. NACA RM L8D29, 1948.

11. Jones, Robert T.: Subsonic Flow Over Thin Oblique Airfoils at Zero Lift. NACA TN 1340, 1947.

12. Weber, J.: Some Remarks on the Application of the Theory of Incompressible Flow Around a Swept Wing at Zero Incidence to the Flow at High Subsonic Mach Numbers. Rep. No. Aero. 2274, R.A.E. (British) 1948.

TABLE I

COORDINATES FOR THE NACA 64_1-212 AIRFOIL SECTION

[Stations and ordinates given in percent of airfoil chord]

Upper surface		Lower surface	
Station	Ordinate	Station	Ordinate
0	0	0	0
.418	1.025	.582	-.925
.659	1.245	.841	-1.105
1.147	1.593	1.353	-1.379
2.382	2.218	2.618	-1.846
4.868	3.123	5.132	-2.491
7.364	3.815	7.636	-2.967
9.865	4.386	10.135	-3.352
14.872	5.291	15.128	-3.945
19.886	5.968	20.114	-4.376
24.903	6.470	25.097	-4.680
29.921	6.815	30.079	-4.871
34.941	7.008	35.059	-4.948
39.961	7.052	40.039	-4.910
44.982	6.893	45.018	-4.703
50.000	6.583	50.000	-4.377
55.016	6.151	54.984	-3.961
60.029	5.619	59.971	-3.477
65.039	5.004	64.961	-2.944
70.045	4.322	69.955	-2.378
75.047	3.590	74.953	-1.800
80.045	2.825	79.955	-1.233
85.038	2.054	84.962	-.708
90.027	1.303	89.973	-.269
95.013	.604	94.987	.028
100.000	0	100.000	0

L.E. radius: 1.040. Slope of radius through L.E.: 0.084.

TABLE II

COORDINATES FOR SECTIONS
PARALLEL TO FREE AIR STREAM
[Stations and ordinates given in
percent of airfoil chord]

Upper surface		Lower surface	
Station	Ordinate	Station	Ordinate
0	0	0	0
.465	.908	.647	-.820
.733	1.103	.935	-.979
1.275	1.411	1.504	-1.221
2.644	1.961	2.905	-1.632
5.388	2.754	5.679	-2.196
8.129	3.355	8.426	-2.608
10.859	3.846	11.153	-2.939
16.279	4.614	16.555	-3.439
21.647	5.175	21.890	-3.794
26.959	5.580	27.163	-4.035
32.213	5.845	32.378	-4.177
37.413	5.978	37.534	-4.220
42.555	5.983	42.635	-4.165
47.644	5.816	47.680	-3.968
52.674	5.525	52.674	-3.673
57.649	5.135	57.618	-3.307
62.569	4.666	62.512	-2.887
67.433	4.133	67.358	-2.432
72.242	3.551	72.156	-1.954
76.998	2.934	76.909	-1.471
81.701	2.297	81.616	-1.003
86.350	1.662	86.279	-.573
90.948	1.049	90.899	-.216
95.497	.484	95.473	.022
100.000	0	100.000	0

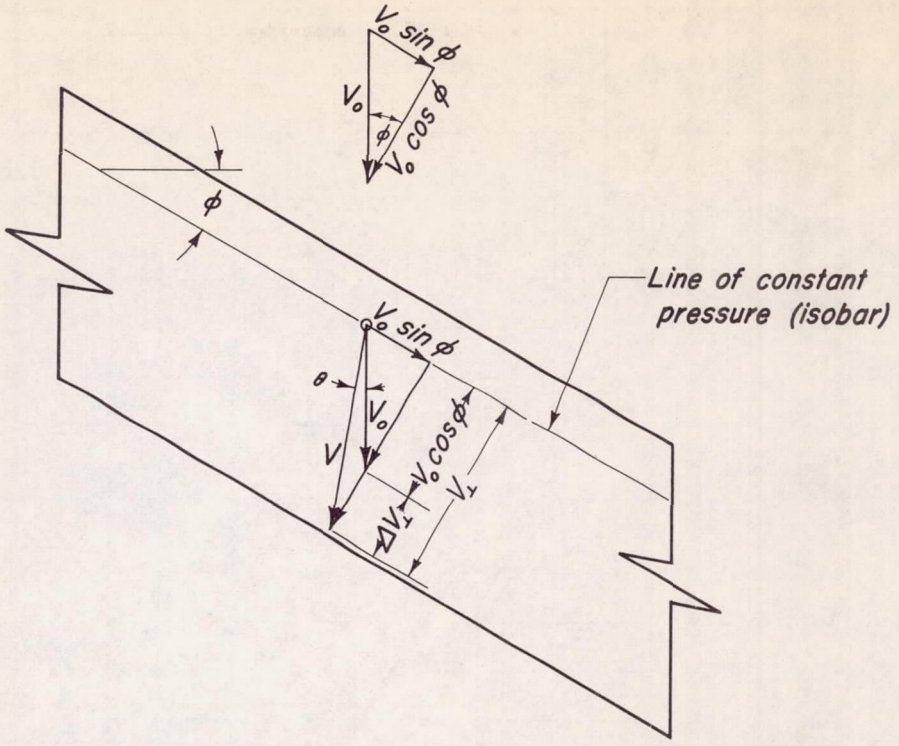

(a) Components of velocity on a yawed wing of infinite span.

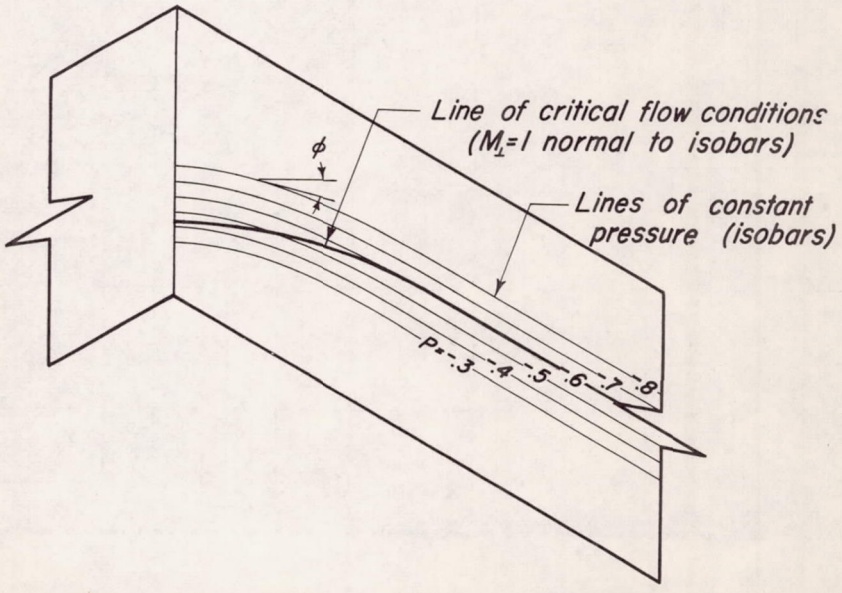

(b) Critical flow conditions on a swept-back wing of infinite span.

NACA

Figure 1.- Concepts used in considering the flow over swept wings.

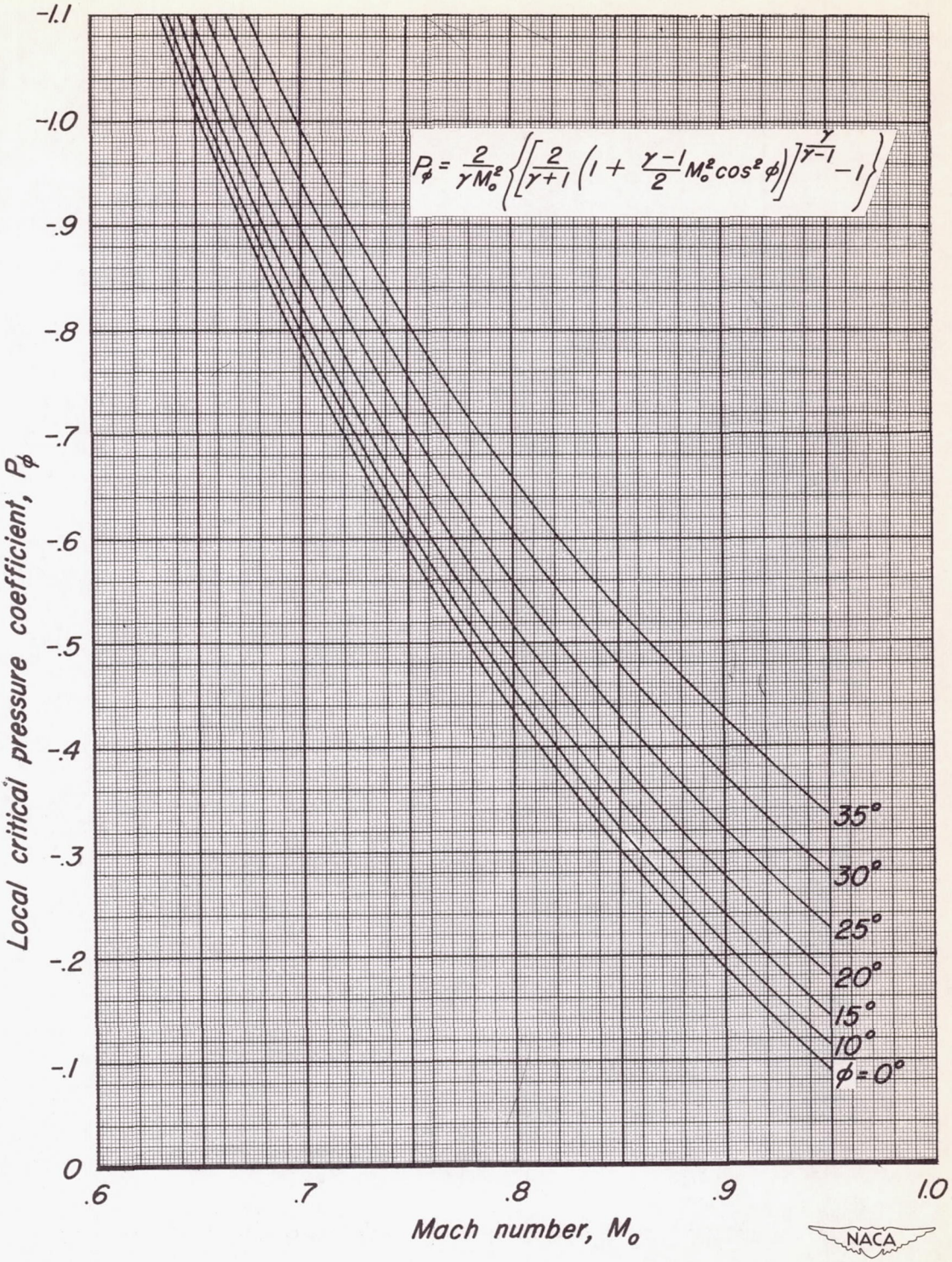

Figure 2.- The variation of local critical pressure coefficient with free-stream Mach number for several local angles of sweep.

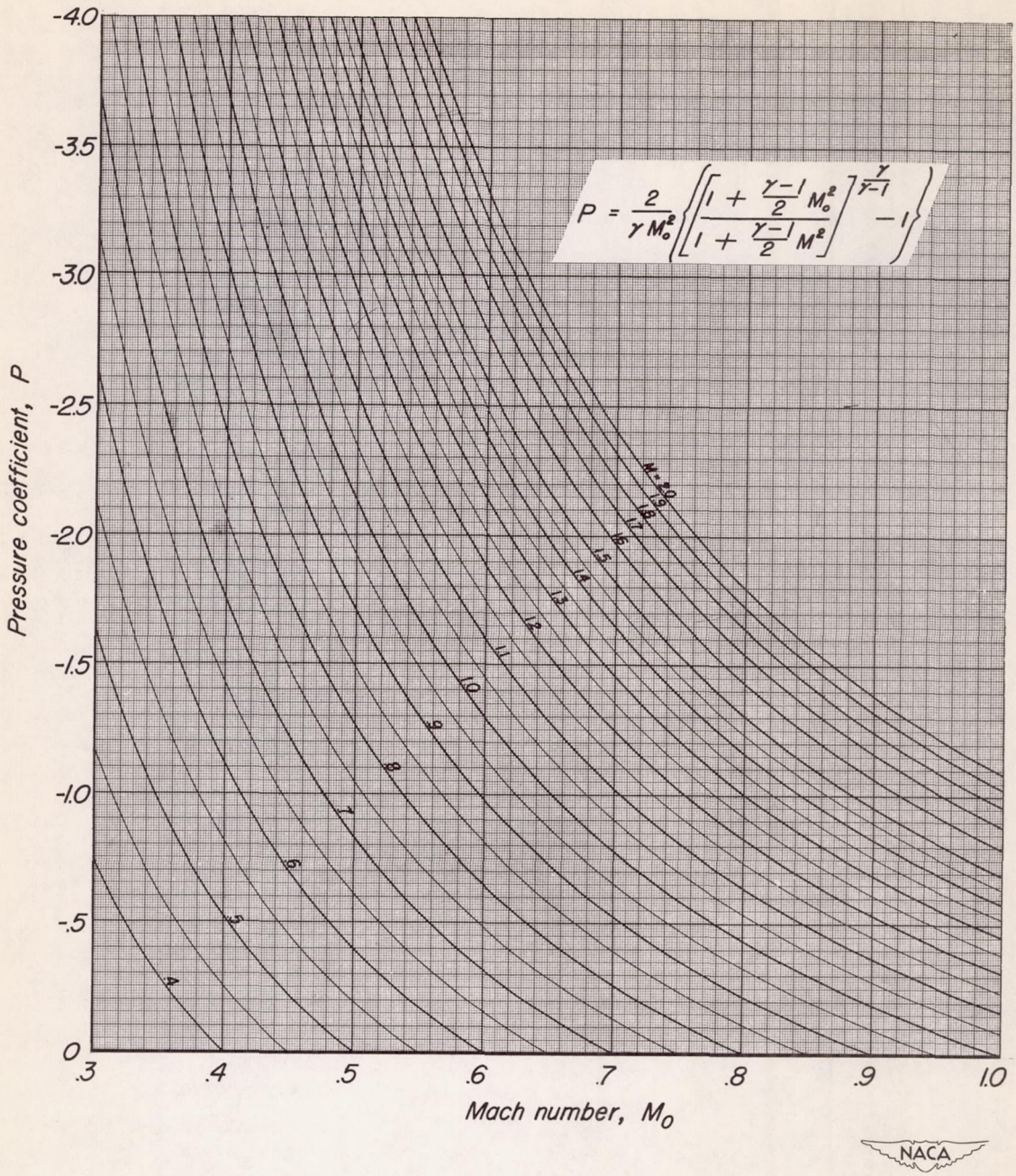

Figure 3.– The variation of pressure coefficient with free-stream Mach number and local Mach number.

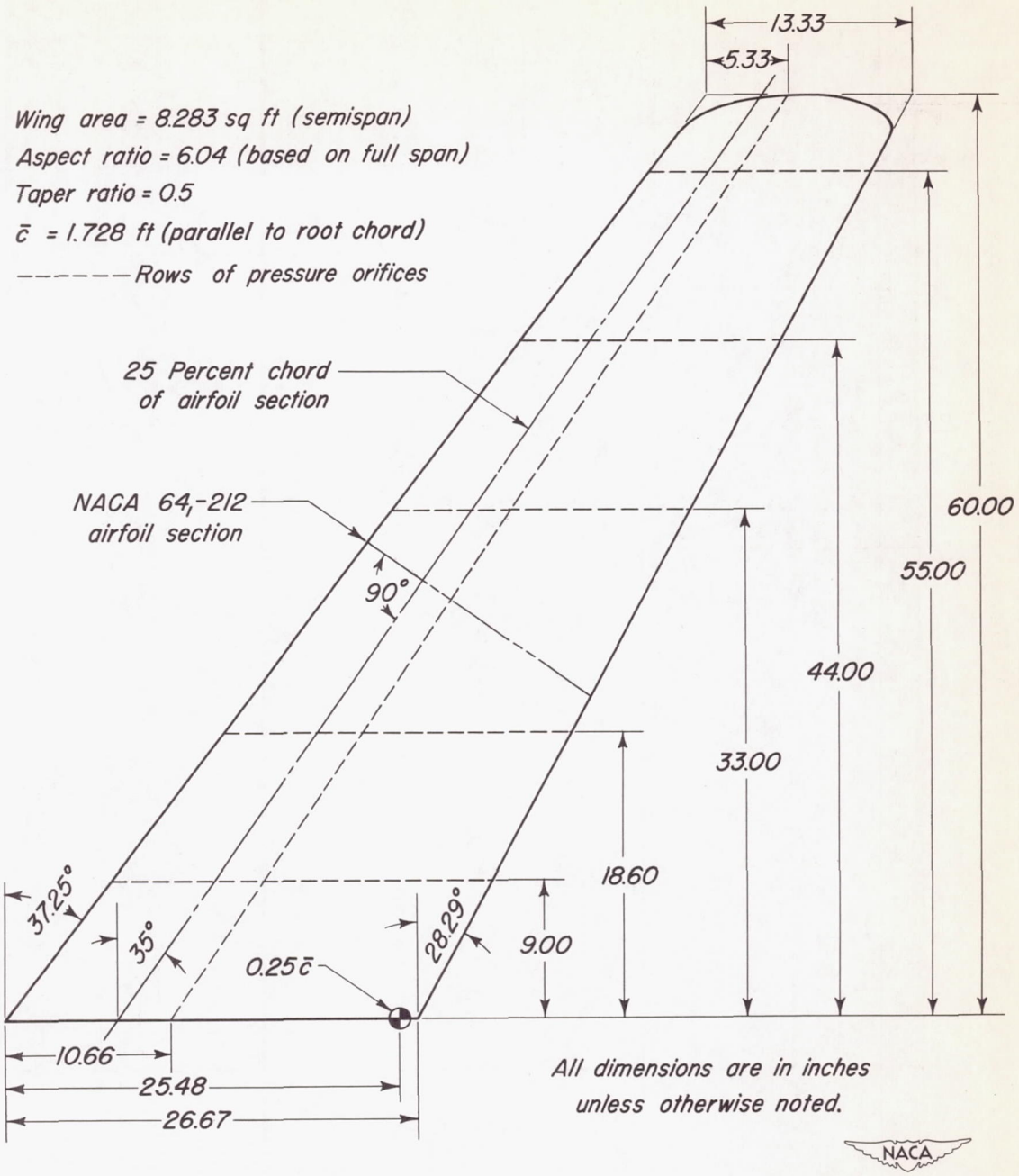

Figure 4.- Semispan model of the wing.

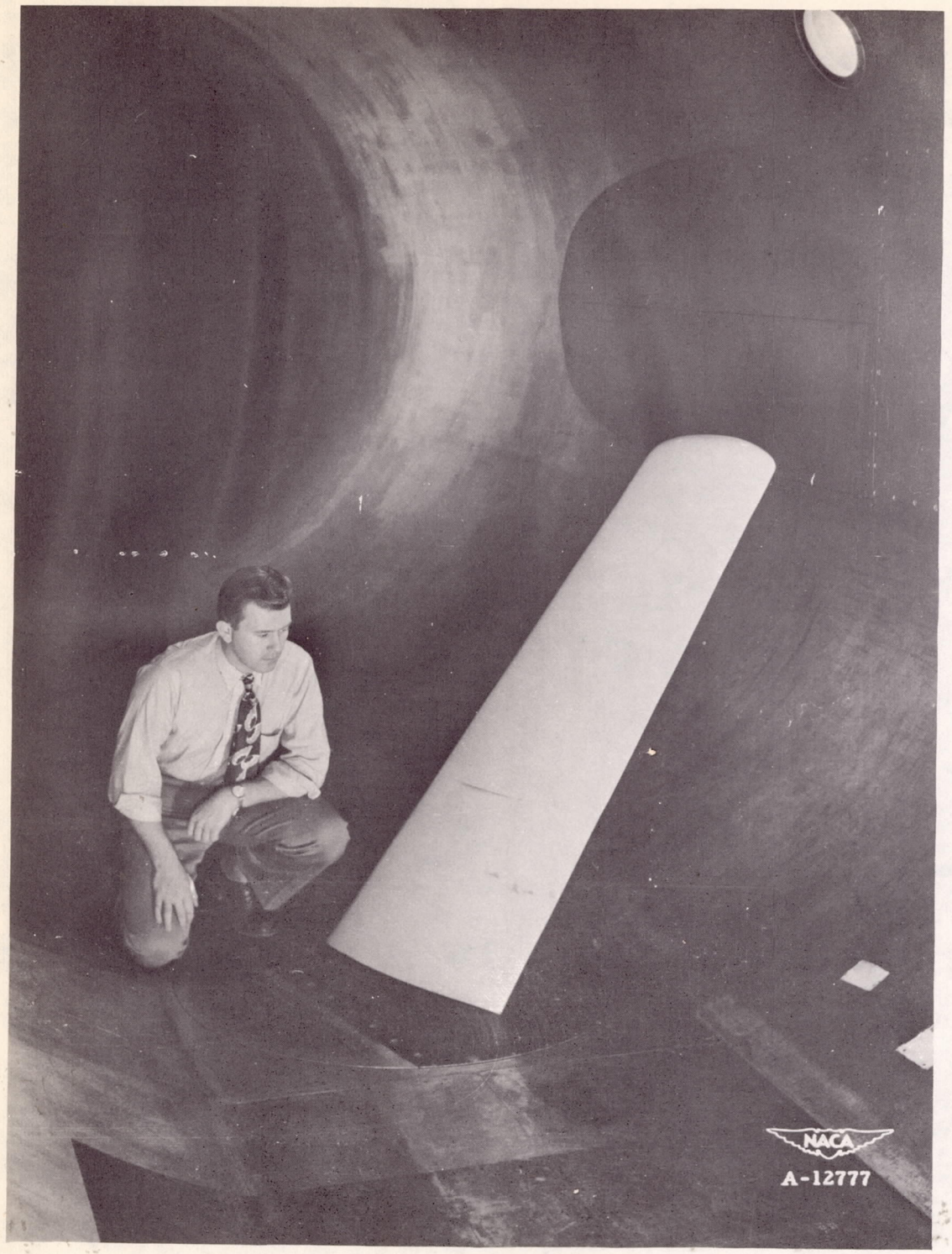

Figure 5.— Semispan wing mounted in the Ames 12-foot pressure wind tunnel.

(a) M, 0.75.

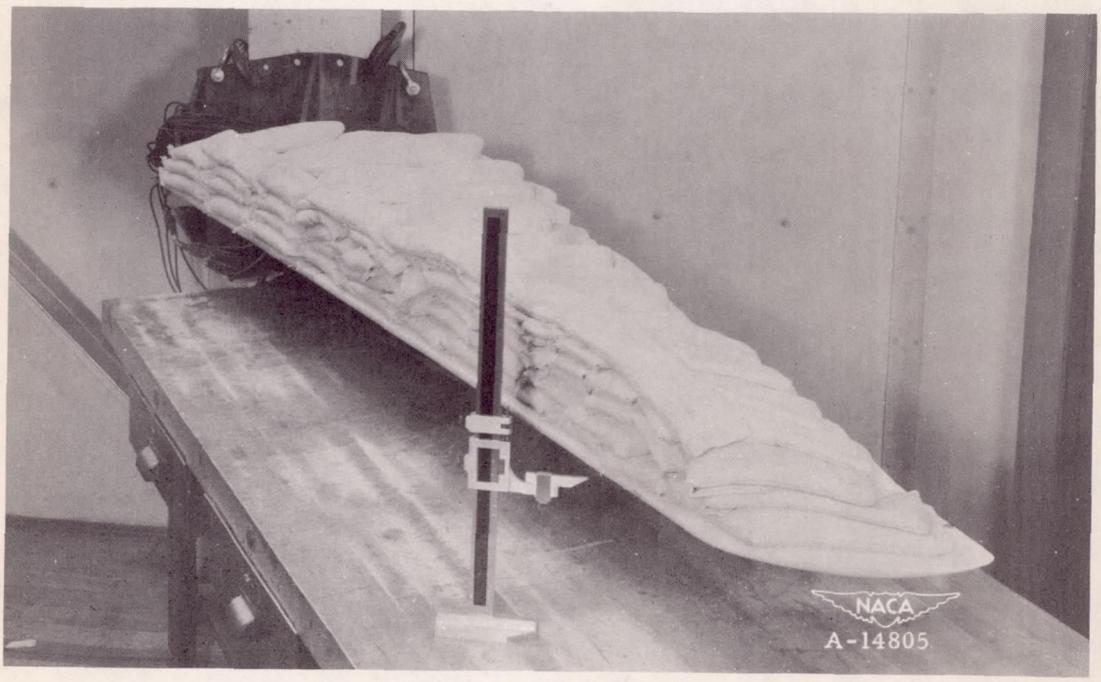

(b) M, 0.90.

Figure 6.- Wing model with weights simulating aerodynamic loadings at Mach numbers of 0.75 and 0.90. R, 2,000,000; α_u, 4°.

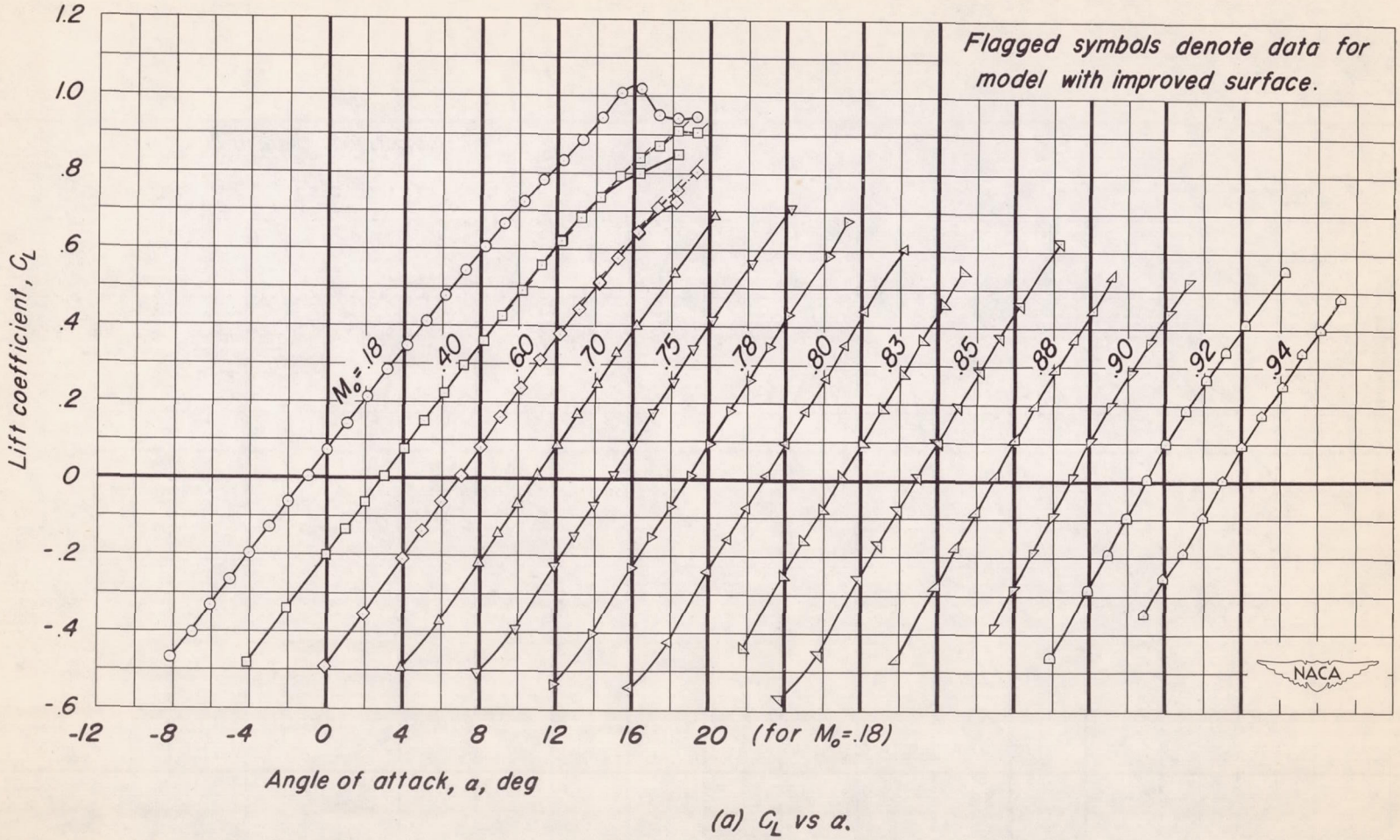

Figure 7.- The effect of Mach number on the lift, drag, and pitching-moment coefficients. R, 2,000,000.

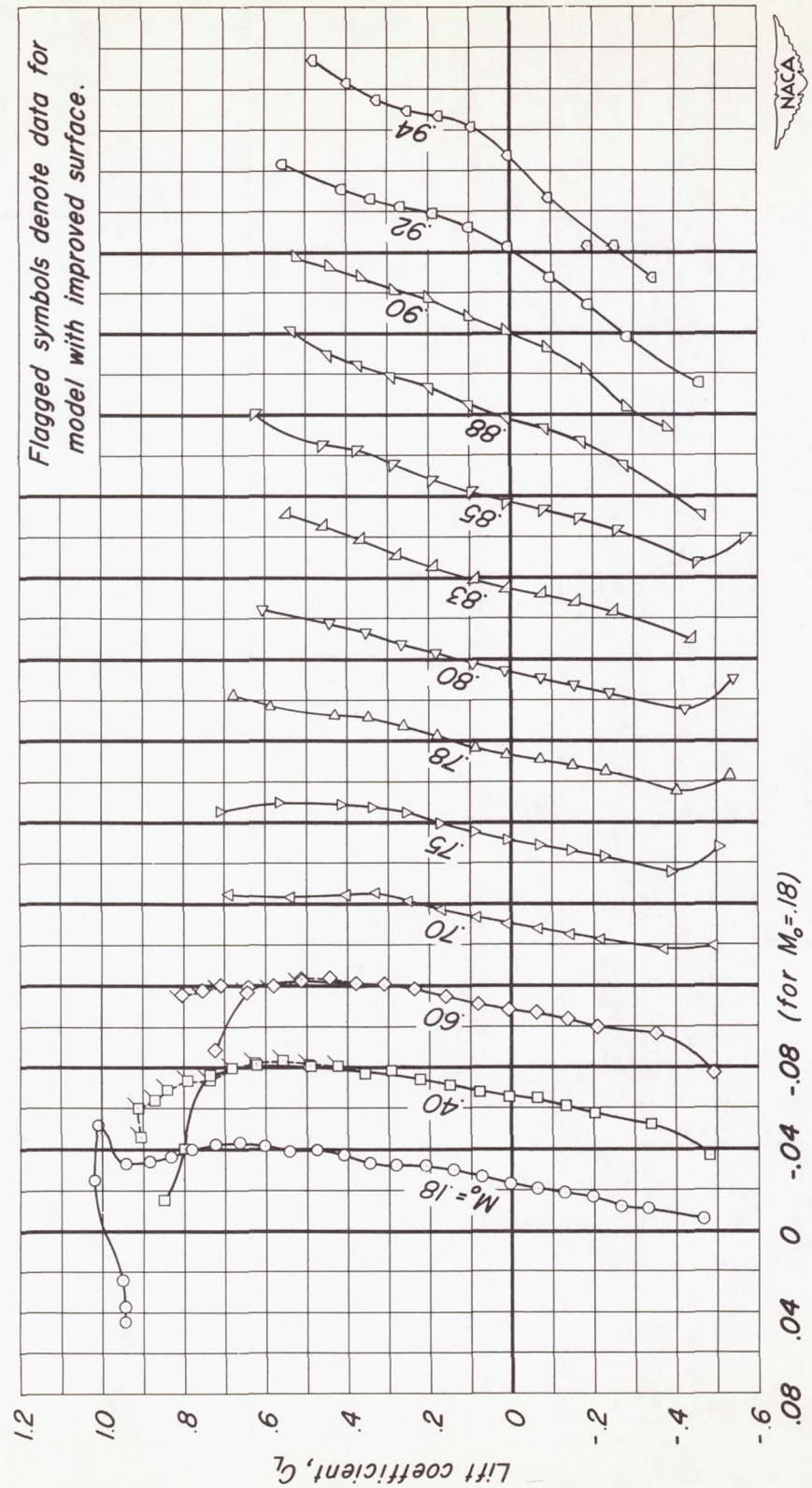

(b) C_L vs C_m.

Figure 7.- Continued.

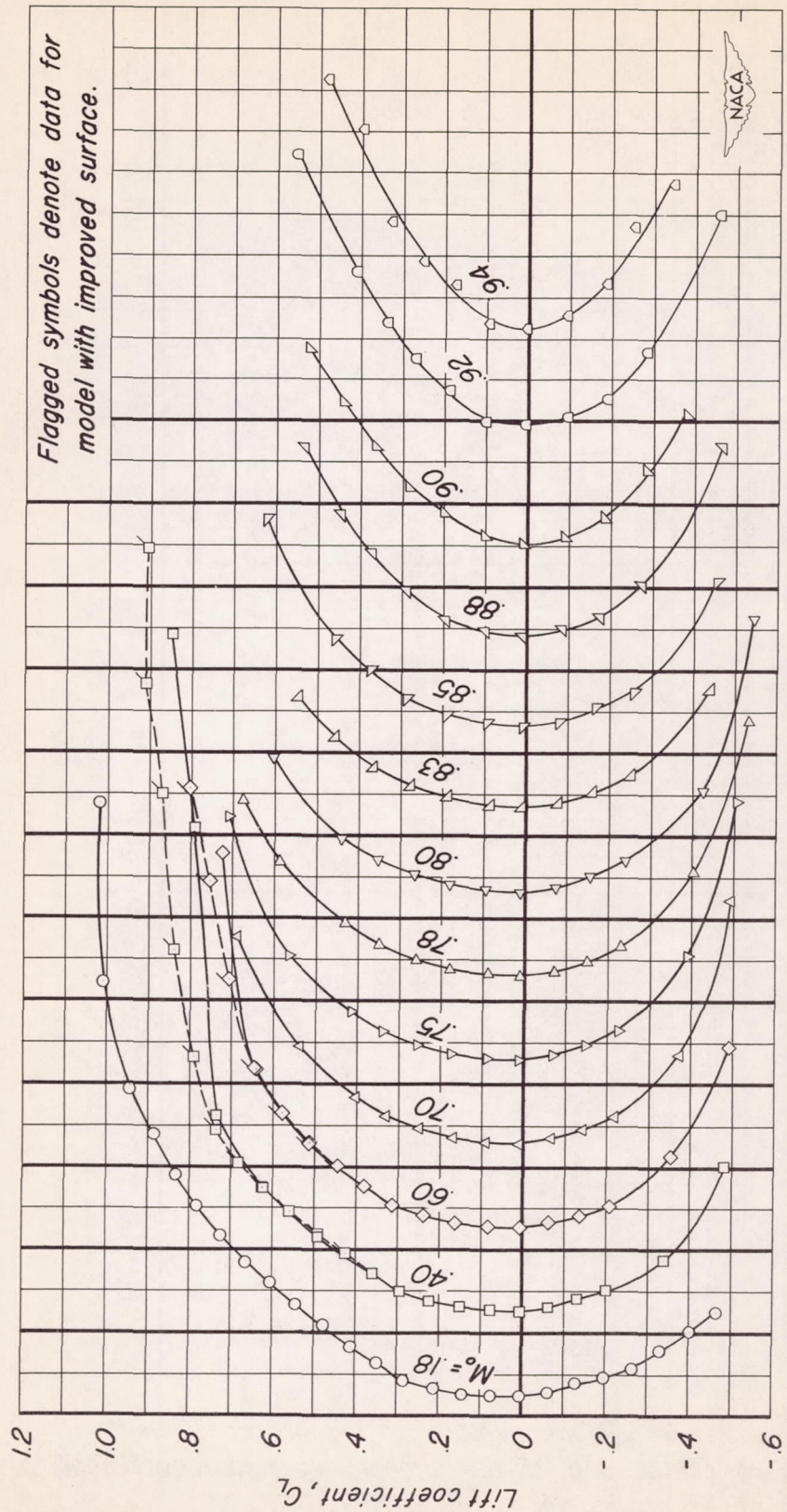

(c) C_L vs C_D.

Figure 7.- Concluded.

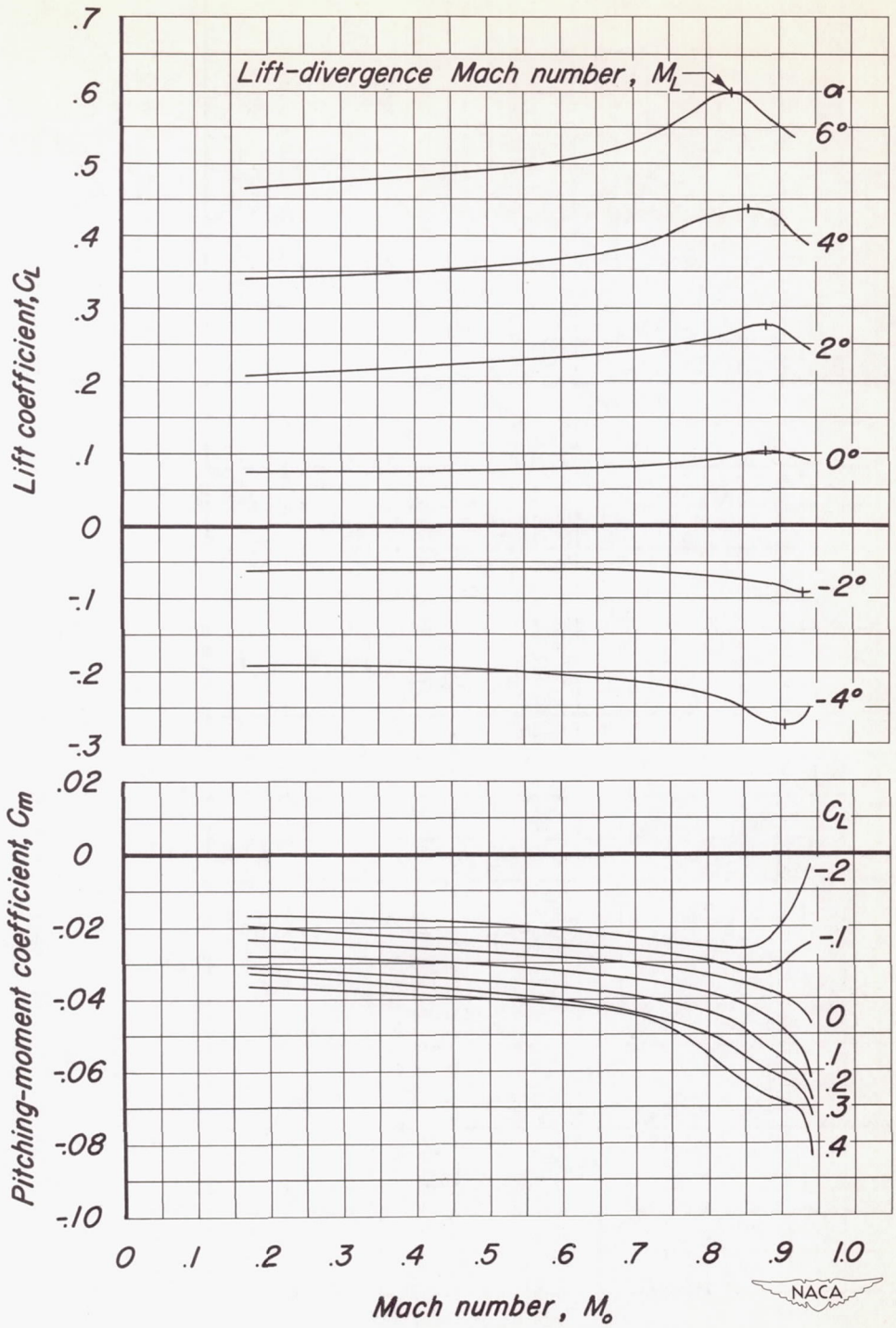

Figure 8.- The variation with Mach number of the lift coefficient at several angles of attack and of the pitching-moment coefficient at several values of lift coefficient. R, 2,000,000.

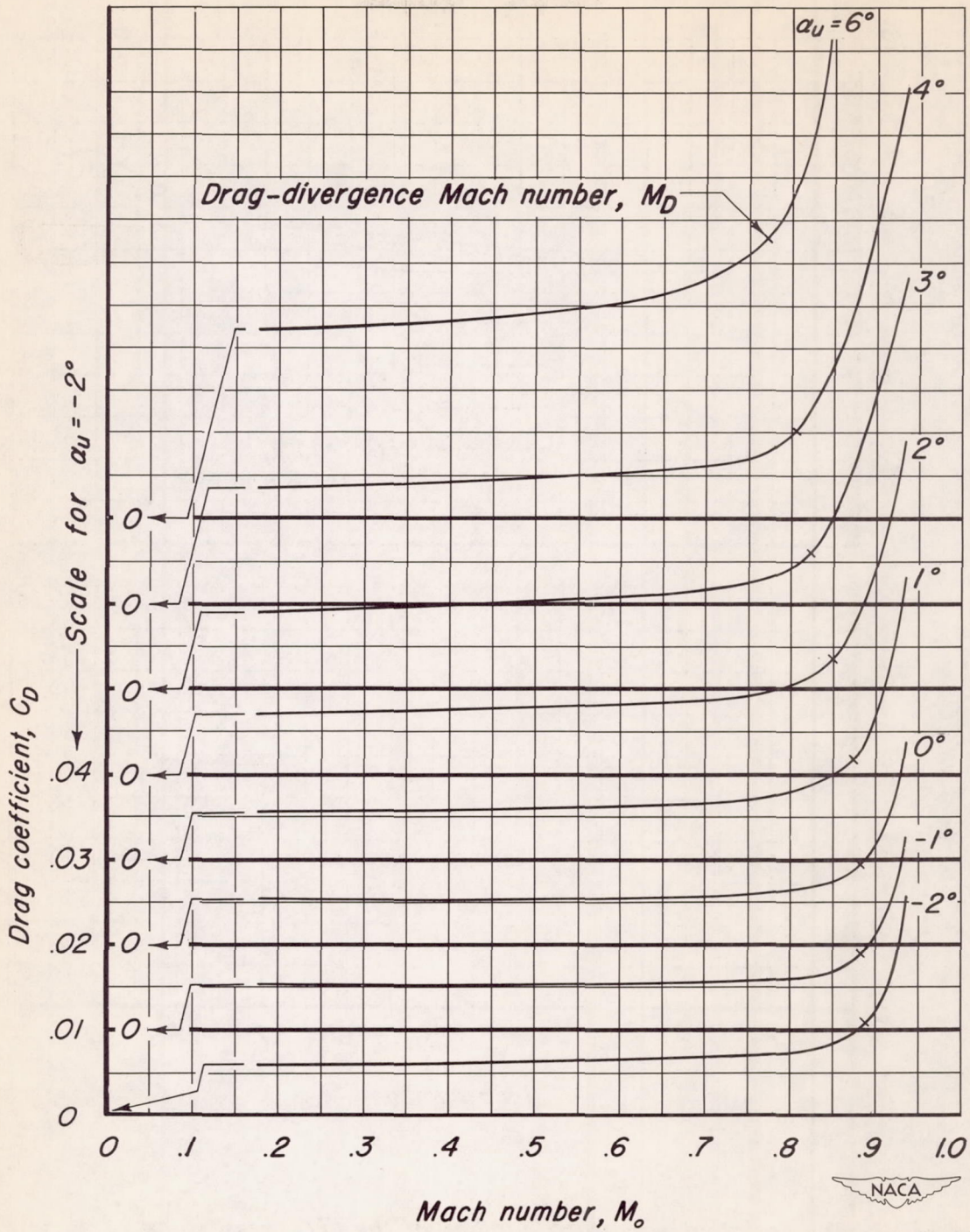

Figure 9.- The variation with Mach number of the drag coefficient at several angles of attack. R, 2,000,000.

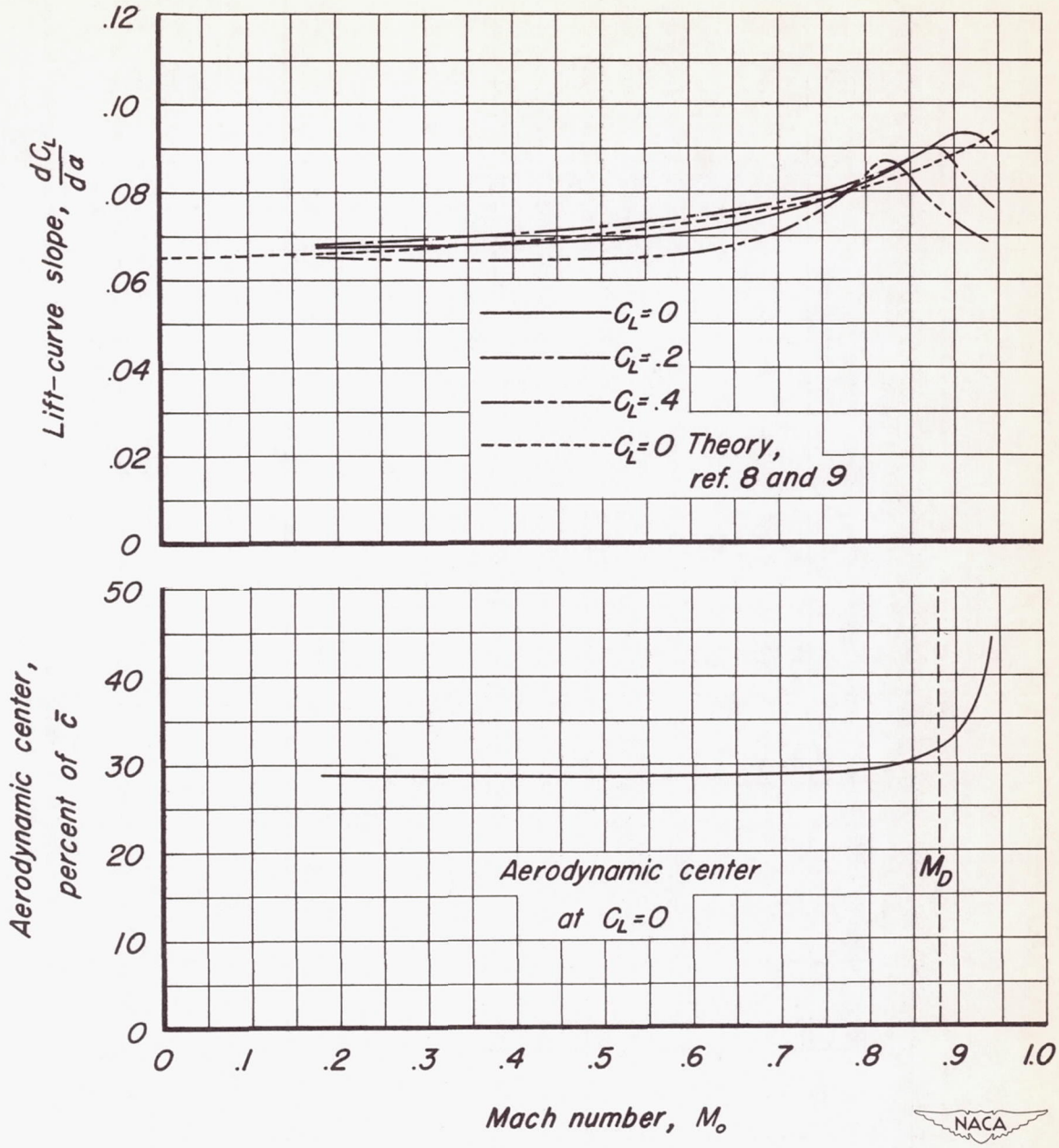

Figure 10.- The variation with Mach number of the lift-curve slope at several values of lift coefficient and of the aerodynamic center at zero lift coefficient. R, 2,000,000.

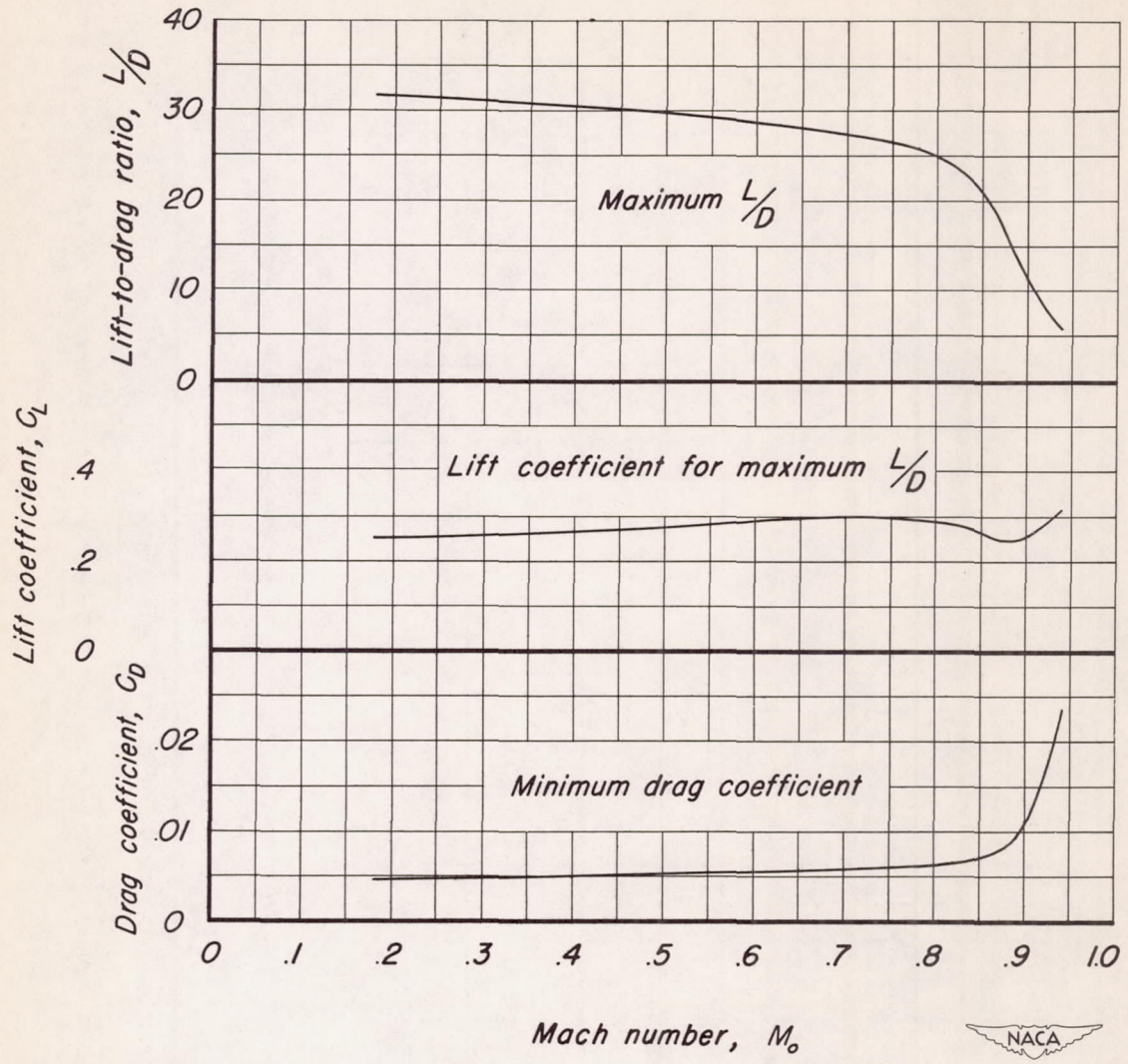

Figure 11. – The variation with Mach number of the maximum lift-to-drag ratio, the lift coefficient for maximum L/D and the minimum drag coefficient. R, 2,000,000.

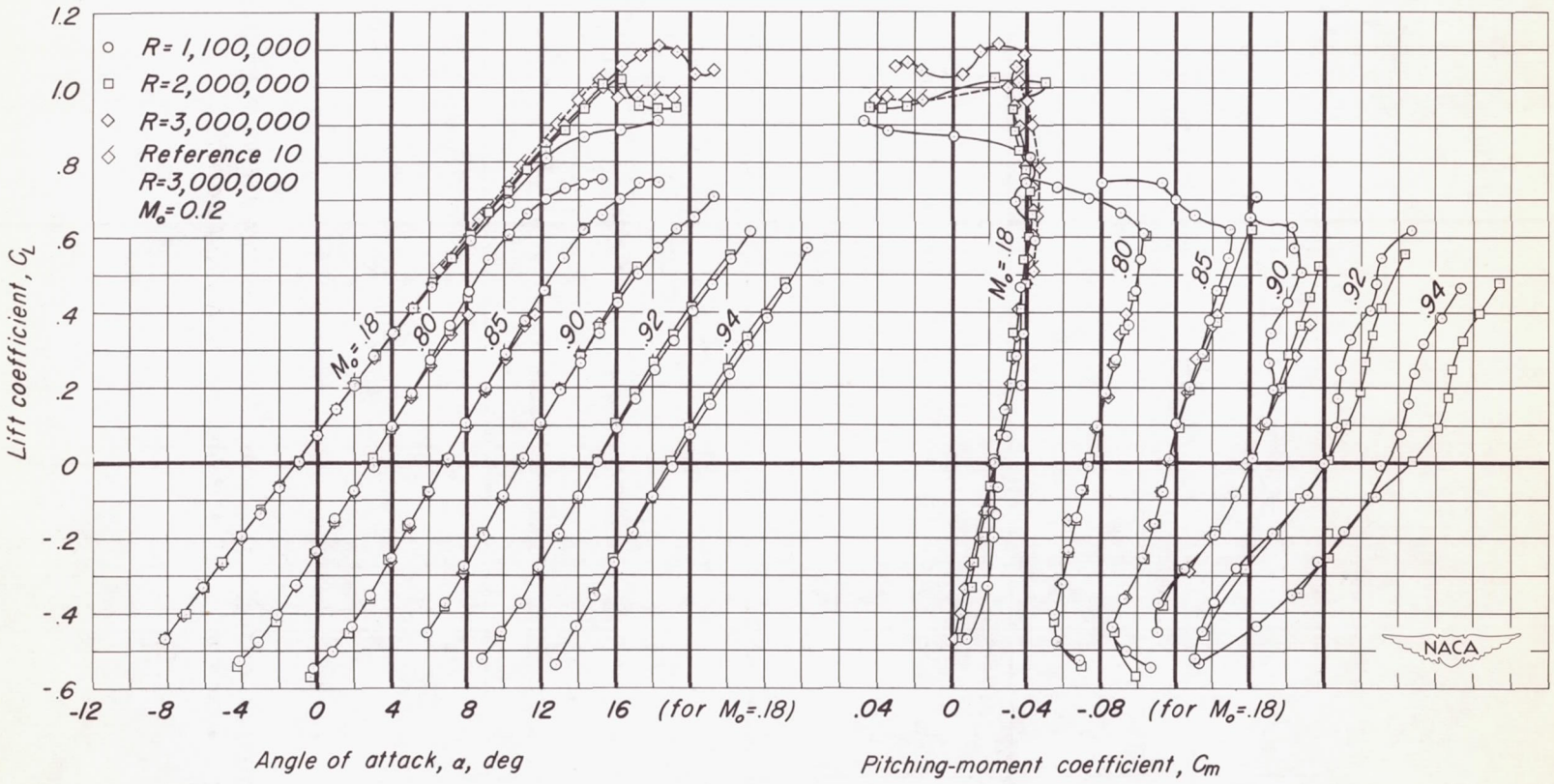

(a) C_L vs α, C_L vs C_m.

Figure 12.- The effect of Reynolds number on the lift, drag, and pitching-moment coefficients at several Mach numbers.

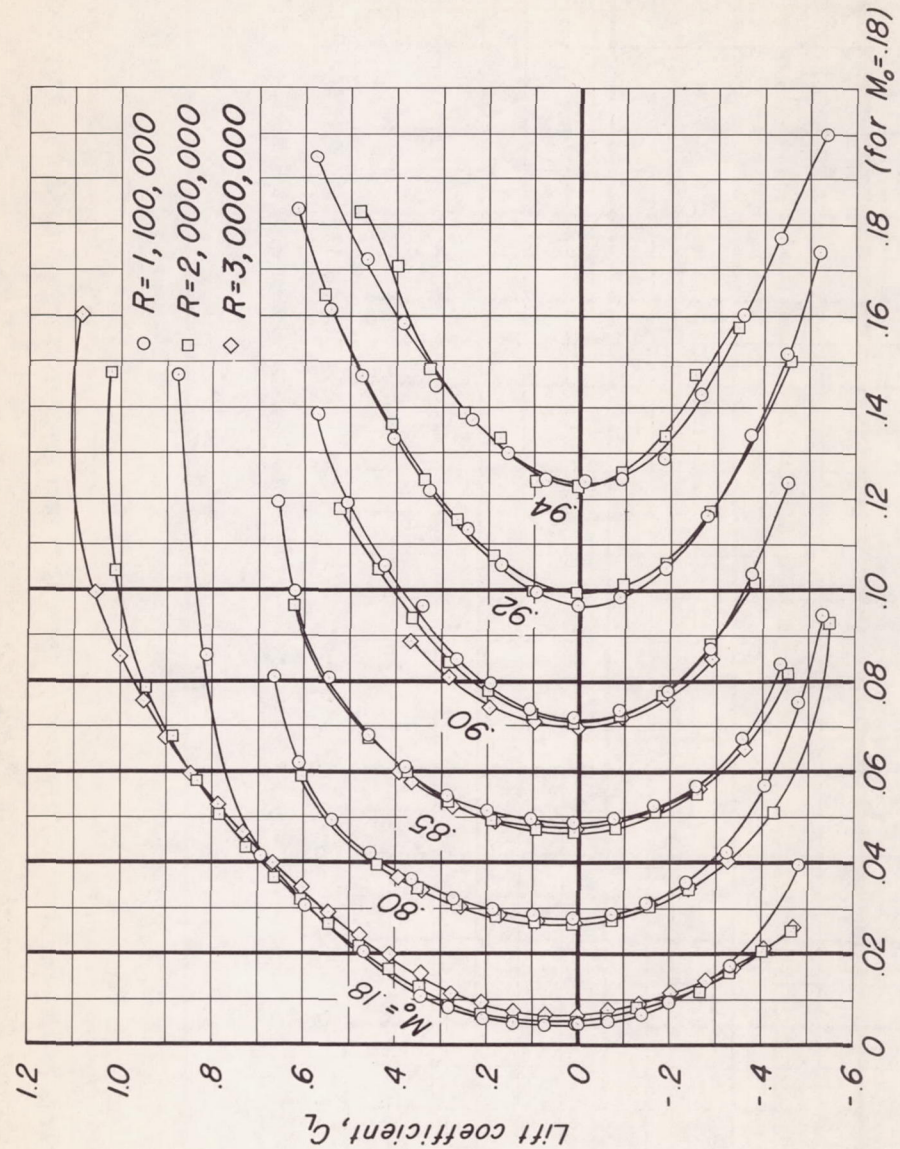

(b) C_L vs C_D.

Figure 12.- Concluded.

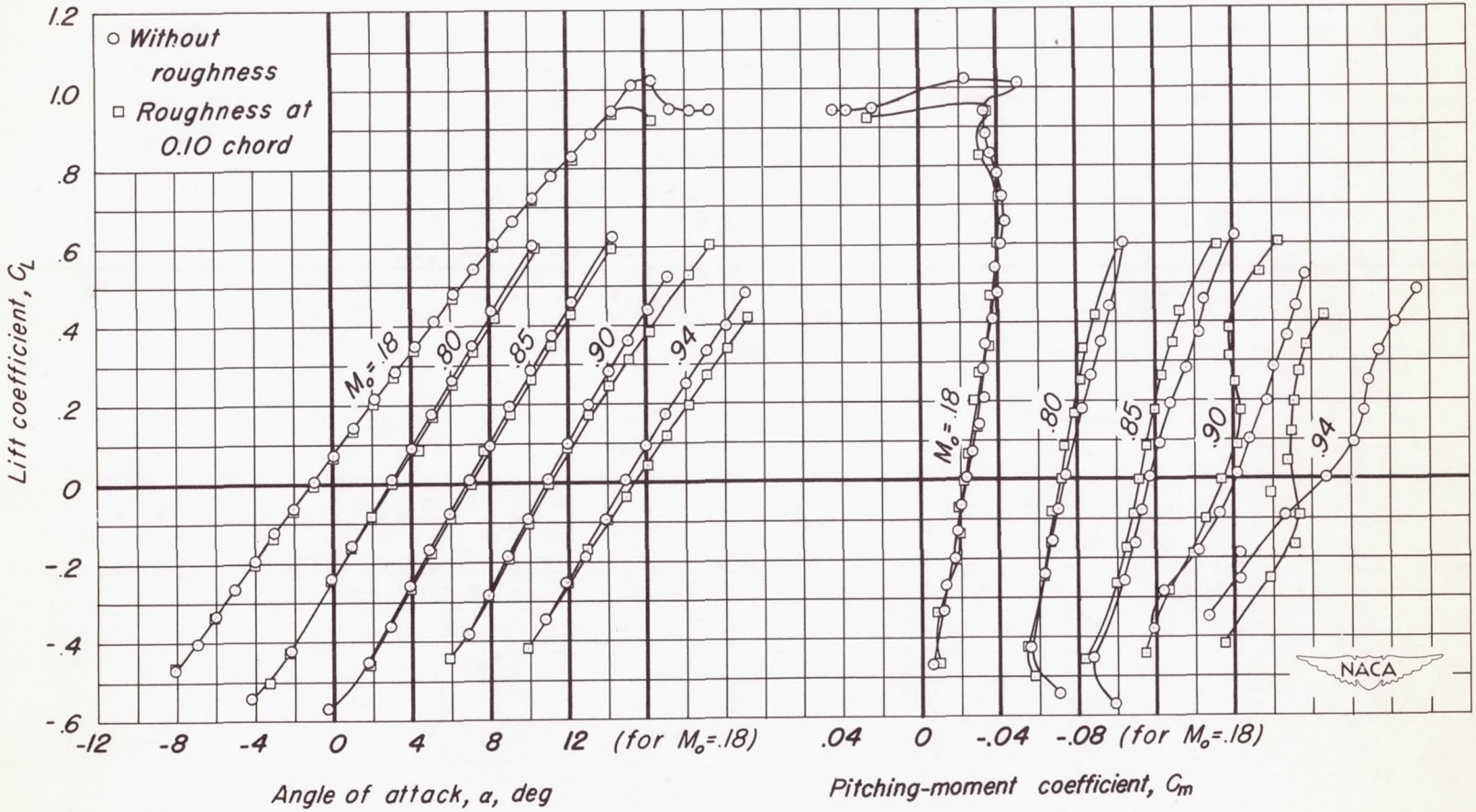

(a) C_L vs α, C_L vs C_m.

Figure 13.- The effects of roughness at 0.10-chord of the upper and lower surfaces on the lift, drag, and pitching-moment coefficients at several Mach numbers. R, 2,000,000.

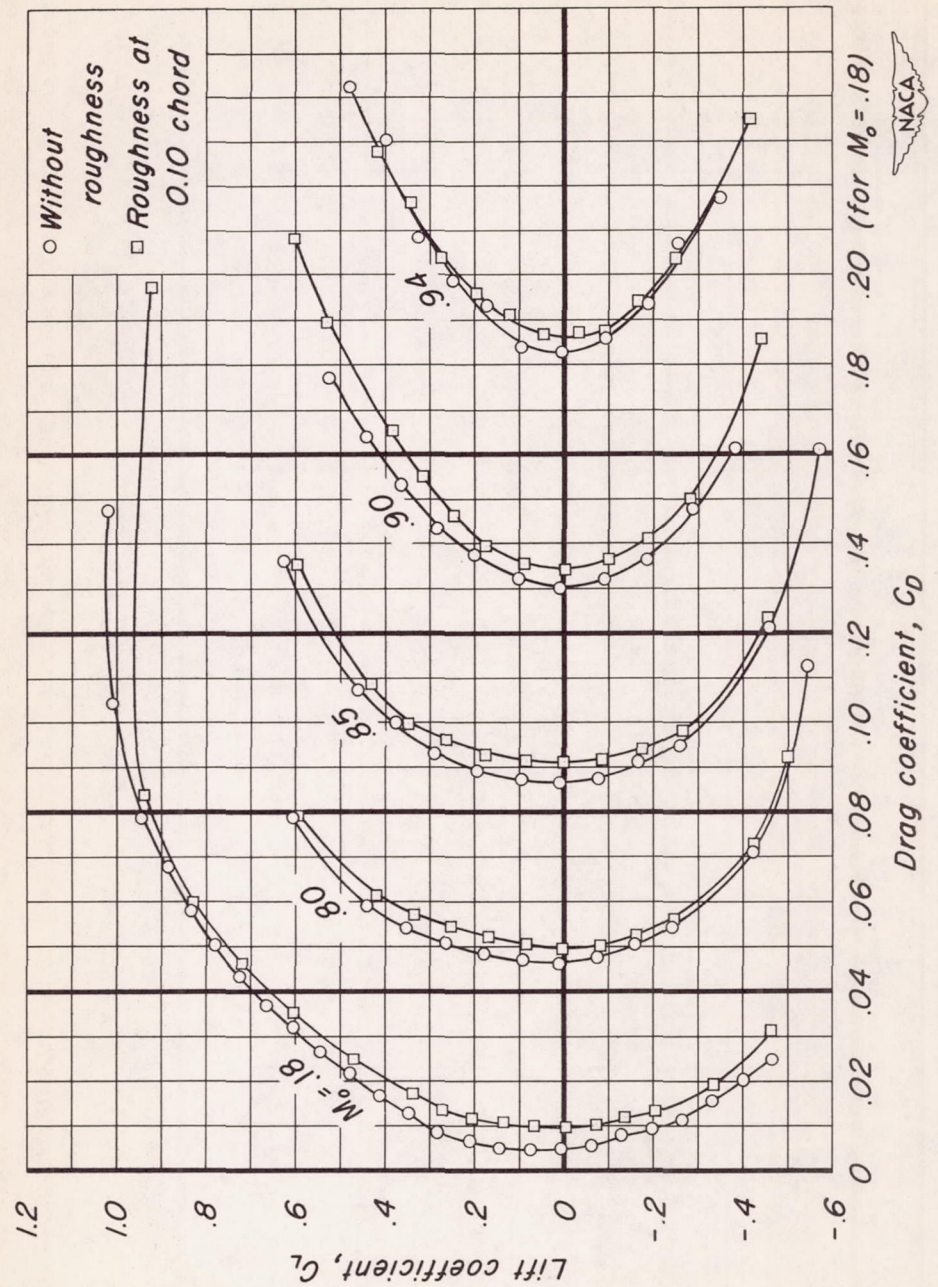

(b) C_L vs C_D.

Figure 13.– Concluded.

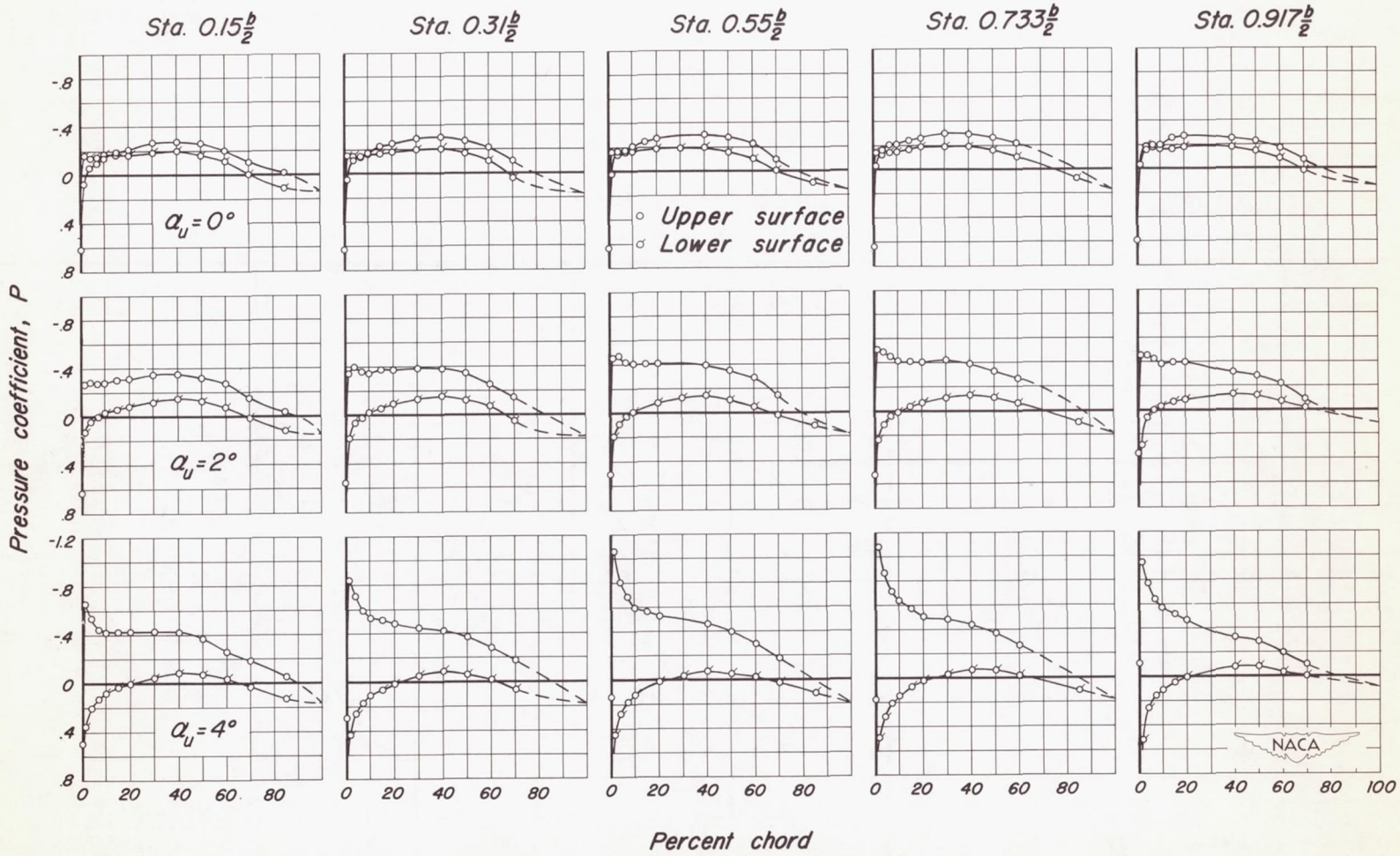

(a) M_o, 0.18 ; α_u, 0°, 2°, 4°.

Figure 14.- The chordwise distribution of pressure coefficient at five semispan stations for several angles of attack. M_o, 0.18; R, 2,000,000.

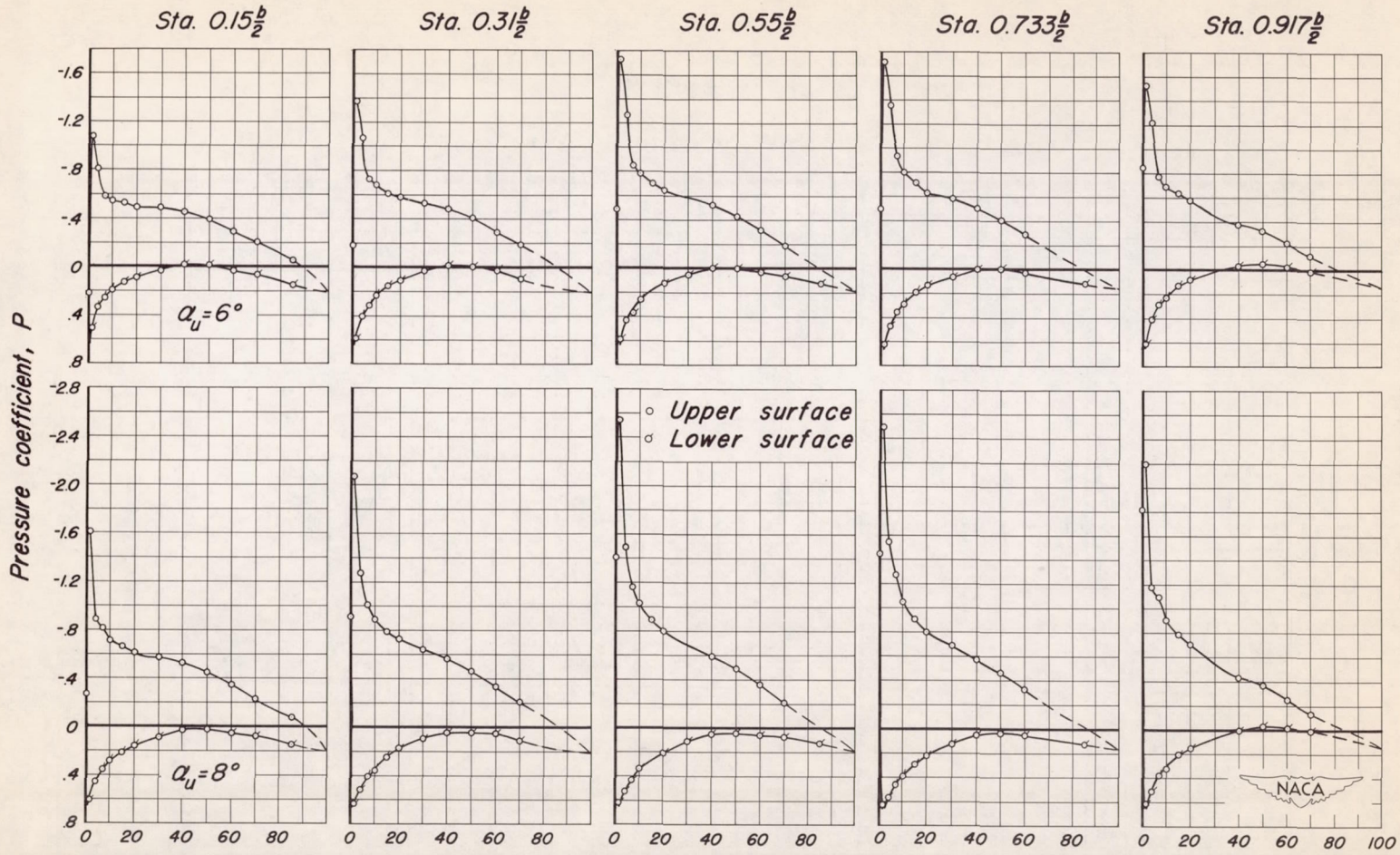

(b) M_o, 0.18 ; α_u, 6°, 8°.

Figure 14.– Continued.

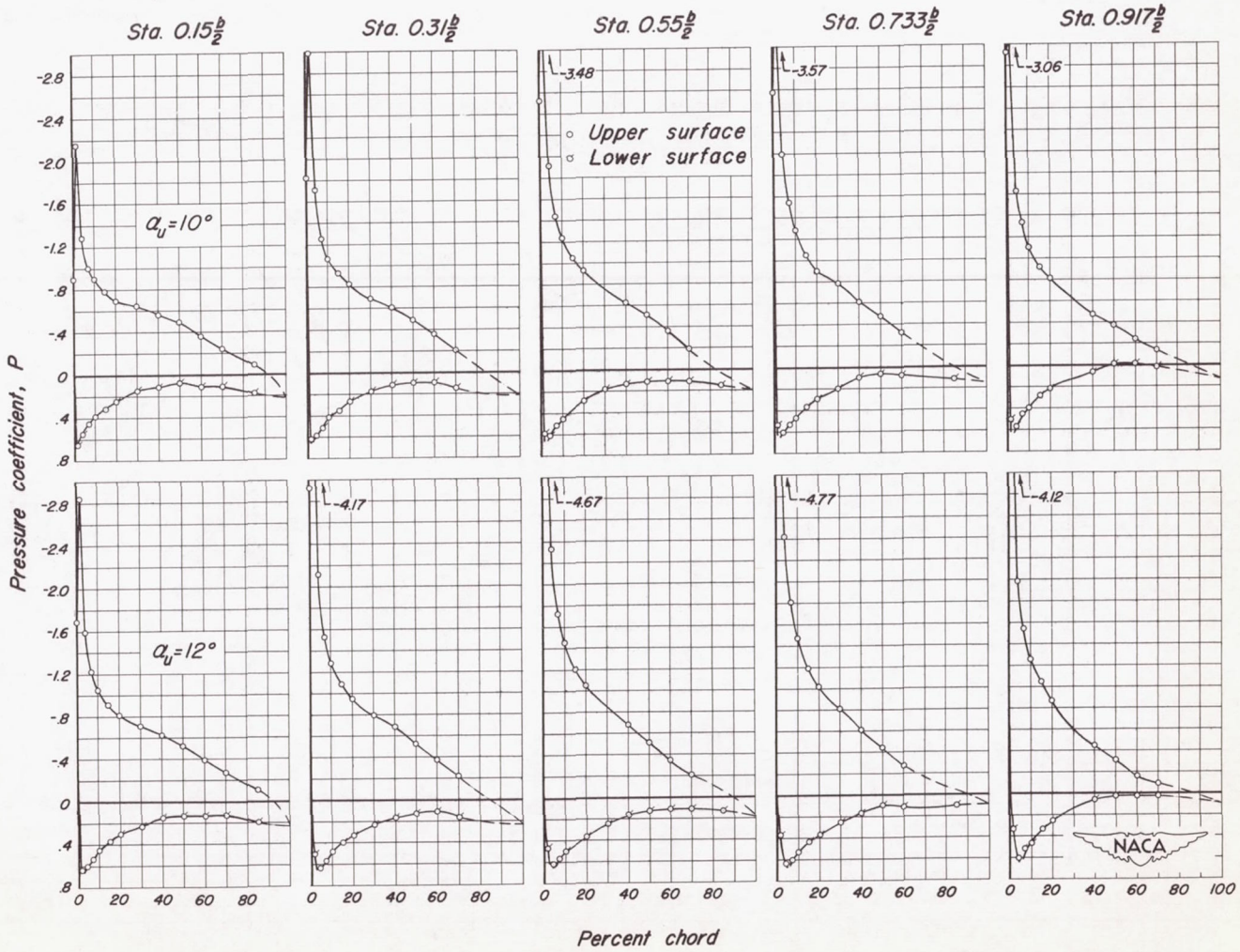

(c) M_o, 0.18 ; α_u, 10°, 12°.

Figure 14.- Continued.

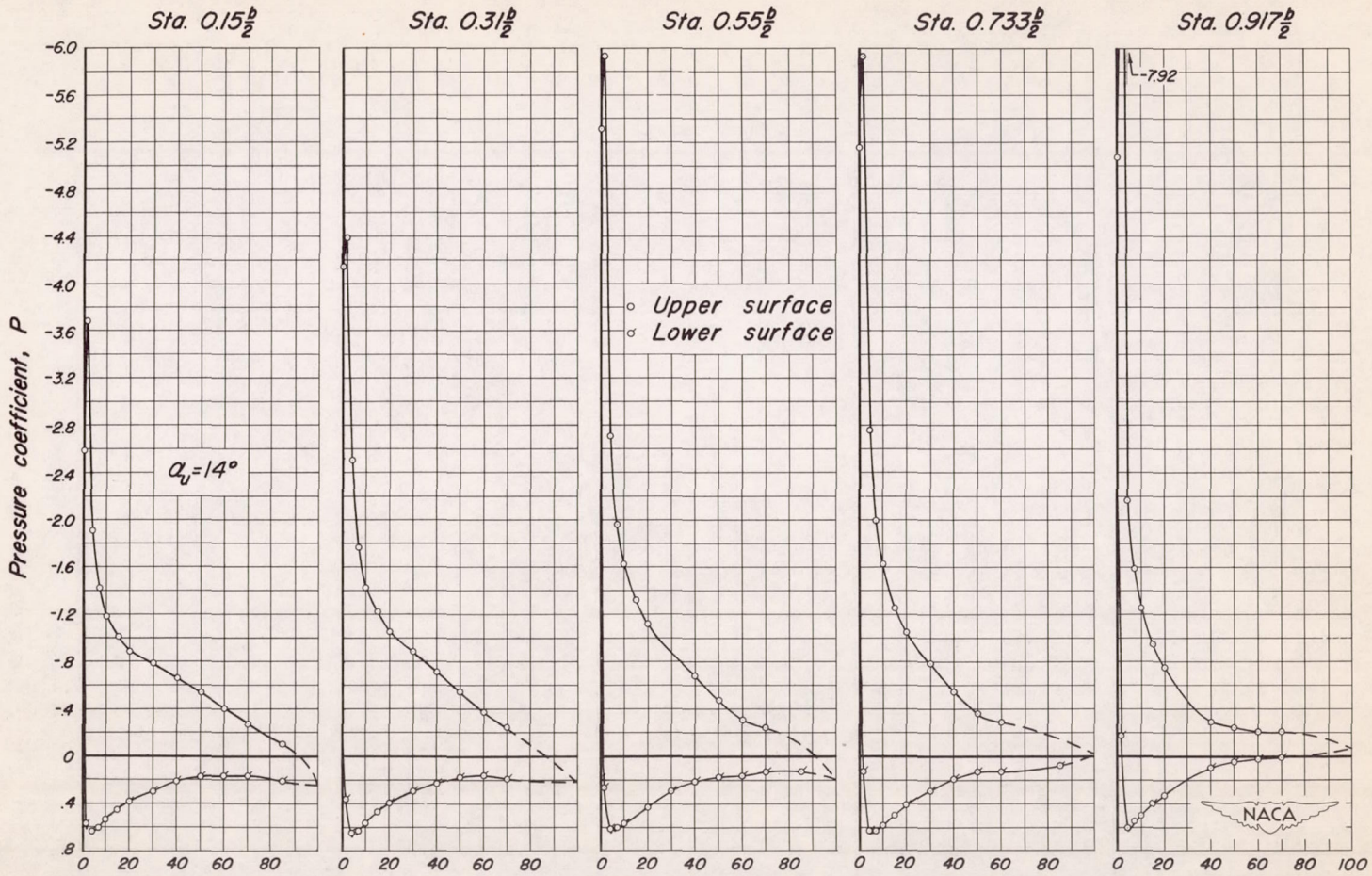

(d) M_o, 0.18 ; α_u, 14°.

Figure 14.- Continued.

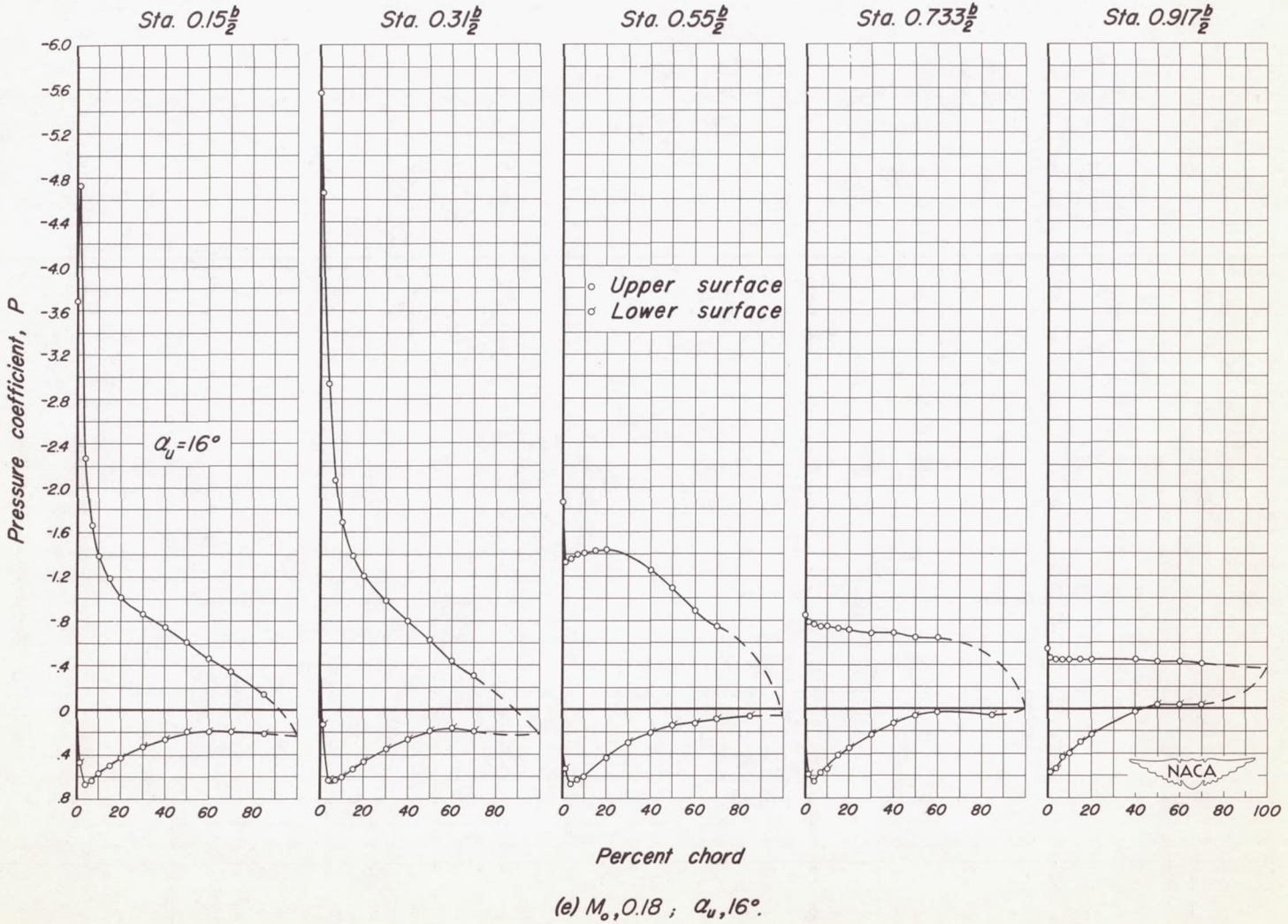

(e) M_o, 0.18 ; α_u, 16°.

Figure 14.- Continued.

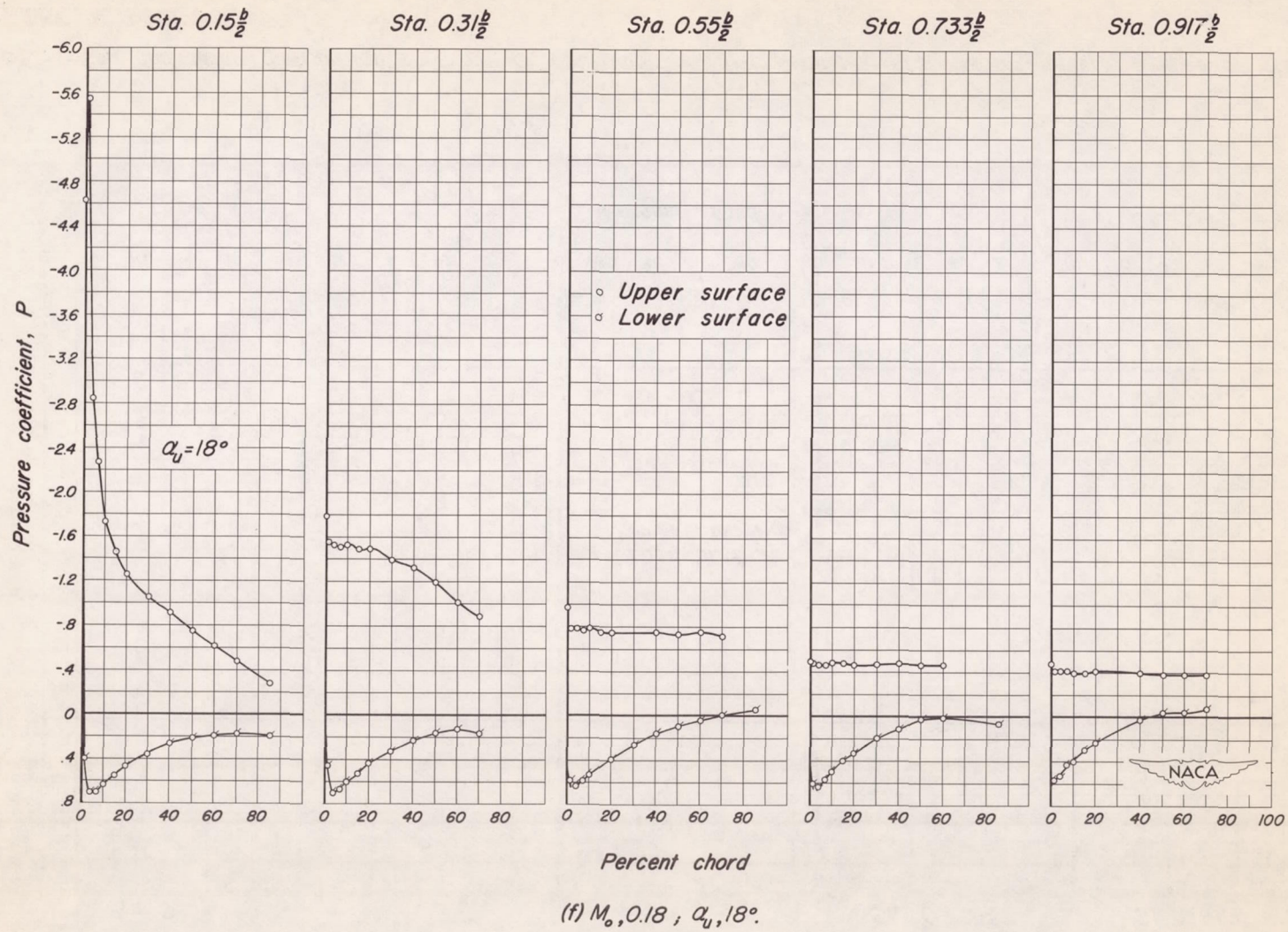

(f) M_o, 0.18 ; α_u, 18°.

Figure 14. - Concluded.

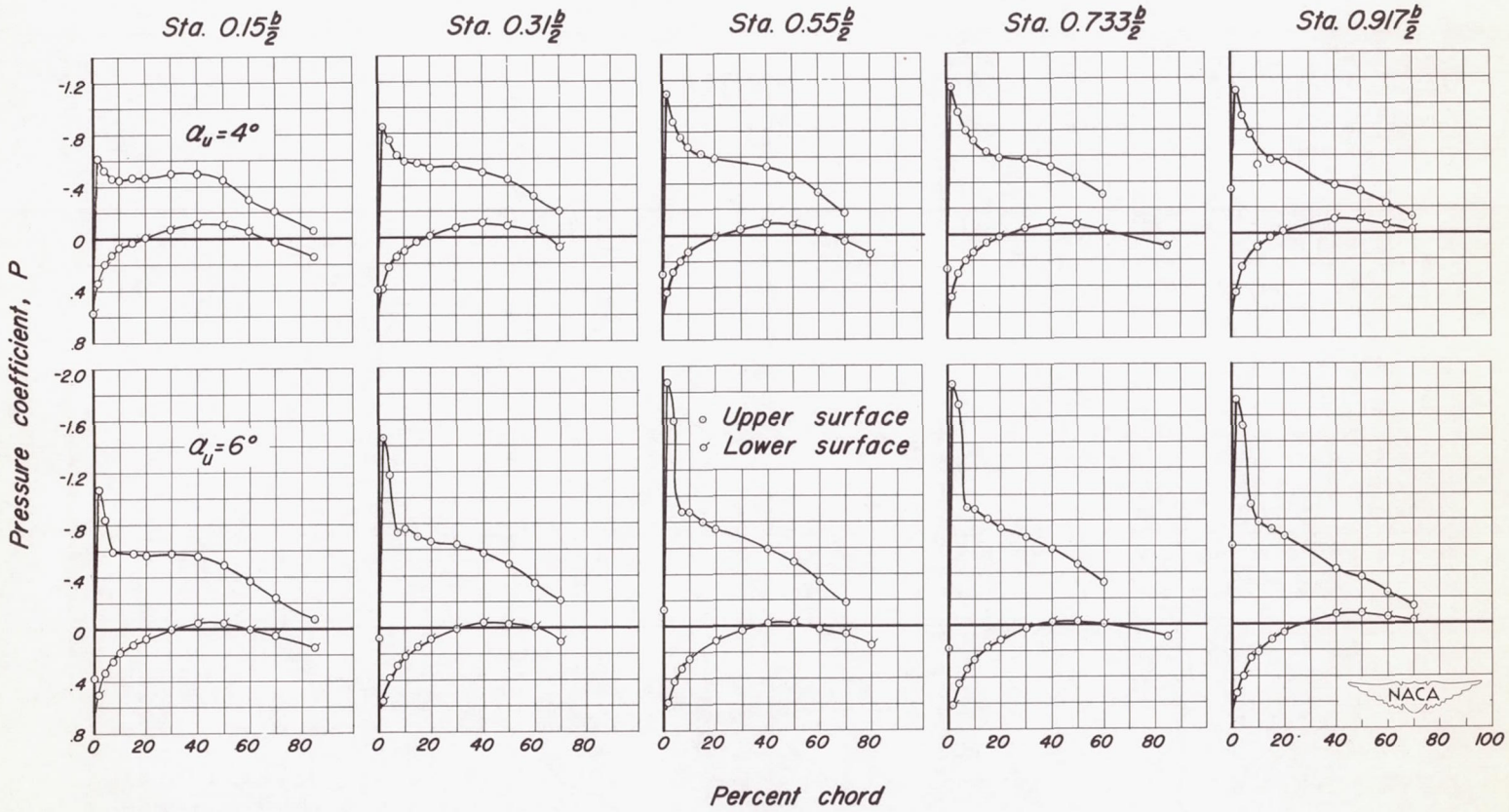

(a) M_o, 0.60; α_u, 4°, 6°.

Figure 15.- The chordwise distribution of pressure coefficient at five semispan stations for several angles of attack. M_o, 0.60; R, 2,000,000.

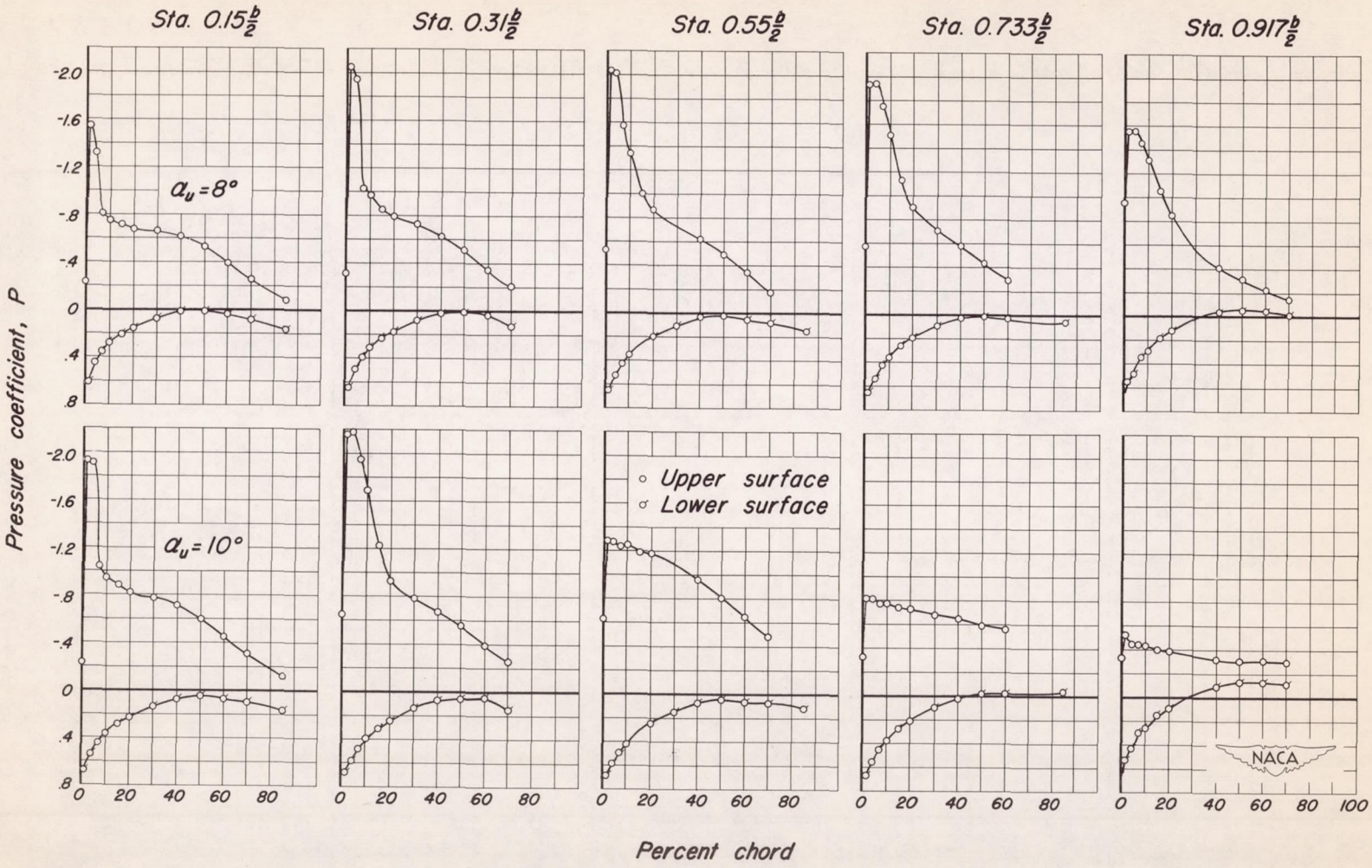

(b) M_o, 0.60; α_u, 8°, 10°.

Figure 15.- Concluded.

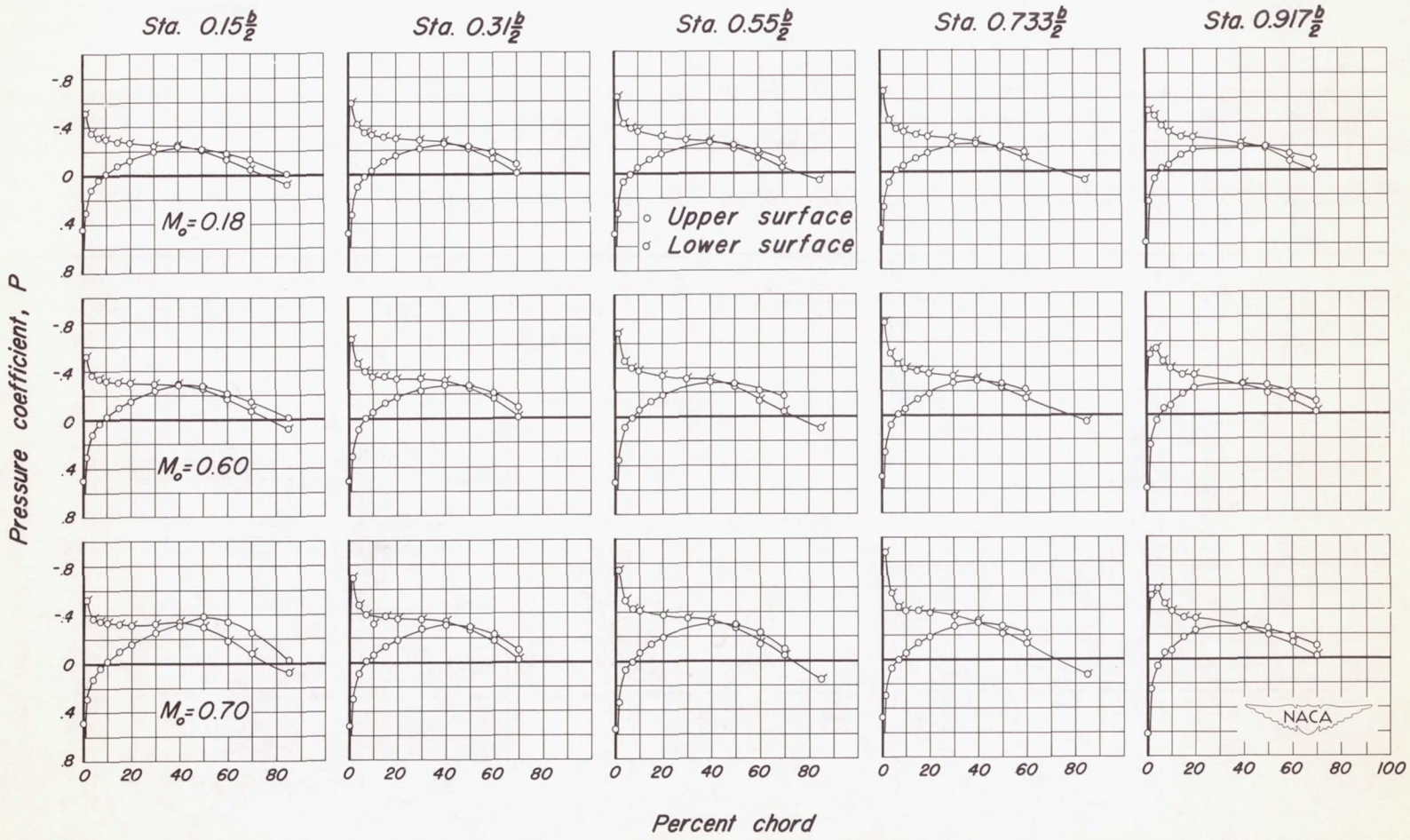

(a) α_u, -2°; M_o, 0.18, 0.60, 0.70.

Figure 16.- The chordwise distribution of pressure coefficient at five semispan stations for several Mach numbers. α_u, -2°; R, 2,000,000.

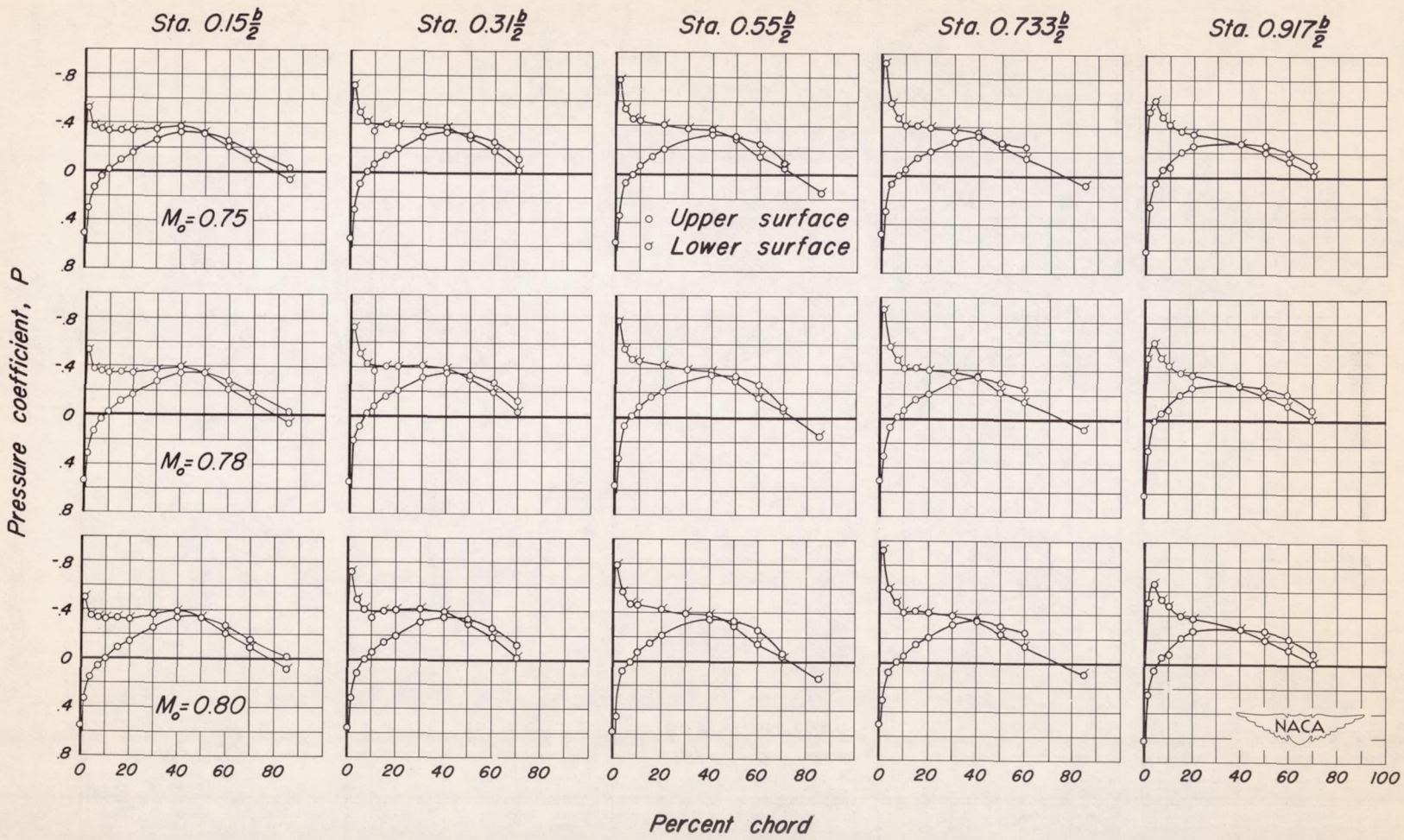

(b) α_u, -2°; M_o, 0.75, 0.78, 0.80.

Figure 16.- Continued.

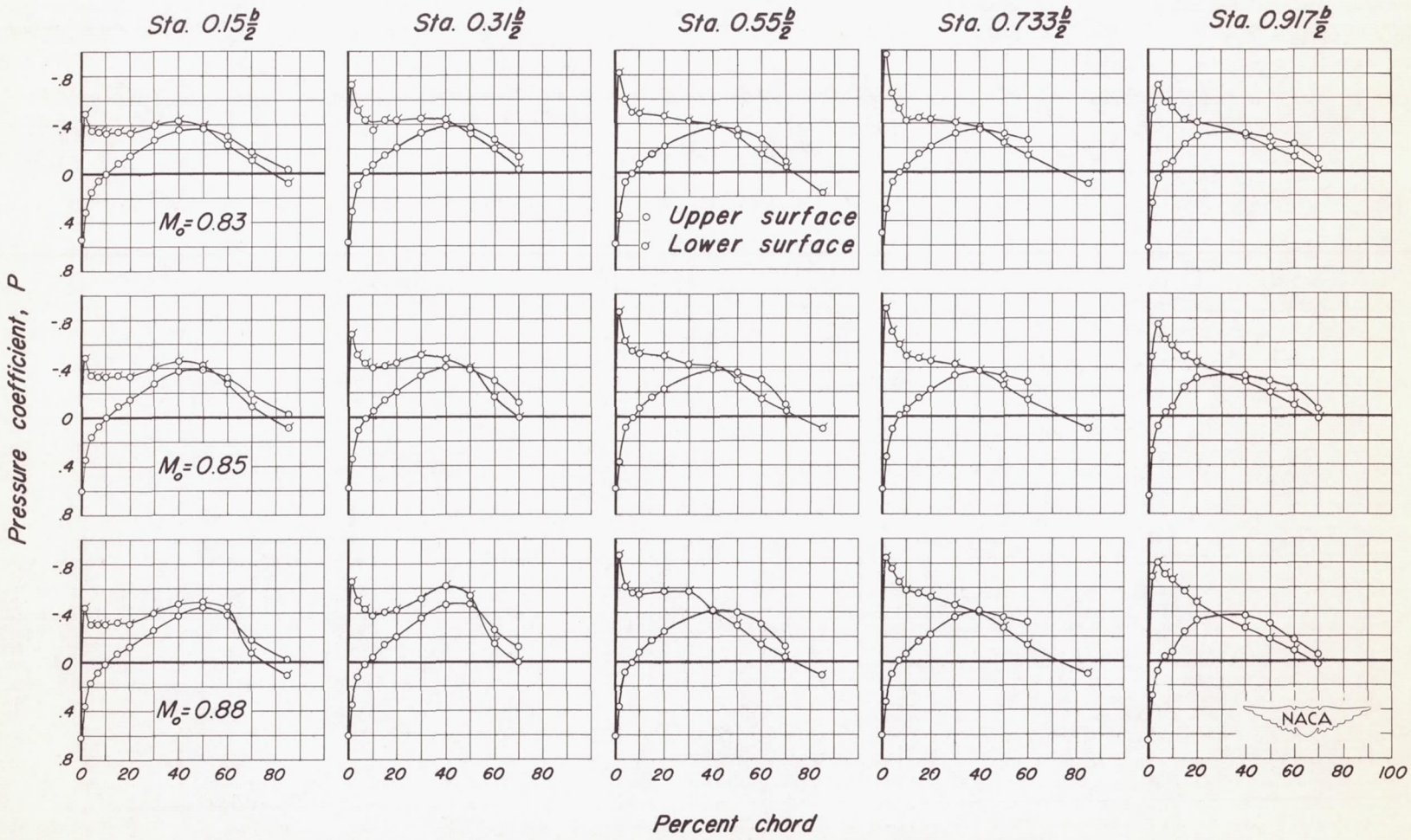

(c) α_u, -2° ; M_o, 0.83, 0.85, 0.88.

Figure 16.- Continued.

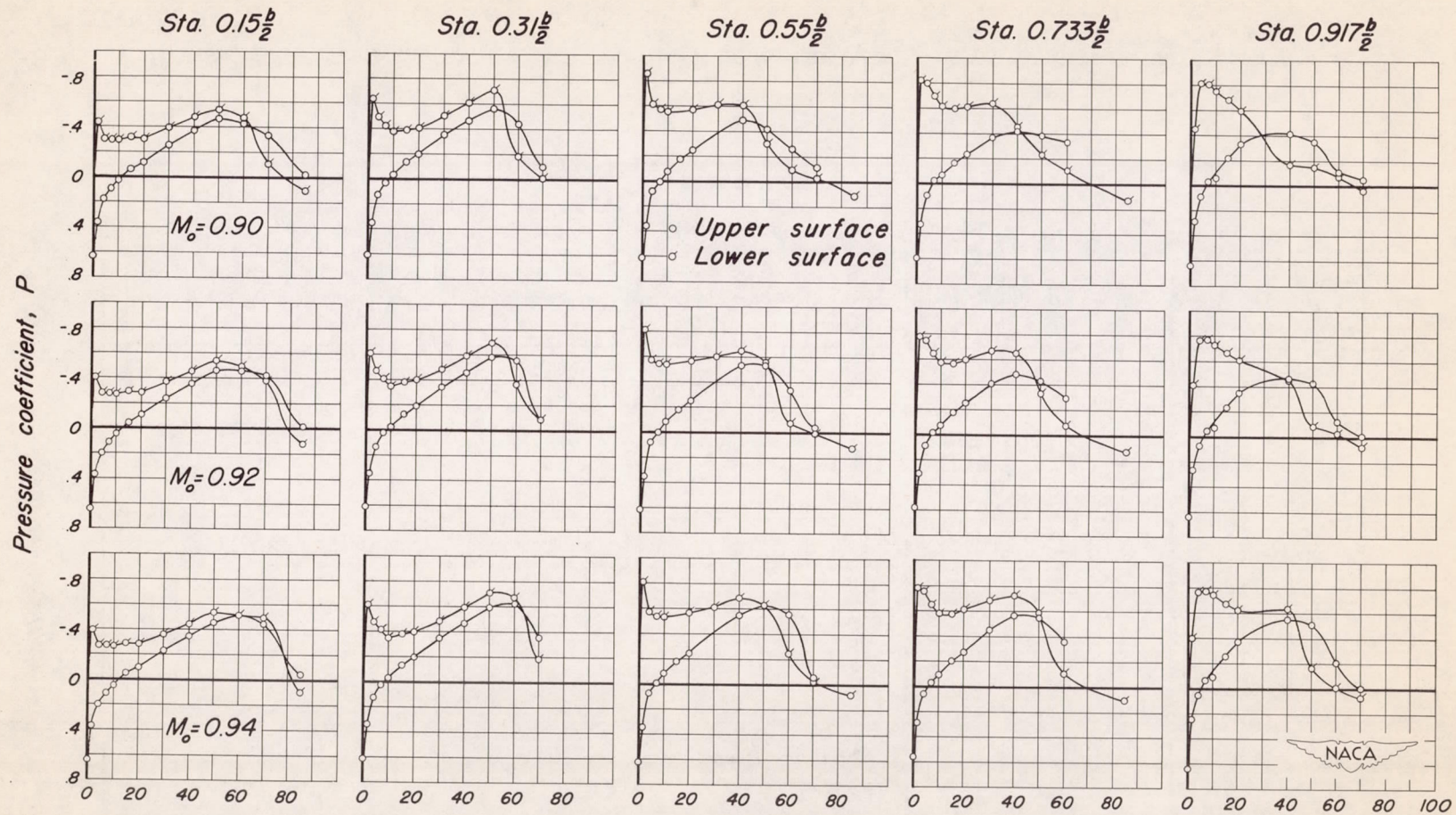

(d) α_u, -2° ; M_o, 0.90, 0.92, 0.94.

Figure 16.- Concluded.

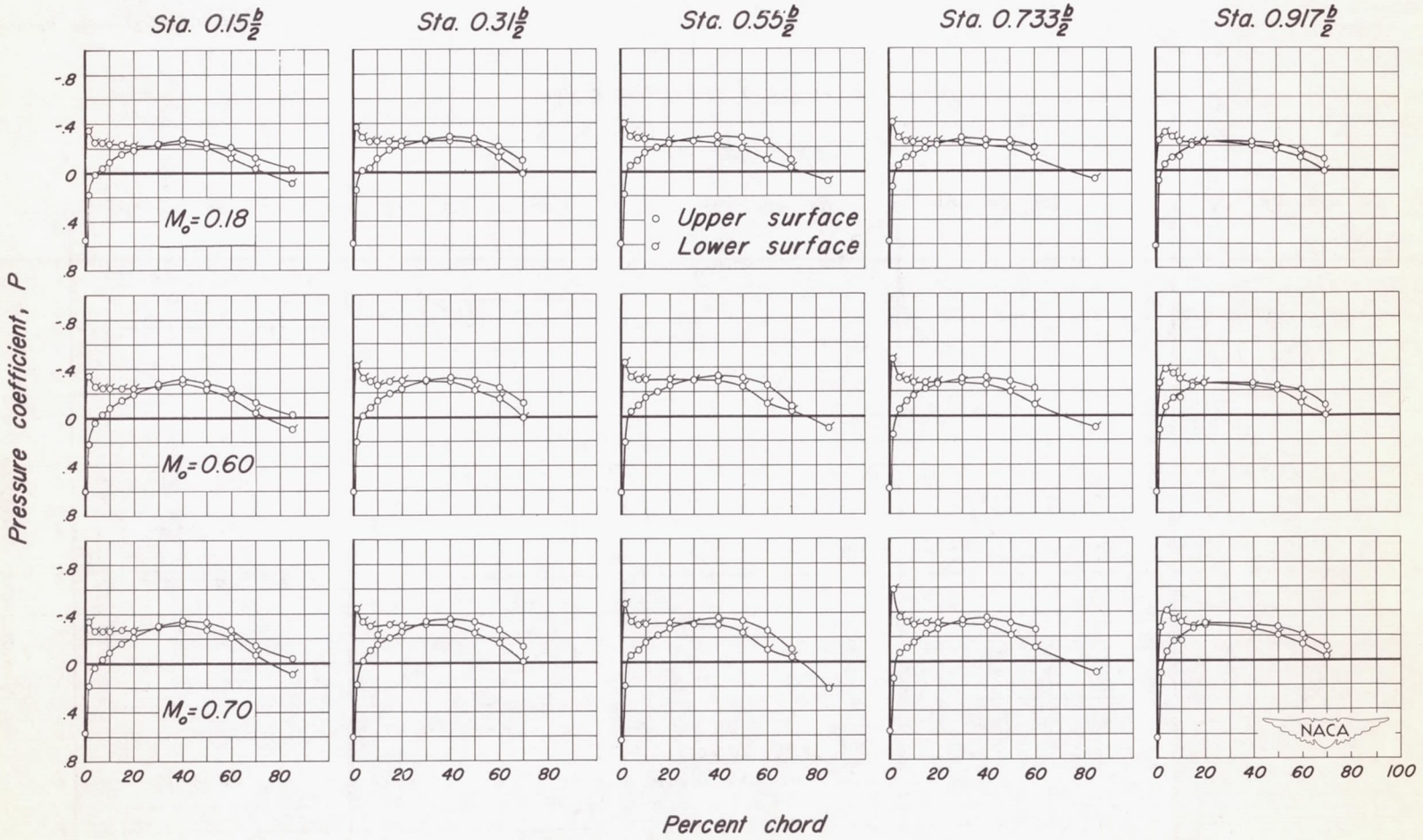

(a) α_u, -1° ; M_o, 0.18, 0.60, 0.70.

Figure 17.- The chordwise distribution of pressure coefficient at five semispan stations for several Mach numbers. α_u, -1°; R, 2,000,000.

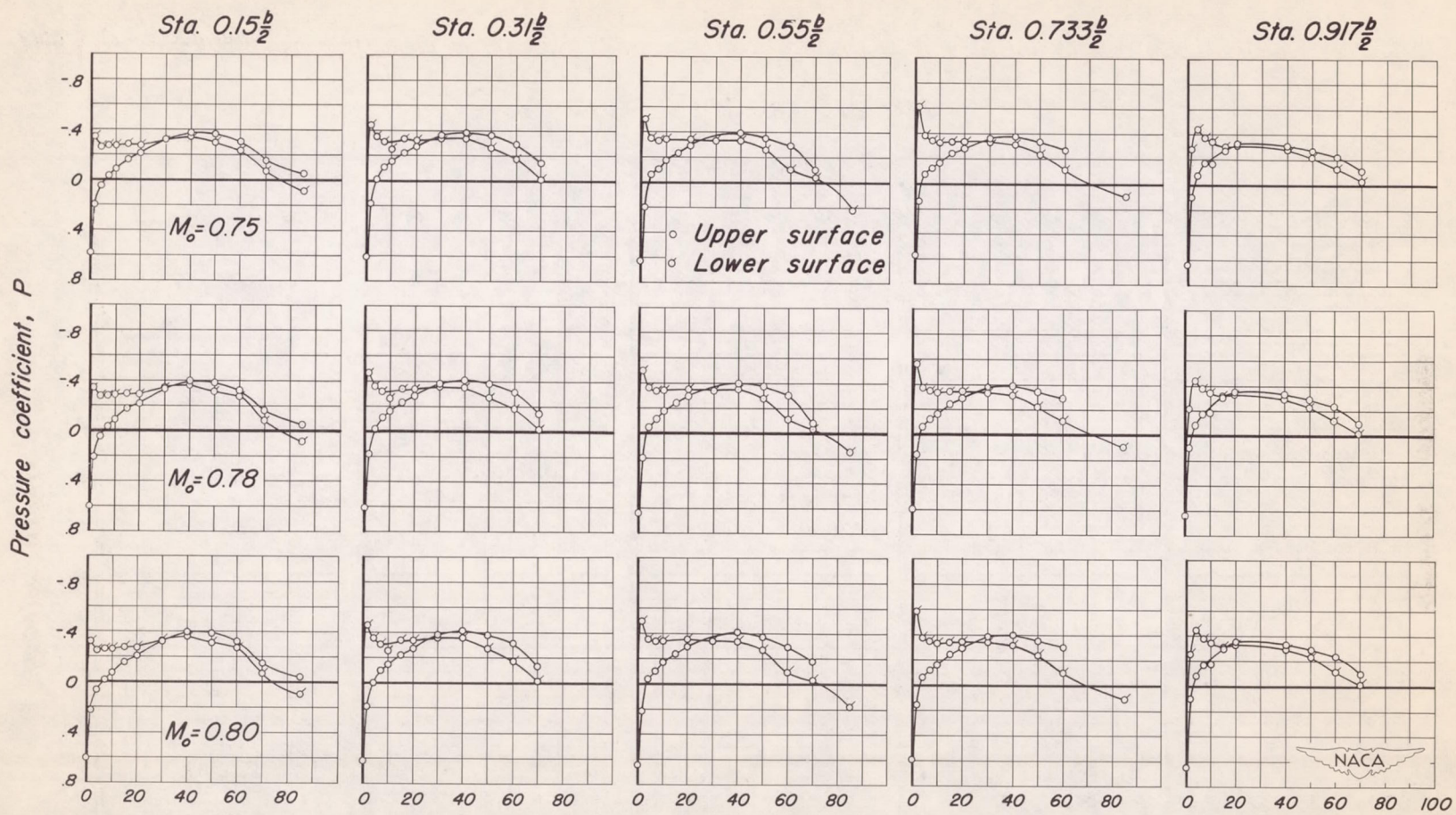

(b) α_u, -1° ; M_o, 0.75, 0.78, 0.80.

Figure 17.- Continued.

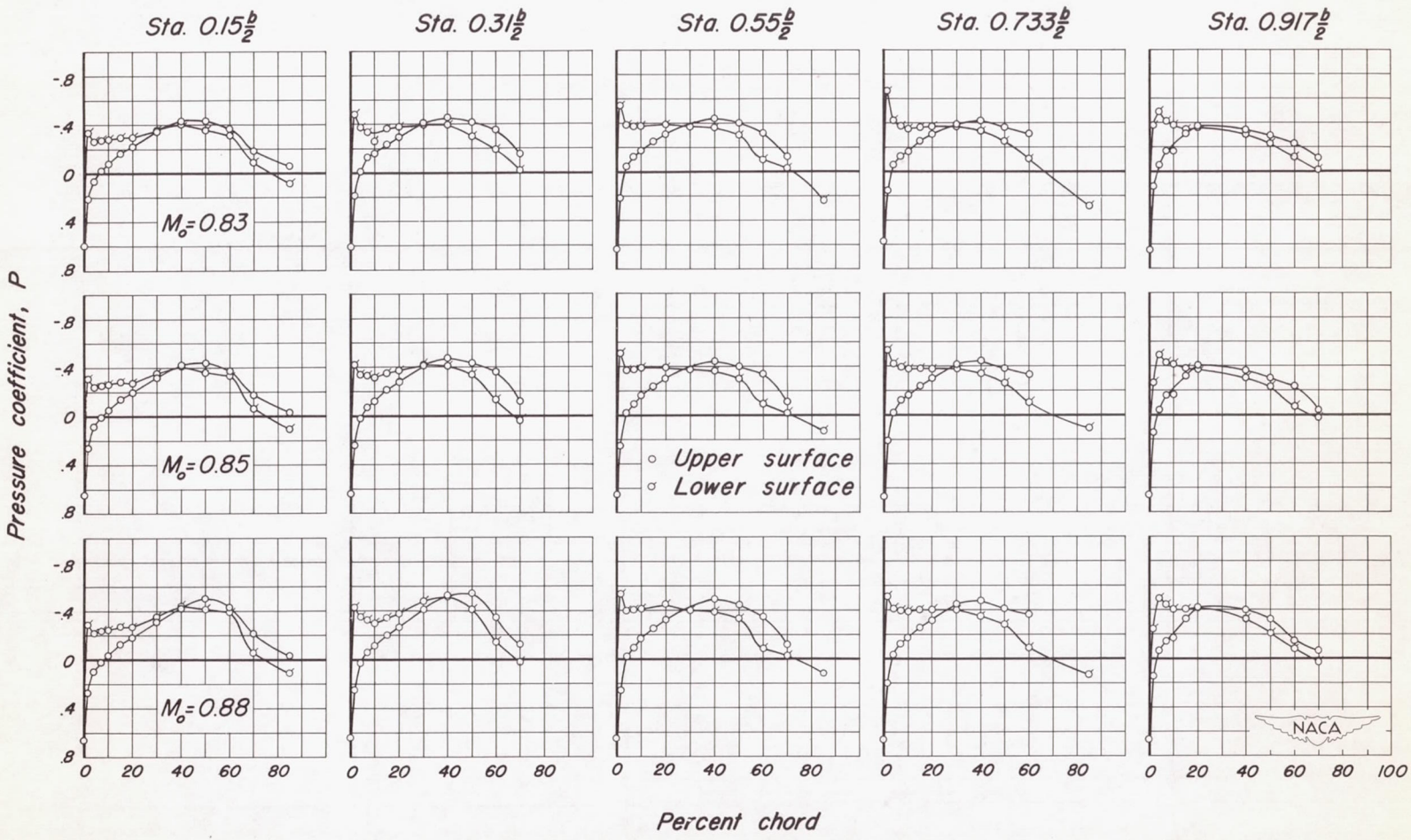

(c) α_u, -1° ; M_o, 0.83, 0.85, 0.88.

Figure 17.- Continued.

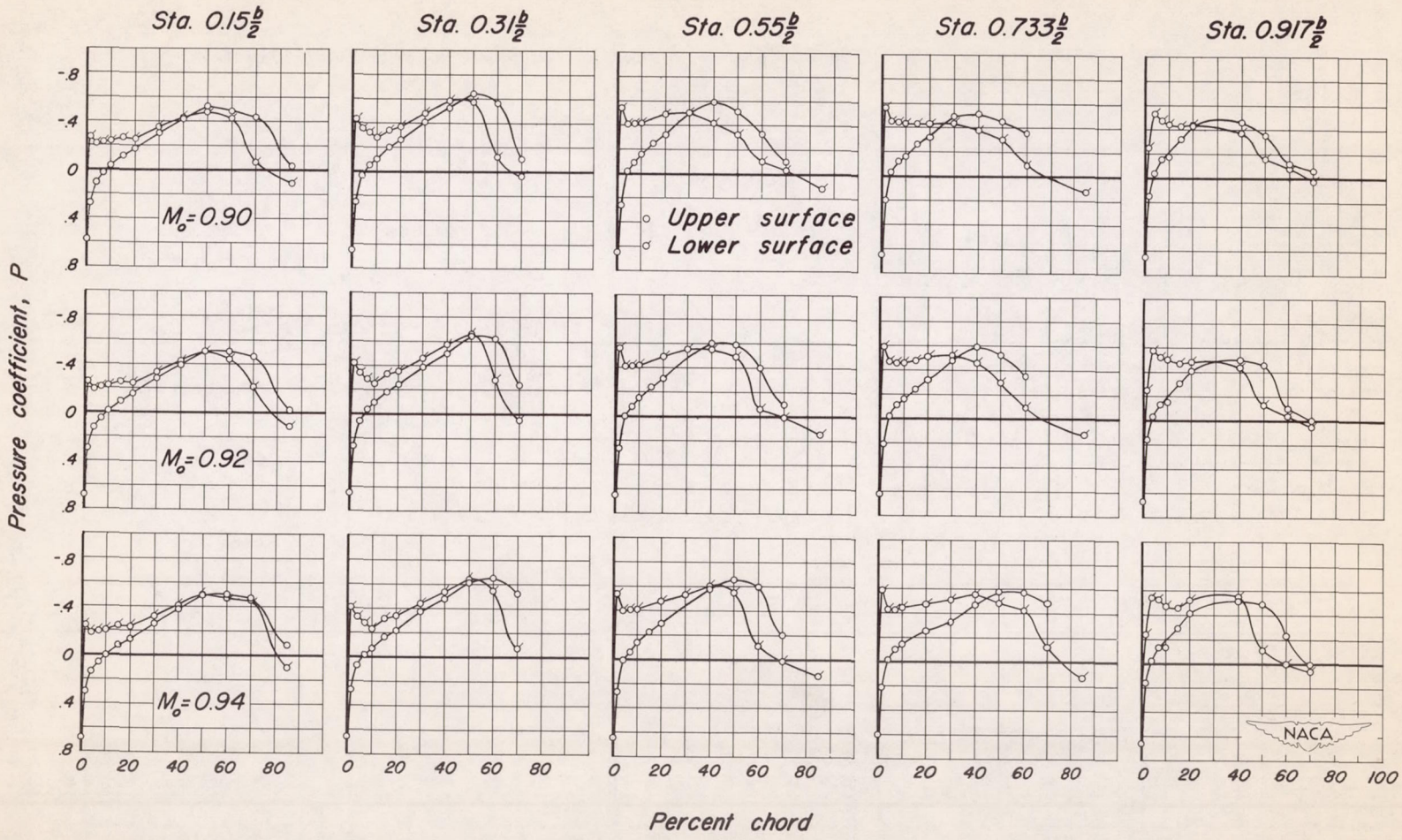

(d) α_u, -1° ; M_o, 0.90, 0.92, 0.94.

Figure 17.- Concluded.

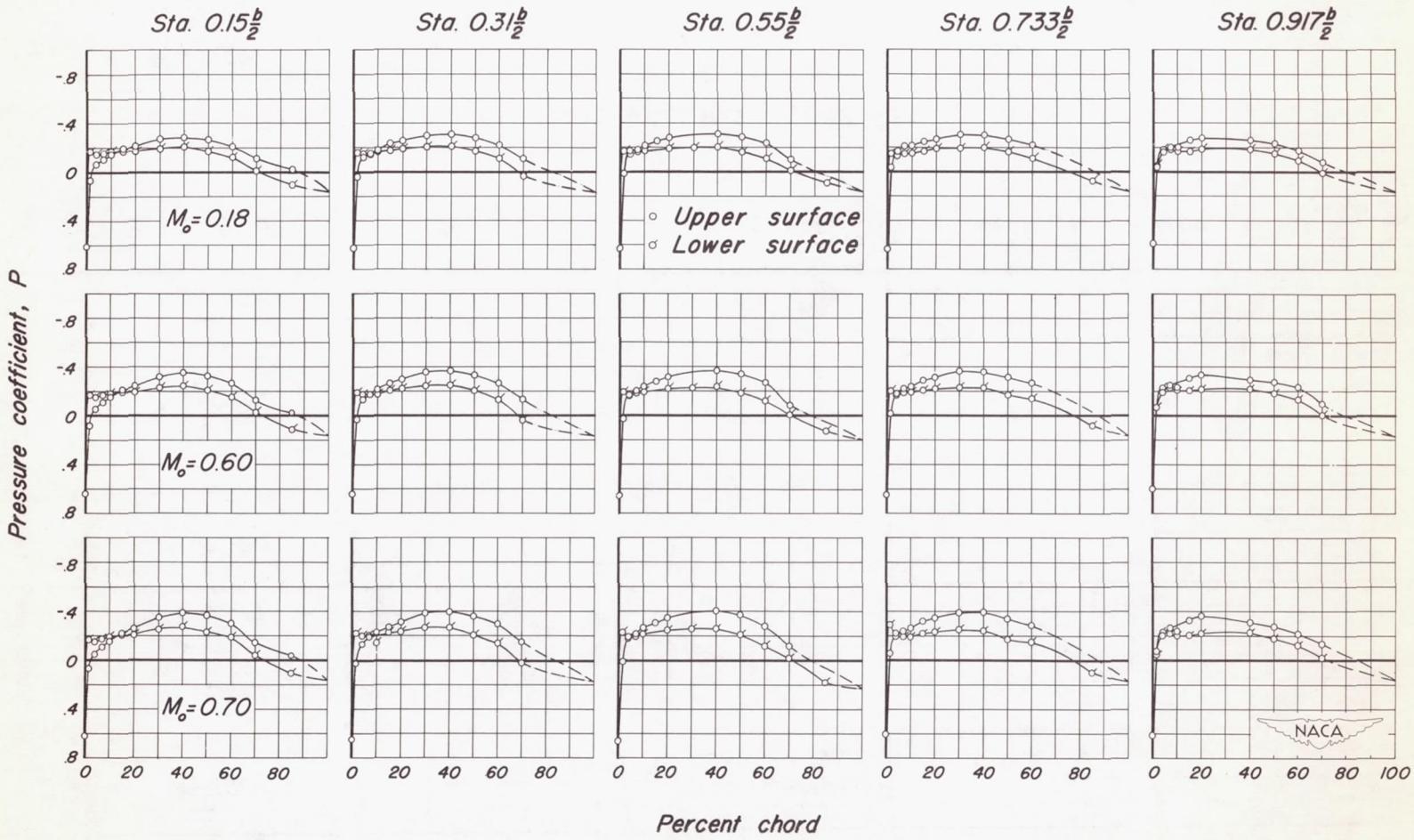

(a) α_u, 0° ; M_o, 0.18, 0.60, 0.70.

Figure 18.– The chordwise distribution of pressure coefficient at five semispan stations for several Mach numbers. α_u, 0°; R, 2,000,000.

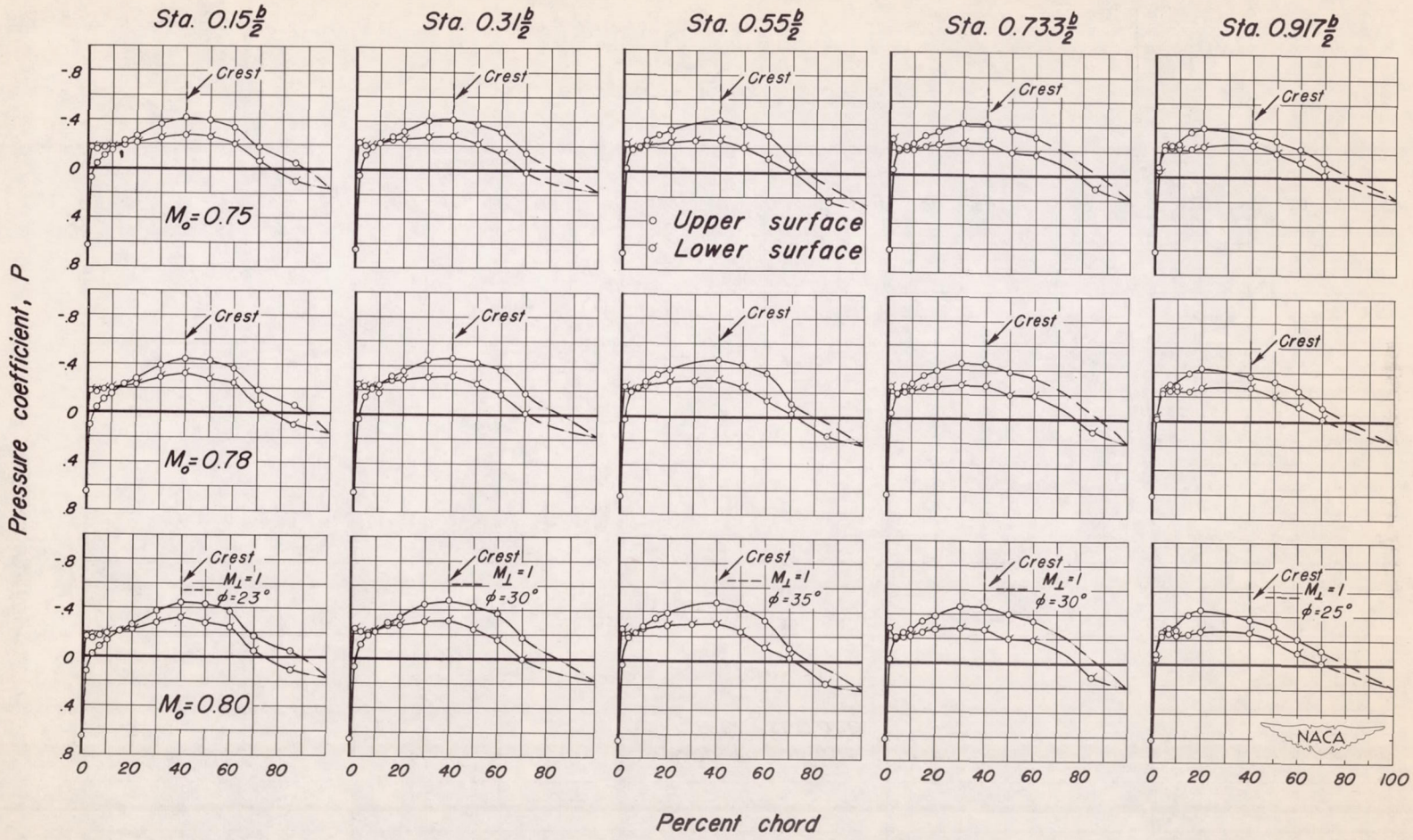

(b) α_u, 0° ; M_o, 0.75, 0.78, 0.80.

Figure 18.- Continued.

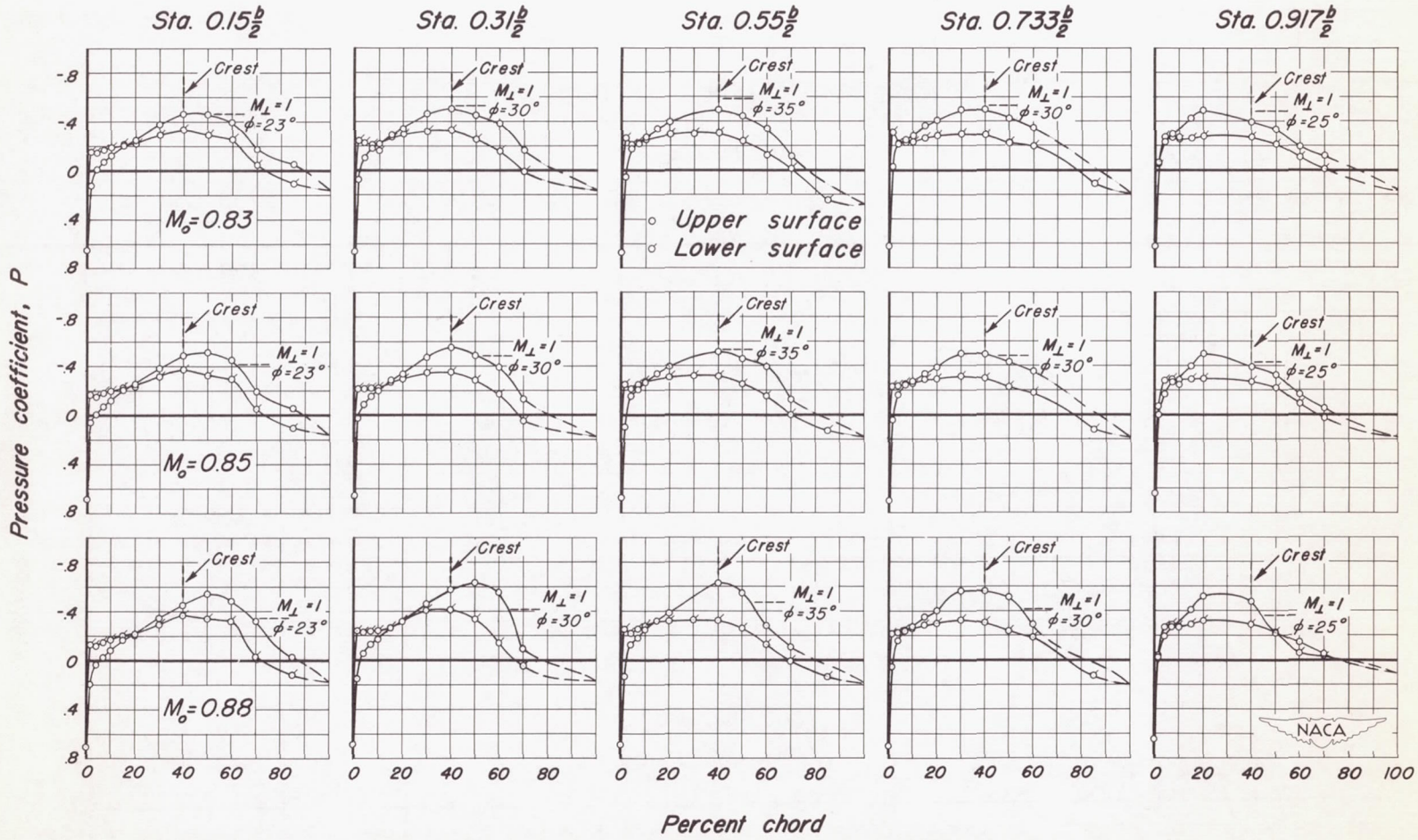

(c) α_u, 0° ; M_o, 0.83, 0.85, 0.88.

Figure 18.- Continued.

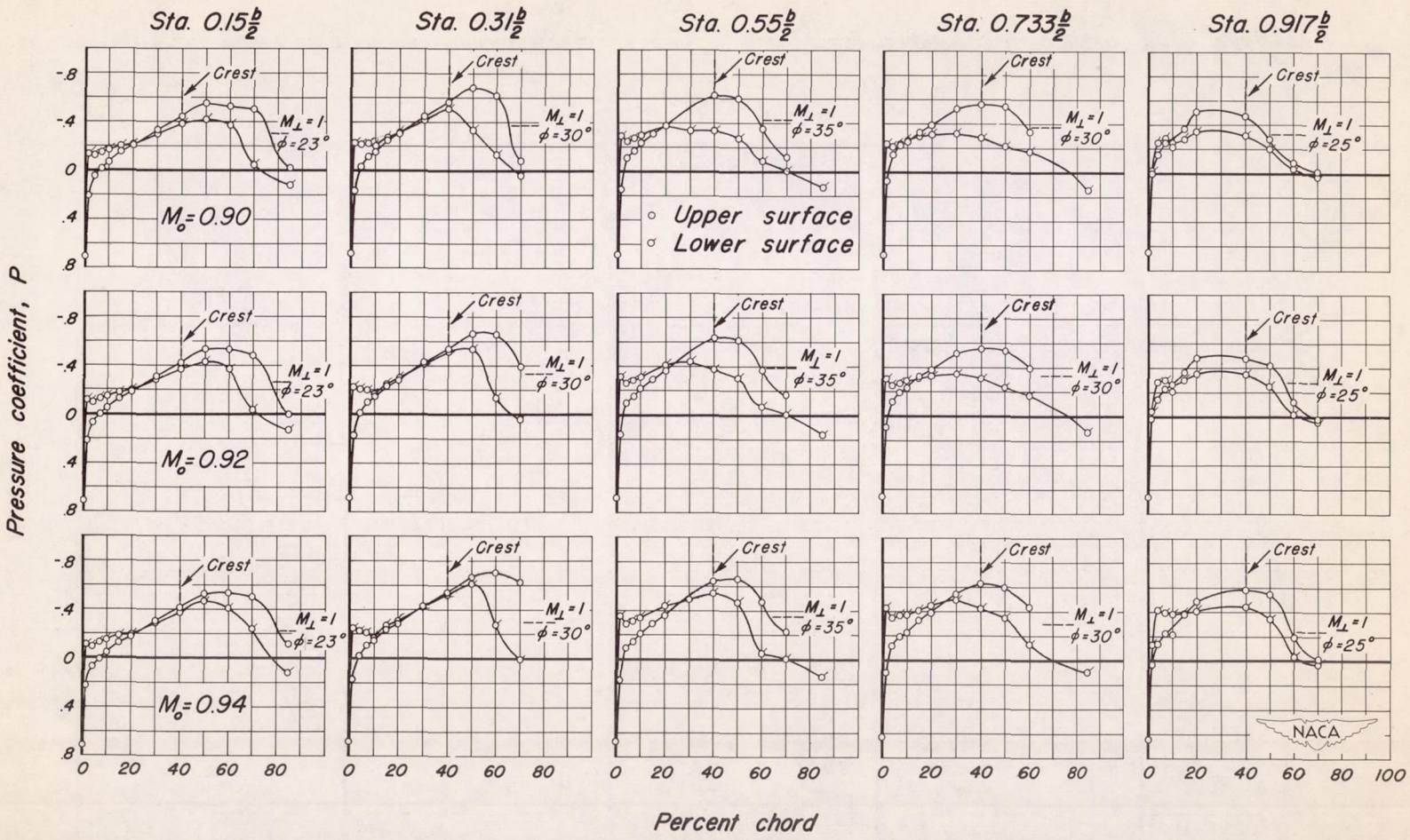

(d) α_u, 0° ; M_o, 0.90, 0.92, 0.94.

Figure 18.- Concluded.

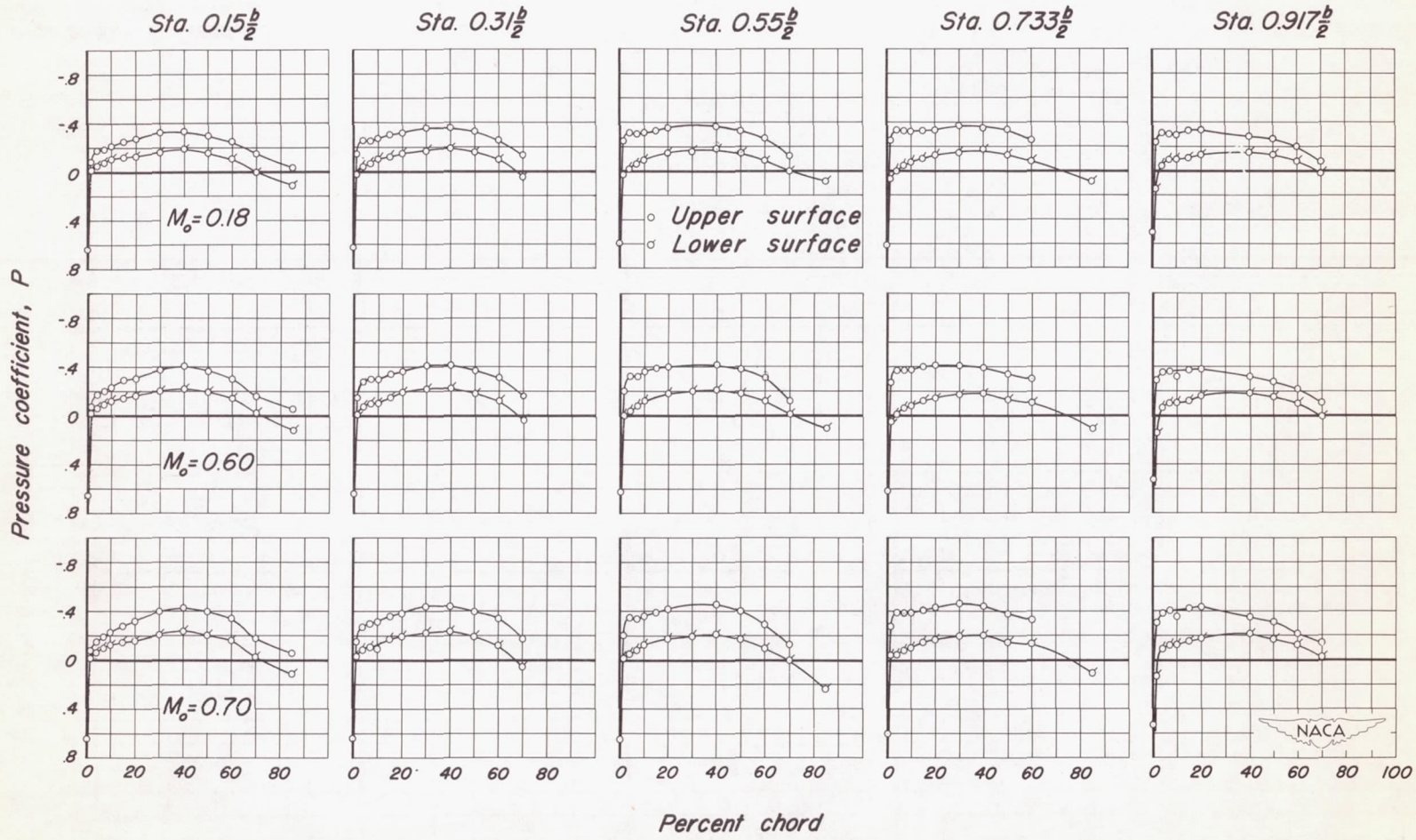

(a) α_u, 1°; M_o, 0.18, 0.60, 0.70.

Figure 19.– The chordwise distribution of pressure coefficient at five semispan stations for several Mach numbers. α_u, 1°; R, 2,000,000.

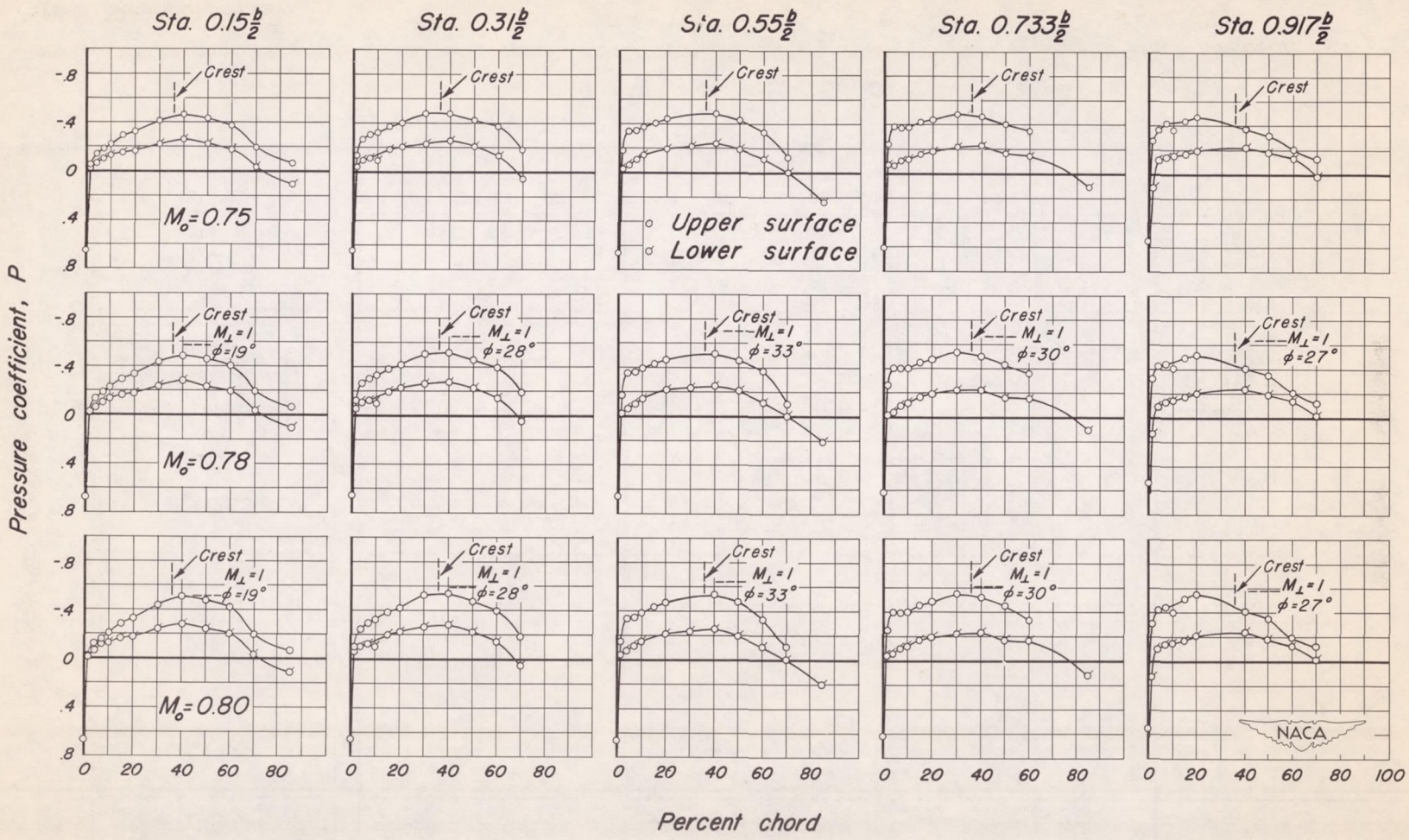

(b) α_u, 1° ; M_o, 0.75, 0.78, 0.80.

Figure 19.– Continued.

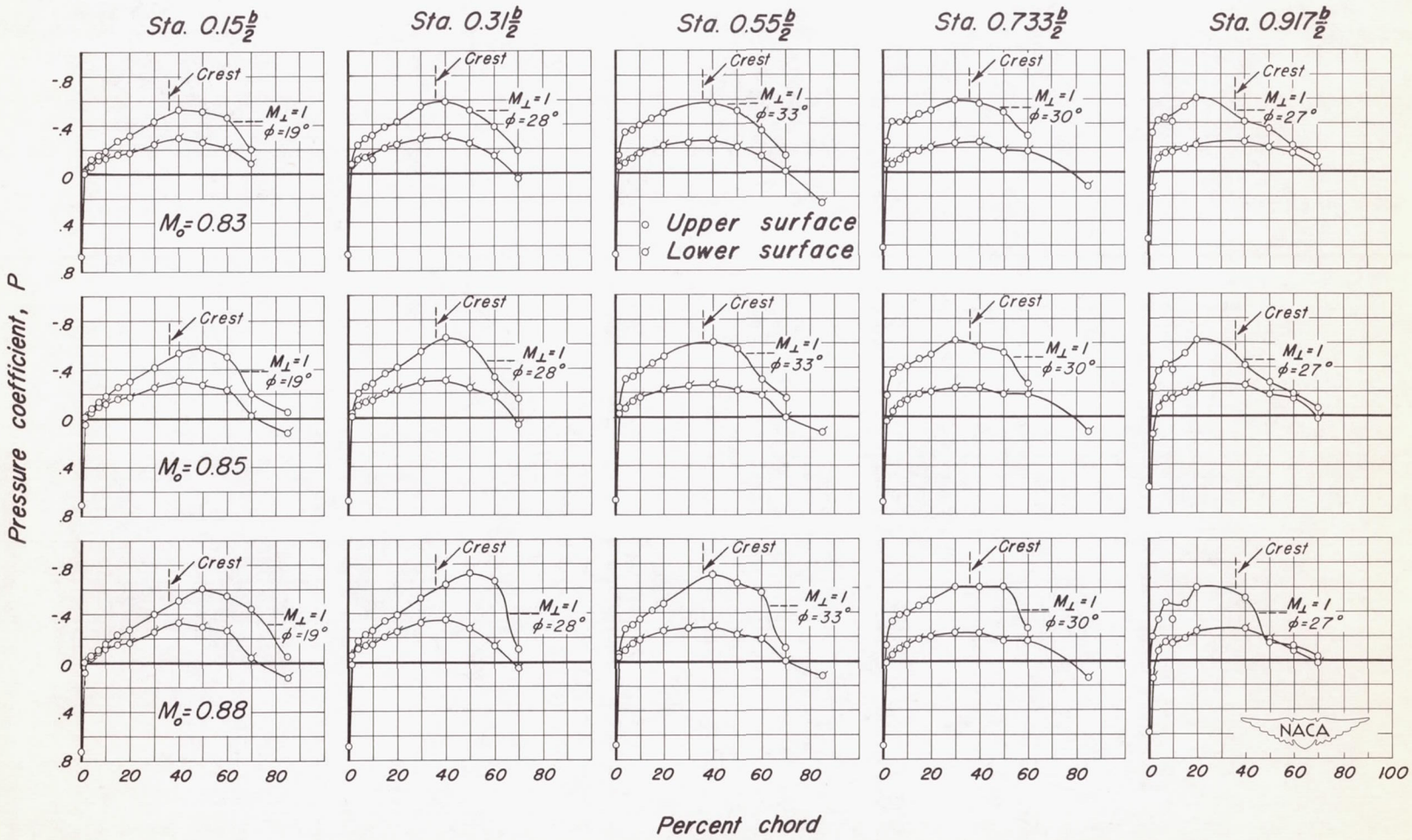

(c) α_u, 1° ; M_o, 0.83, 0.85, 0.88.

Figure 19.- Continued.

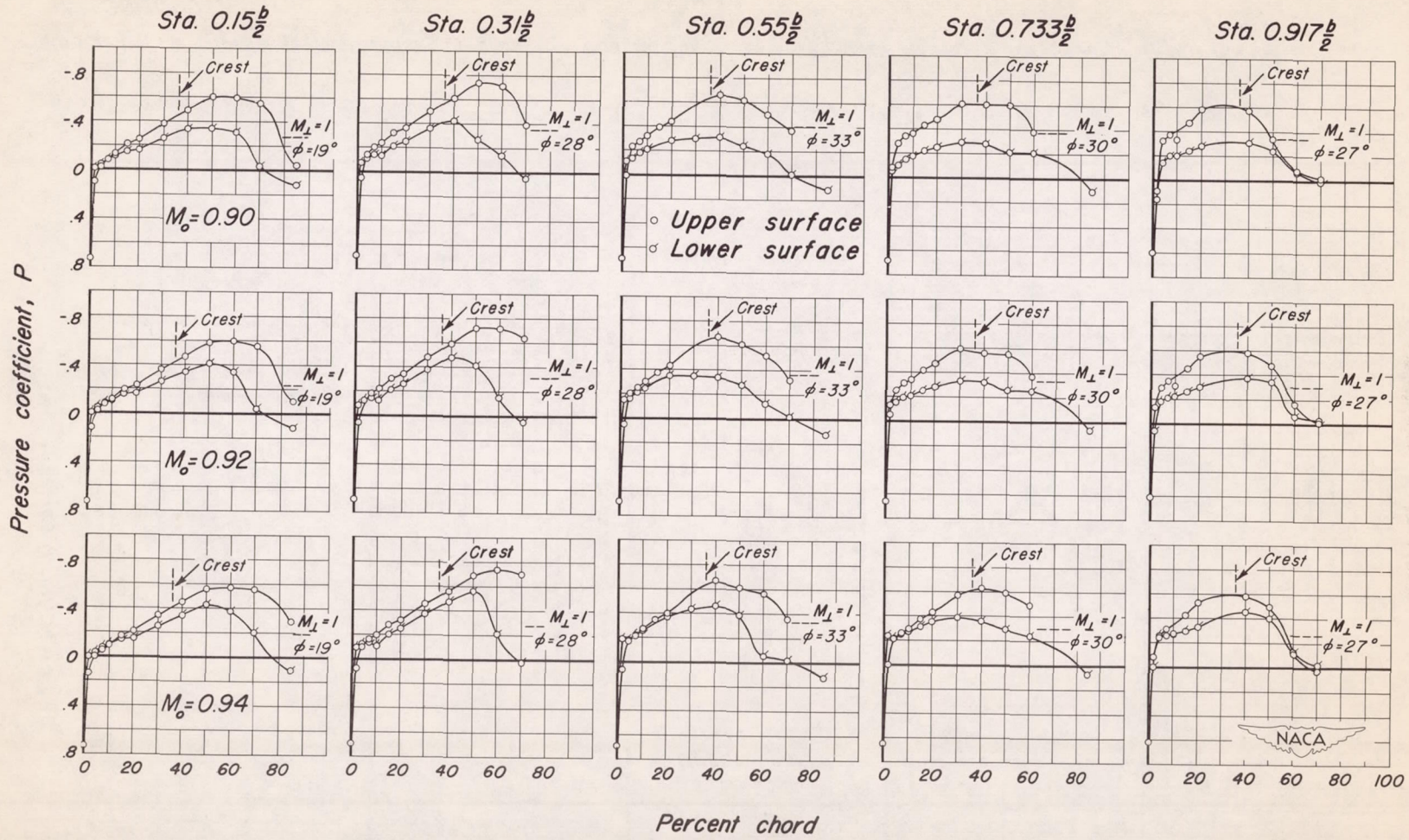

(d) α_u, 1° ; M_o, 0.90, 0.92, 0.94.

Figure 19.- Concluded.

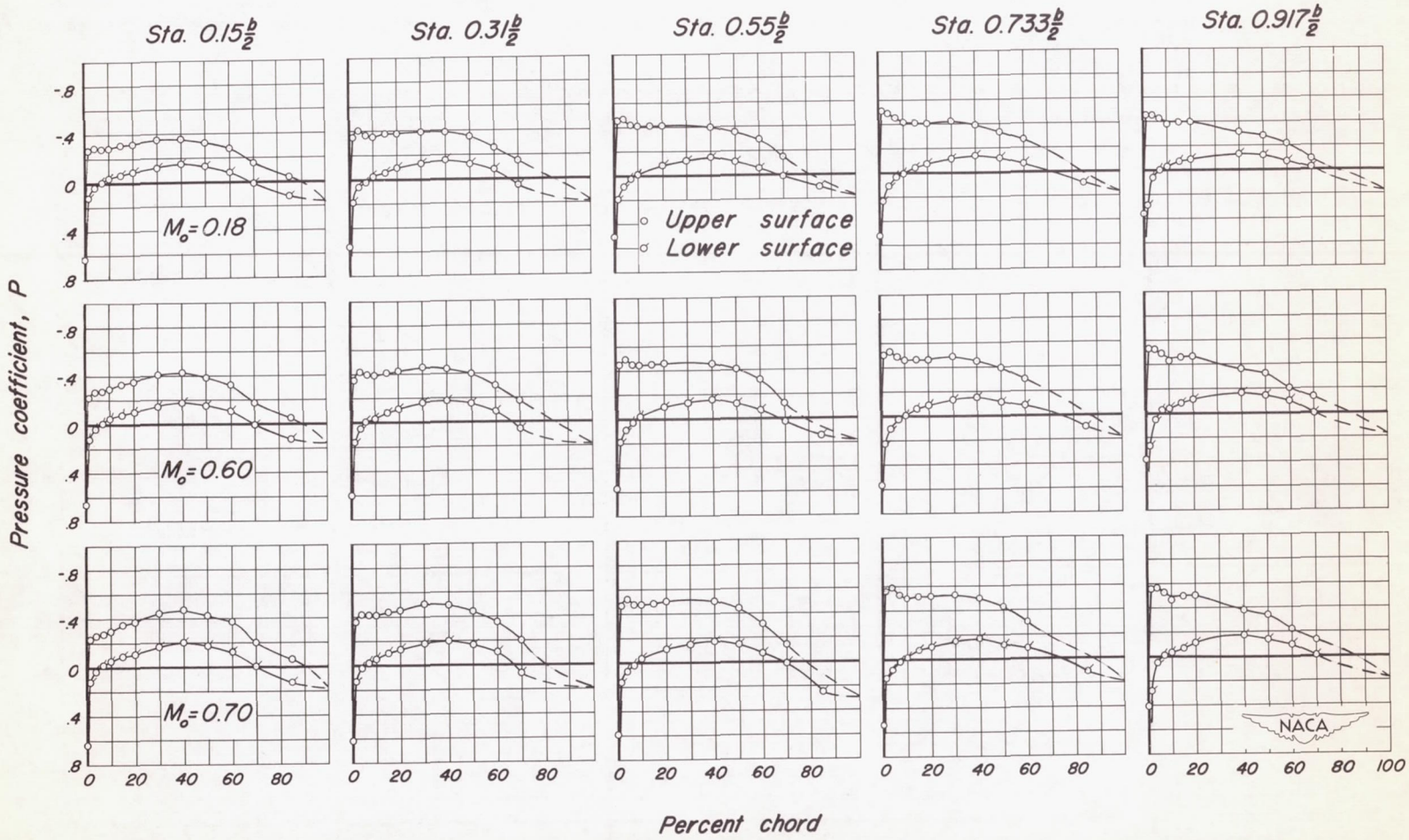

(a) α_u, 2°; M_o, 0.18, 0.60, 0.70.

Figure 20.- The chordwise distribution of pressure coefficient at five semispan stations for several Mach numbers. α_u, 2°; R, 2,000,000.

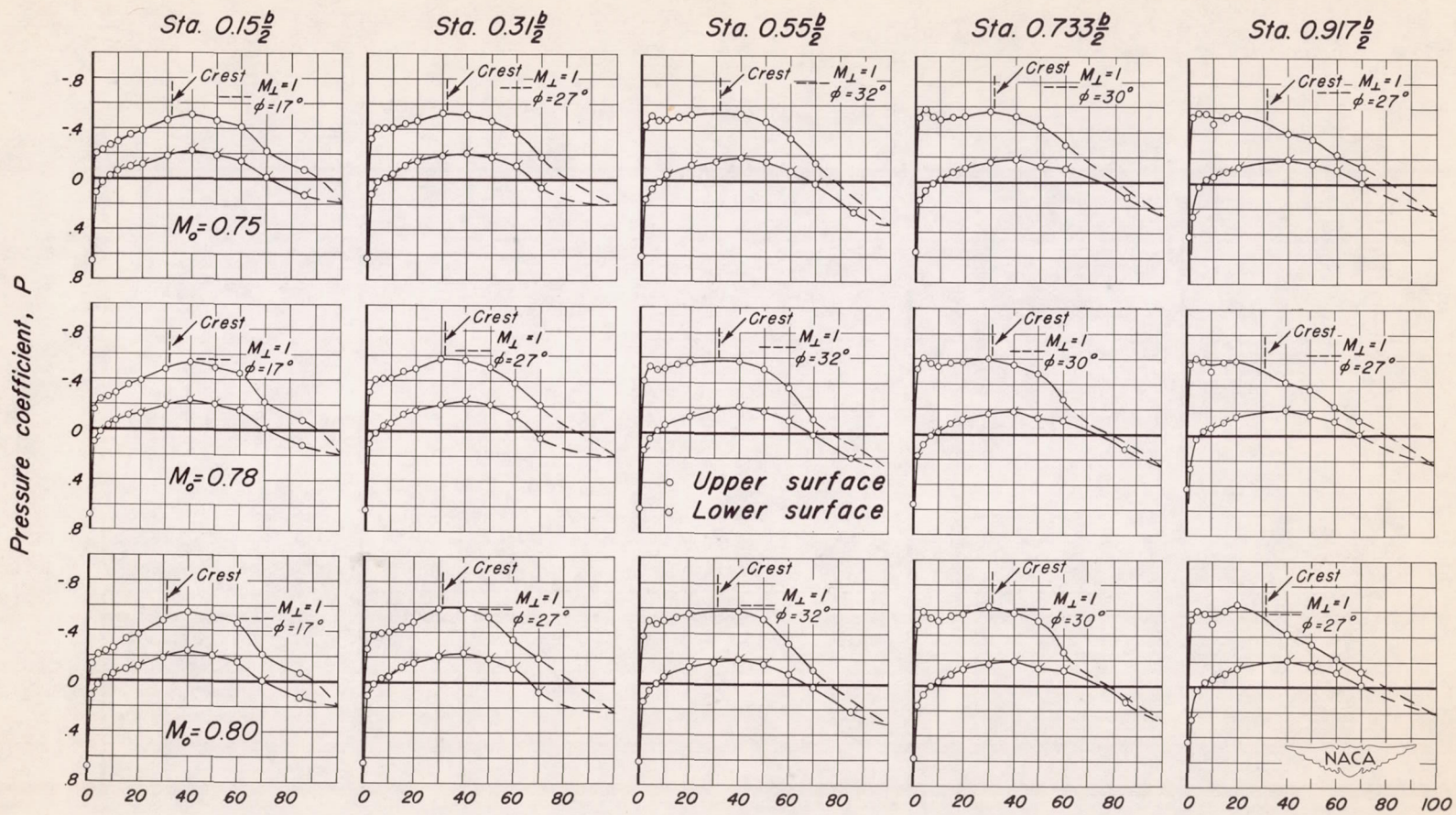

(b) α_u, 2°; M_o, 0.75, 0.78, 0.80.

Figure 20.- Continued.

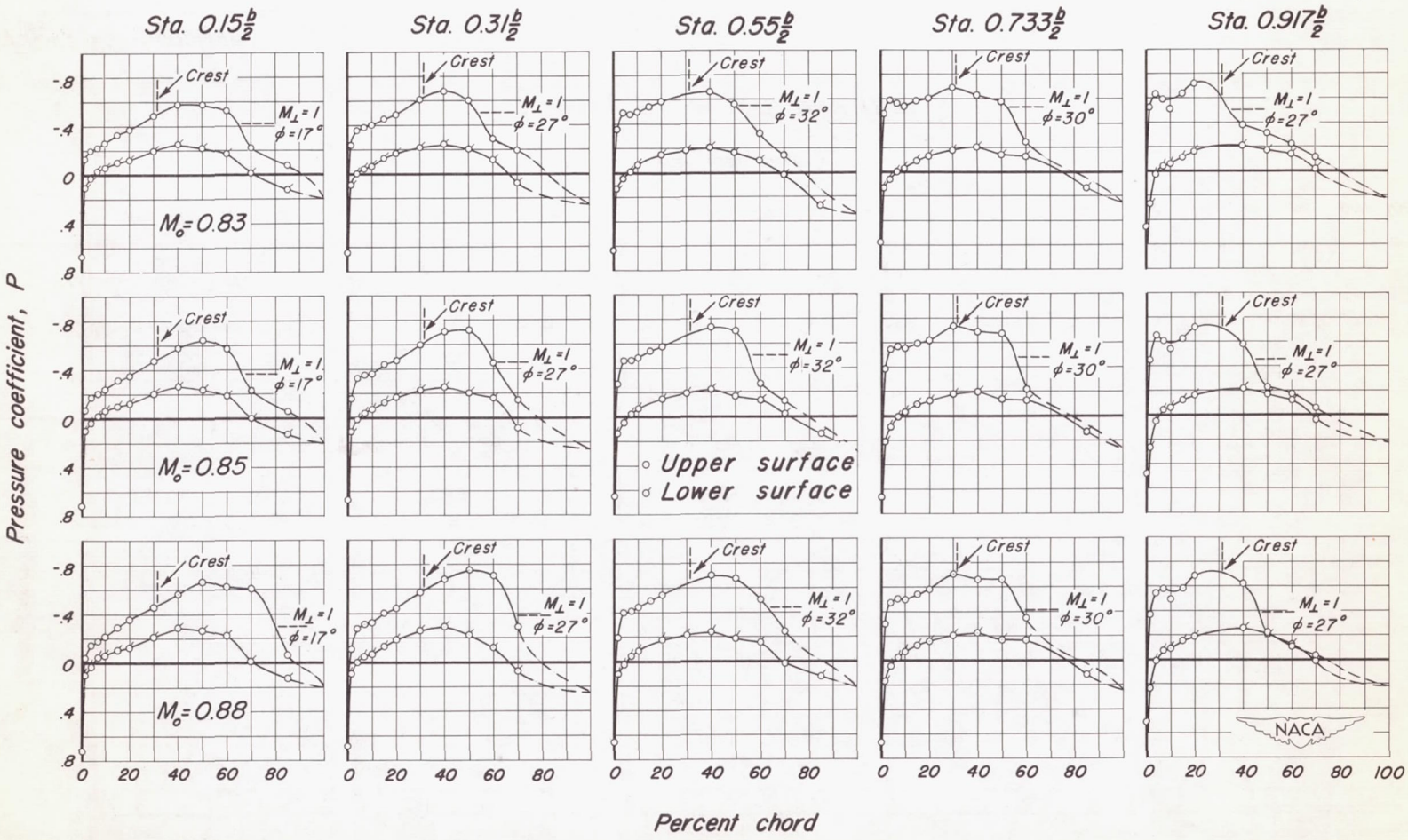

(c) α_u, 2°; M_o, 0.83, 0.85, 0.88.

Figure 20.- Continued.

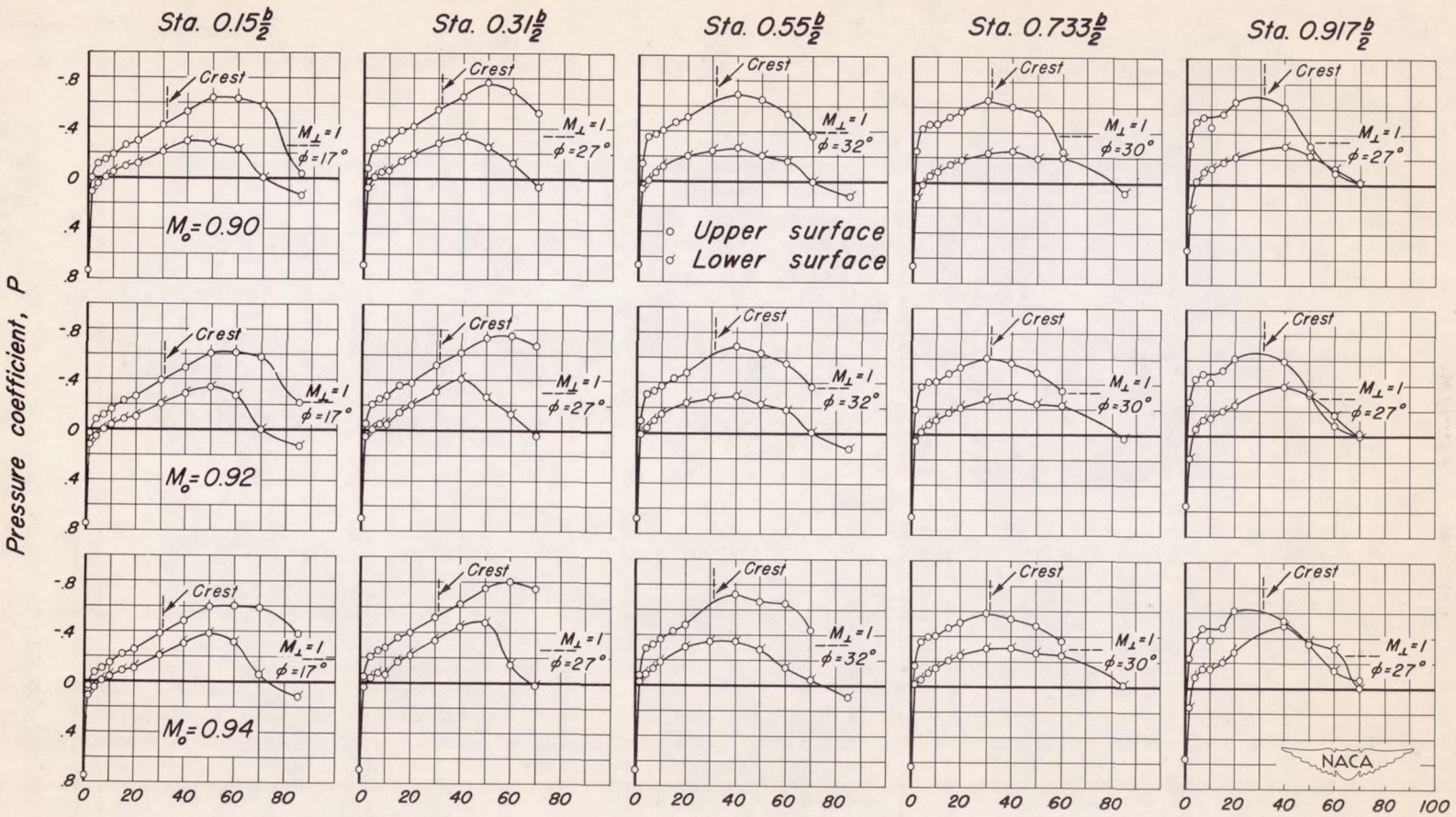

(d) α_u, 2°; M_o, 0.90, 0.92, 0.94.

Figure 20.- Concluded.

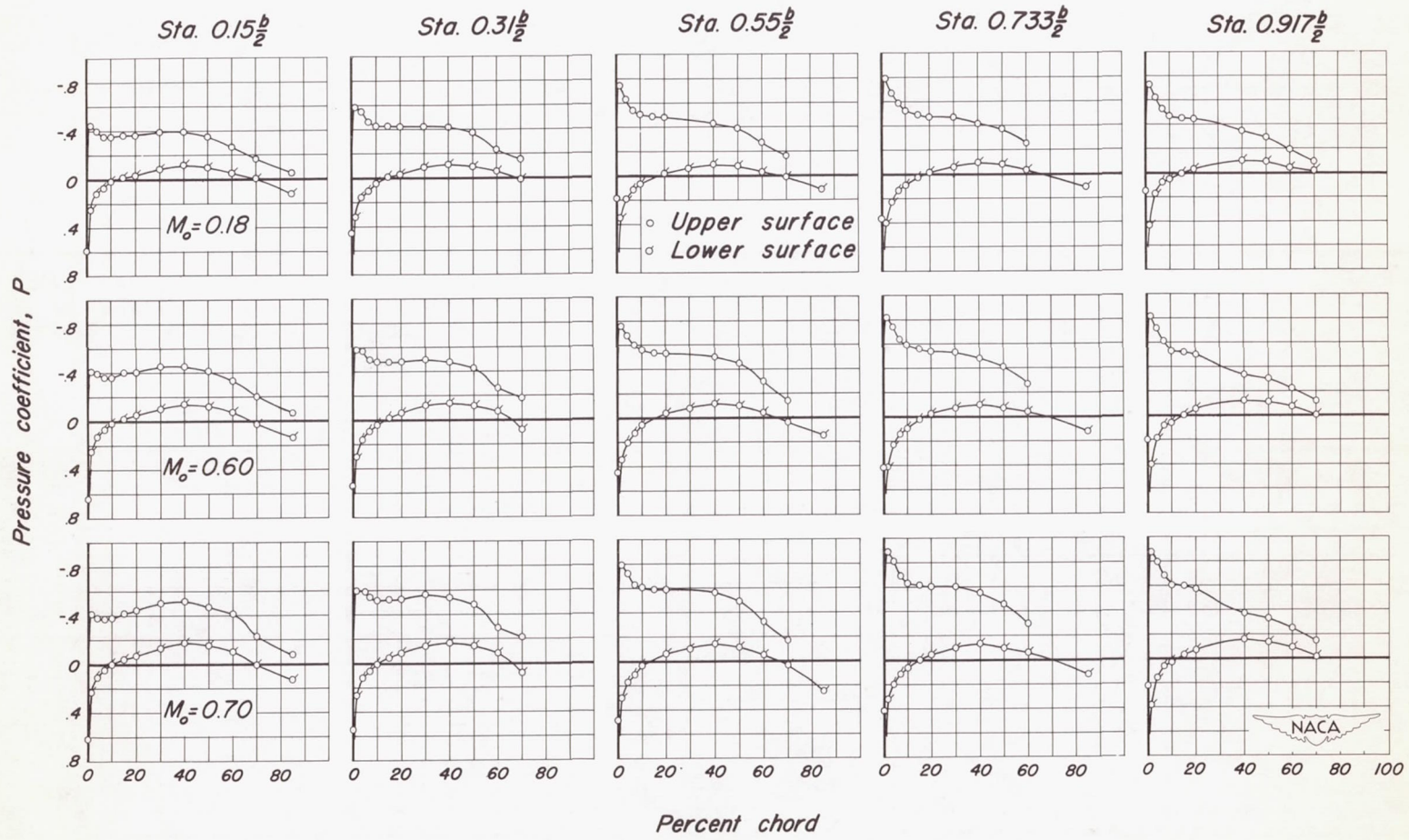

(a) α_u, 3°; M_o, 0.18, 0.60, 0.70.

Figure 21.– The chordwise distribution of pressure coefficient at five semispan stations for several Mach numbers. α_u, 3°; R, 2,000,000.

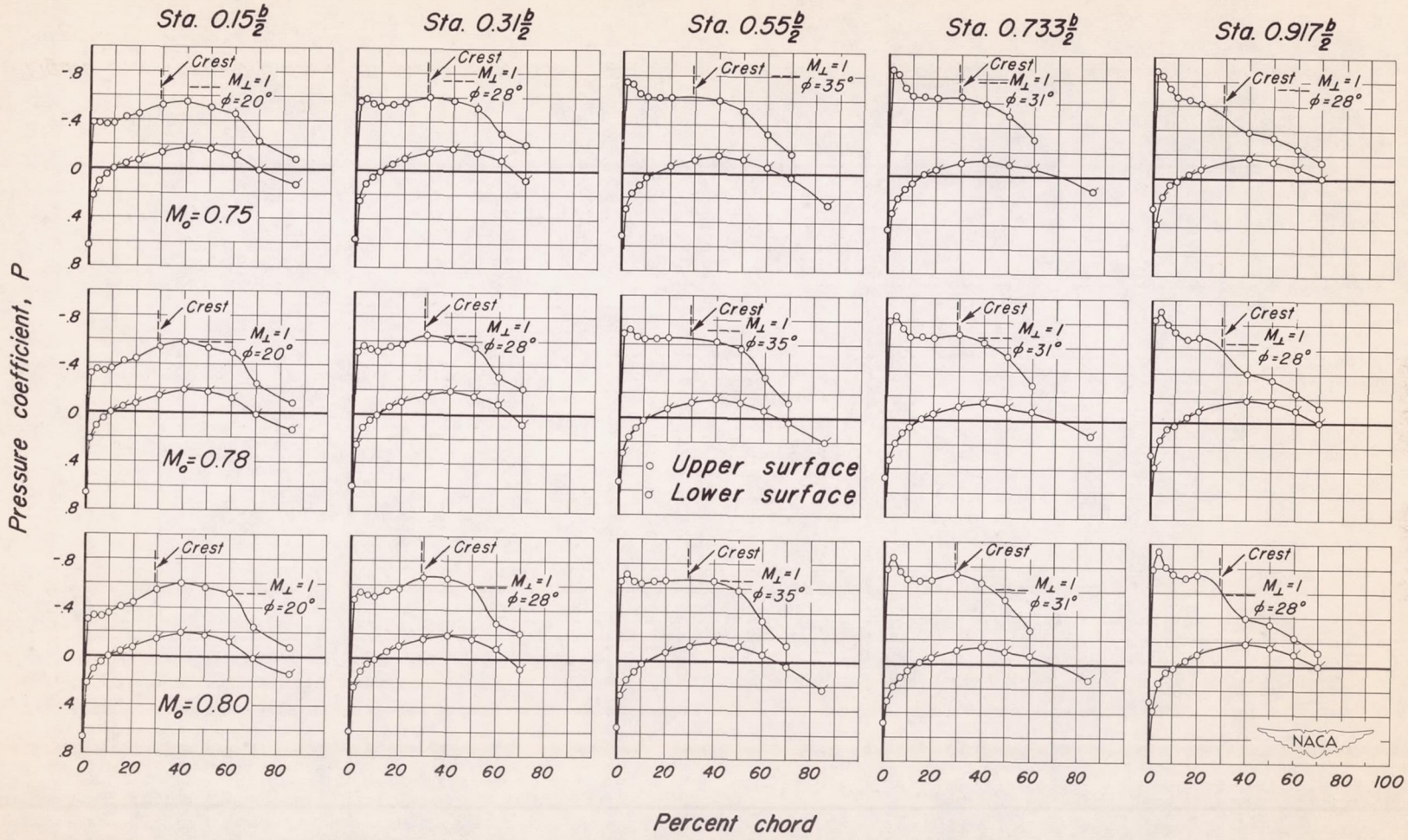

(b) α_u, 3°; M_o, 0.75, 0.78, 0.80.

Figure 21.- Continued.

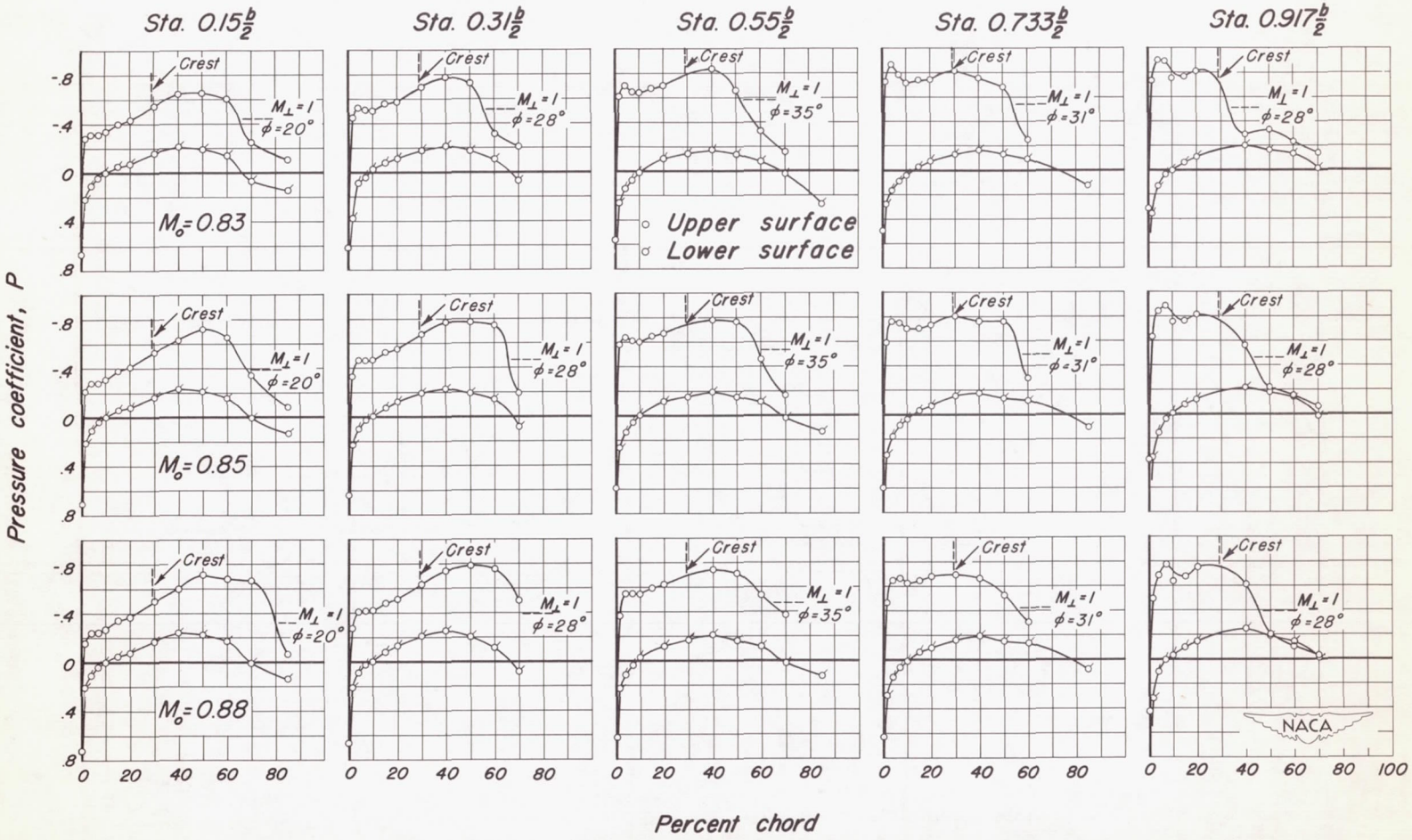

(c) α_u, 3°; M_o, 0.83, 0.85, 0.88.

Figure 21.– Continued.

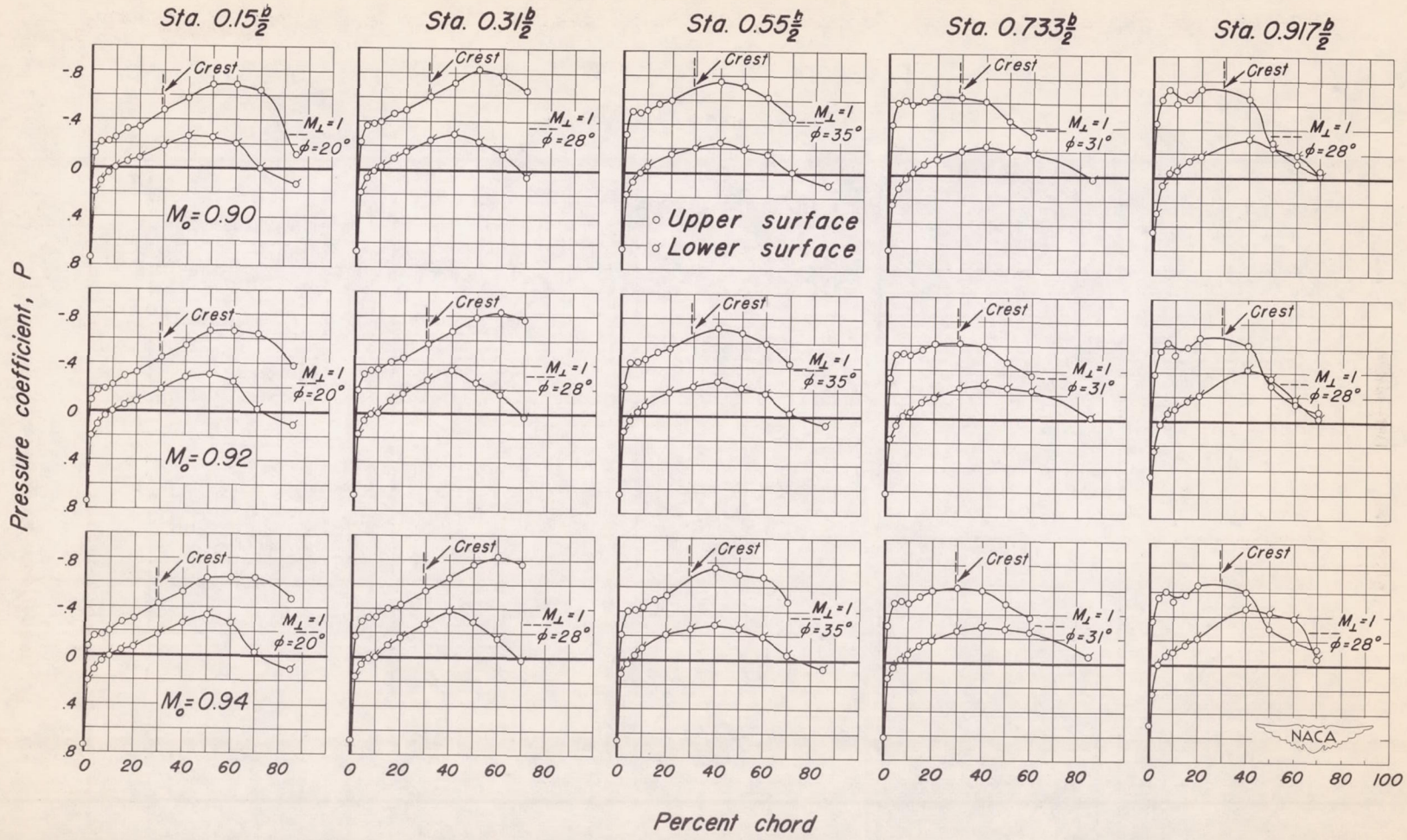

(d) α_u, 3°; M_o, 0.90, 0.92, 0.94.

Figure 21.– Concluded.

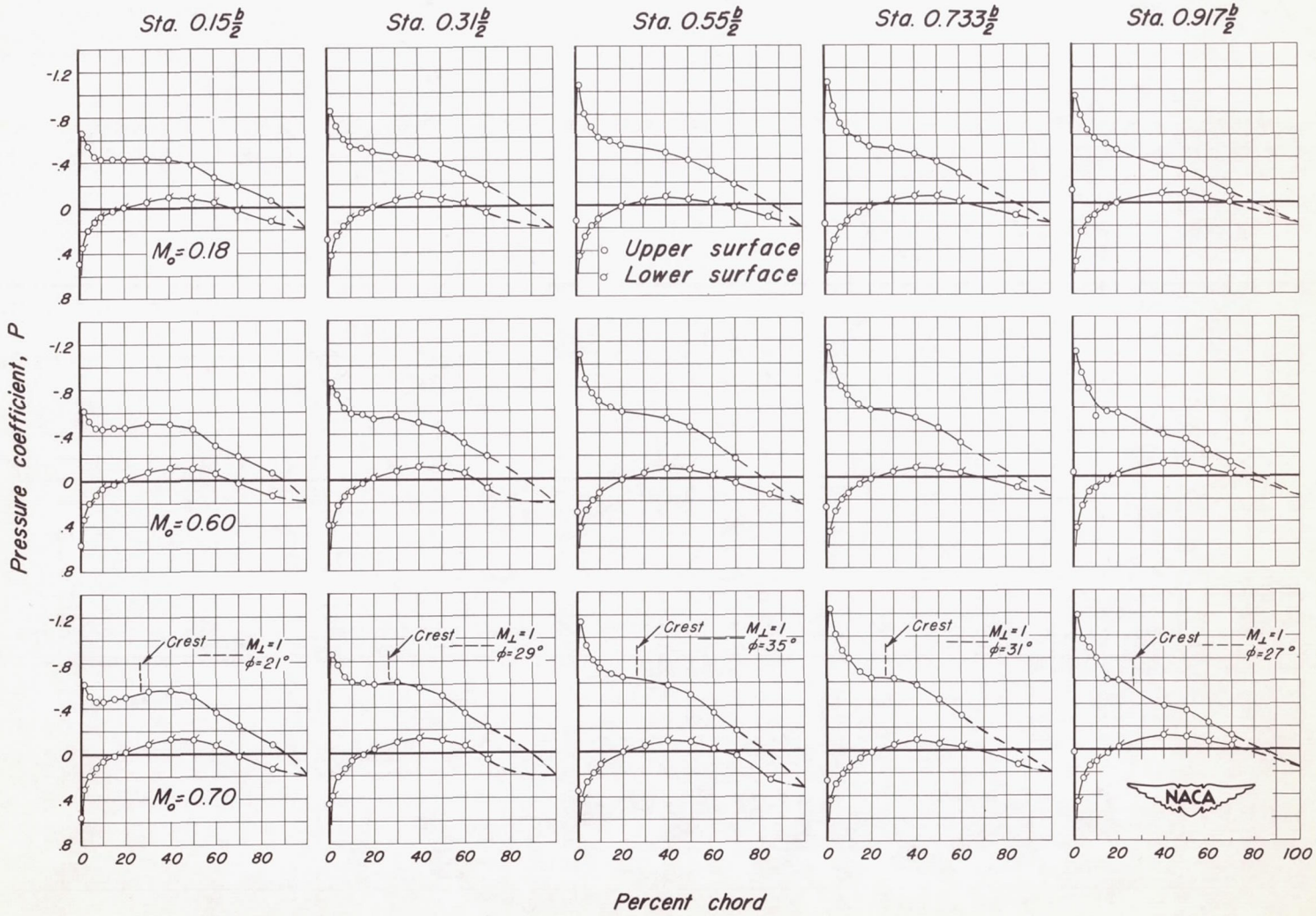

(a) α_u, 4°; M_o, 0.18, 0.60, 0.70.

Figure 22.- The chordwise distribution of pressure coefficient at five semispan stations for several Mach numbers. α_u, 4°; R, 2,000,000.

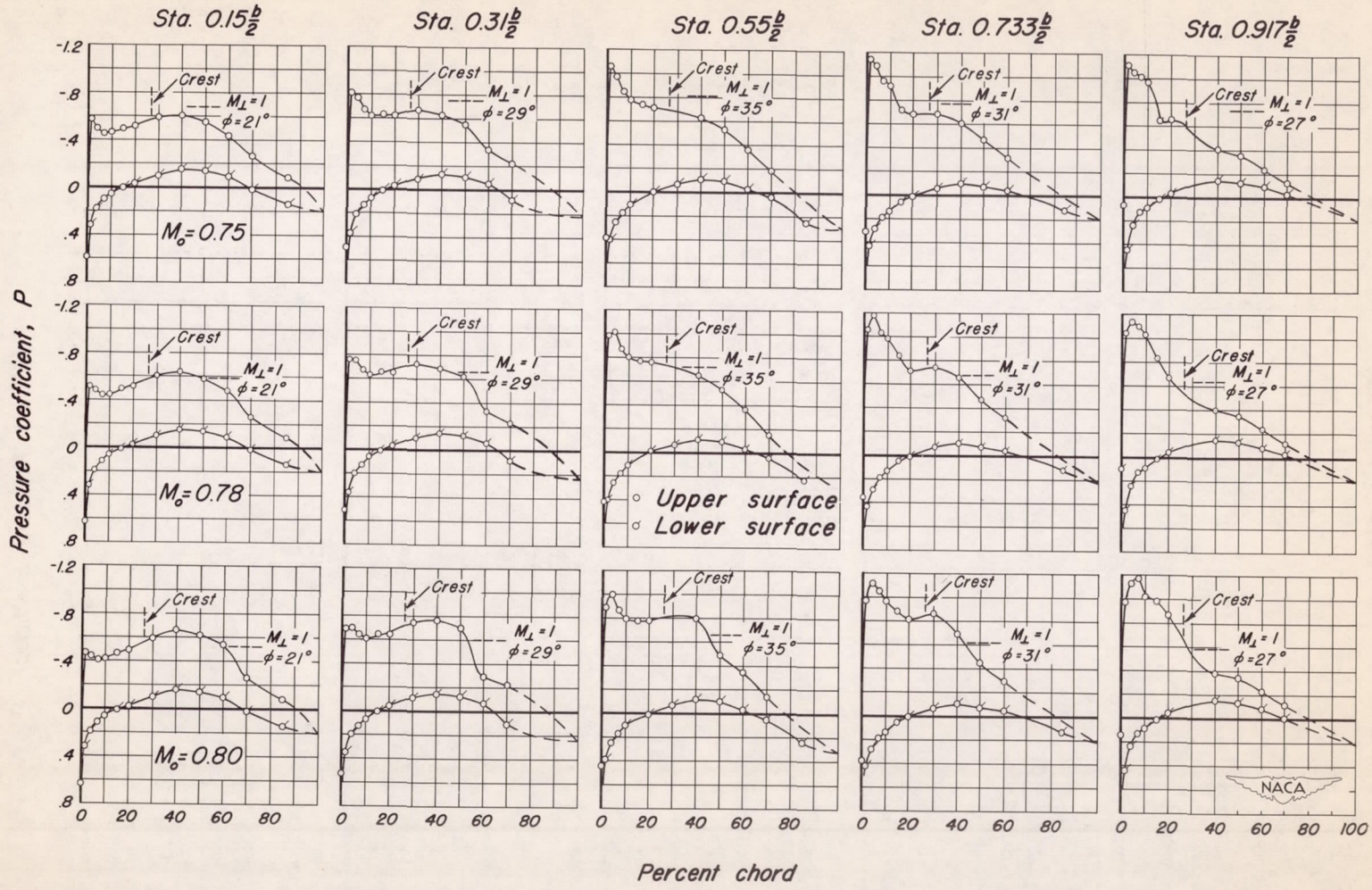

(b) α_u, 4°; M_o, 0.75, 0.78, 0.80.

Figure 22.- Continued.

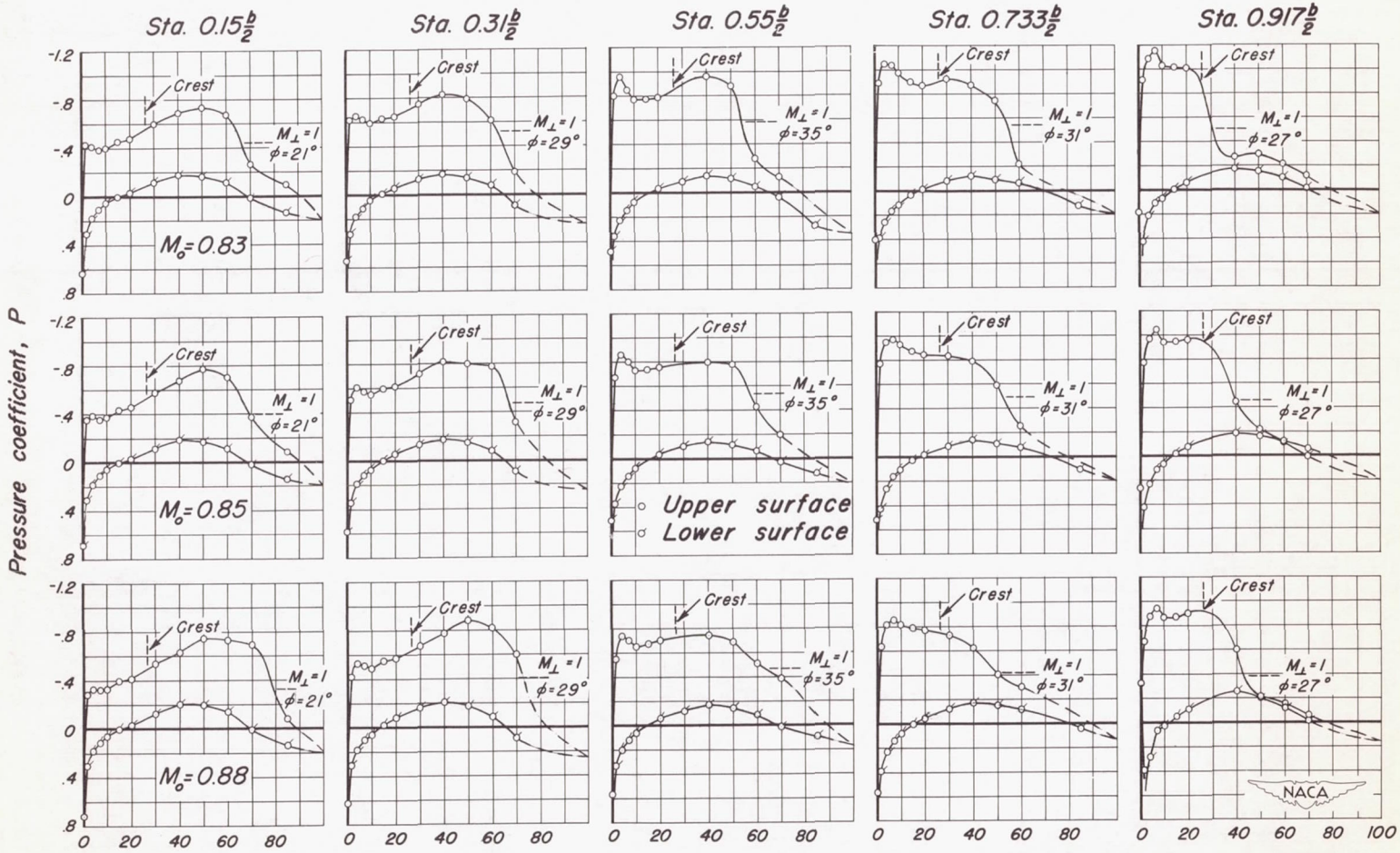

(c) α_u, 4°; M_o, 0.83, 0.85, 0.88.

Figure 22.- Continued.

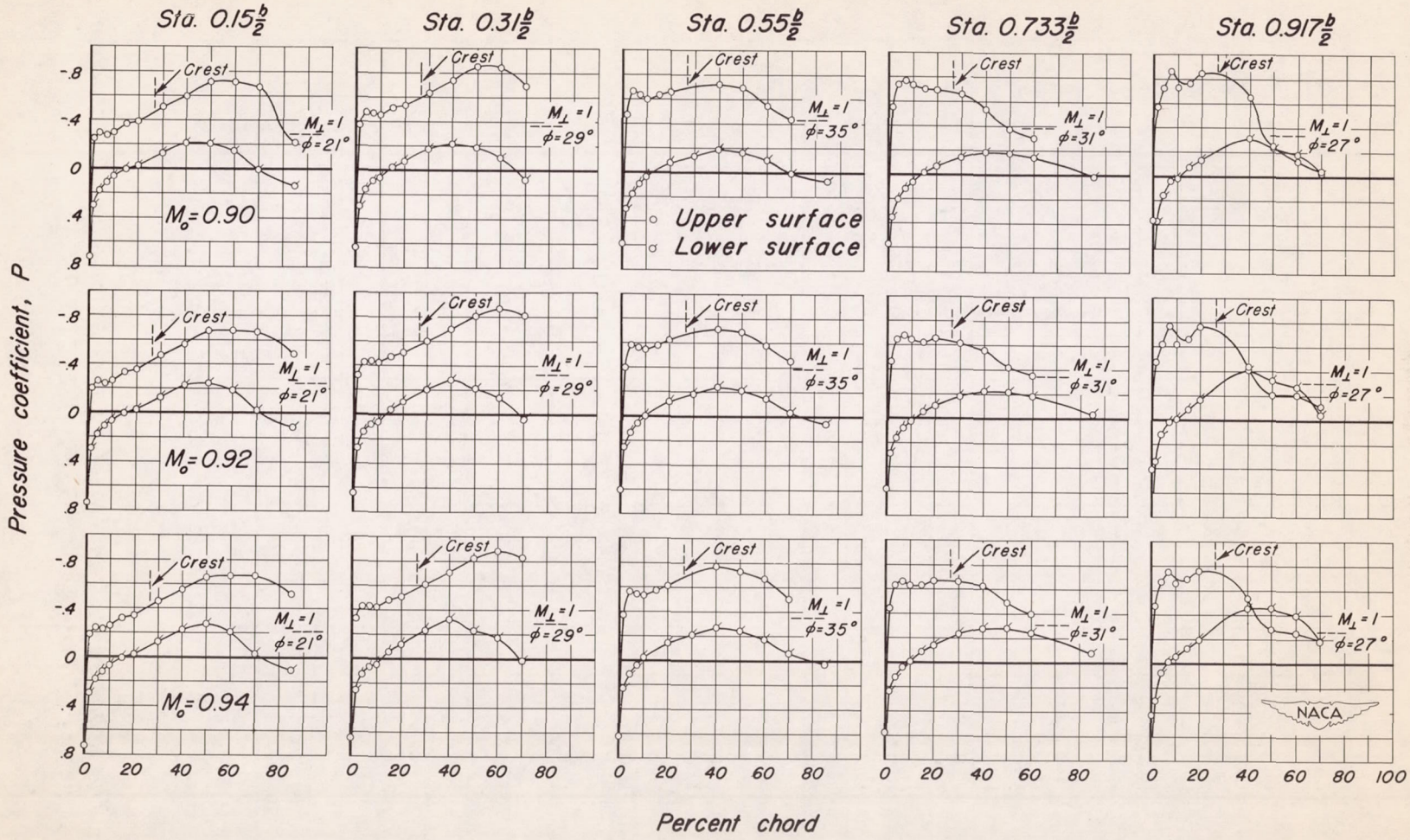

(d) α_u, 4°; M_0, 0.90, 0.92, 0.94.

Figure 22.- Concluded.

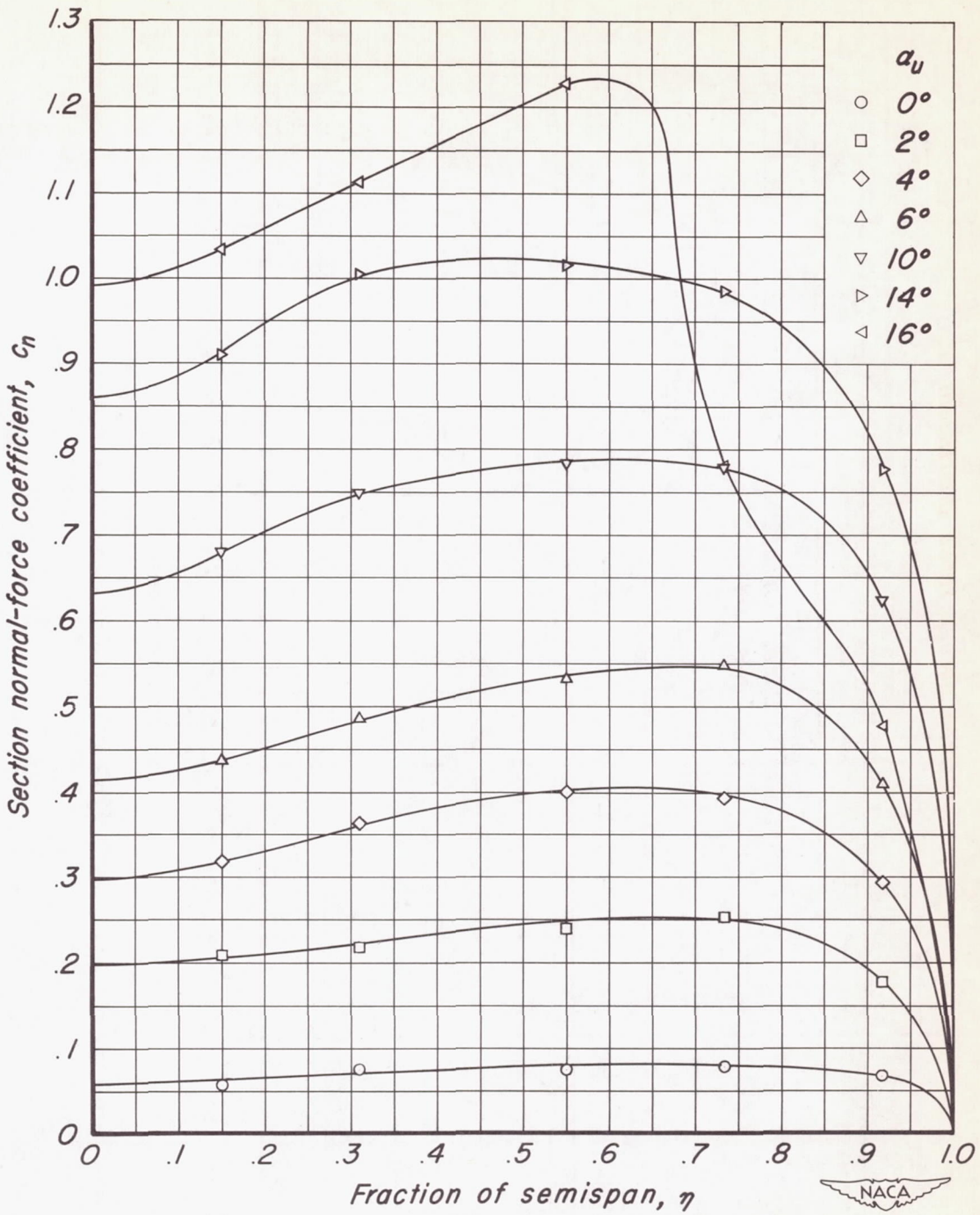

Figure 23.- The spanwise distribution of section normal-force coefficient at several angles of attack. M_o, 0.18; R, 2,000,000.

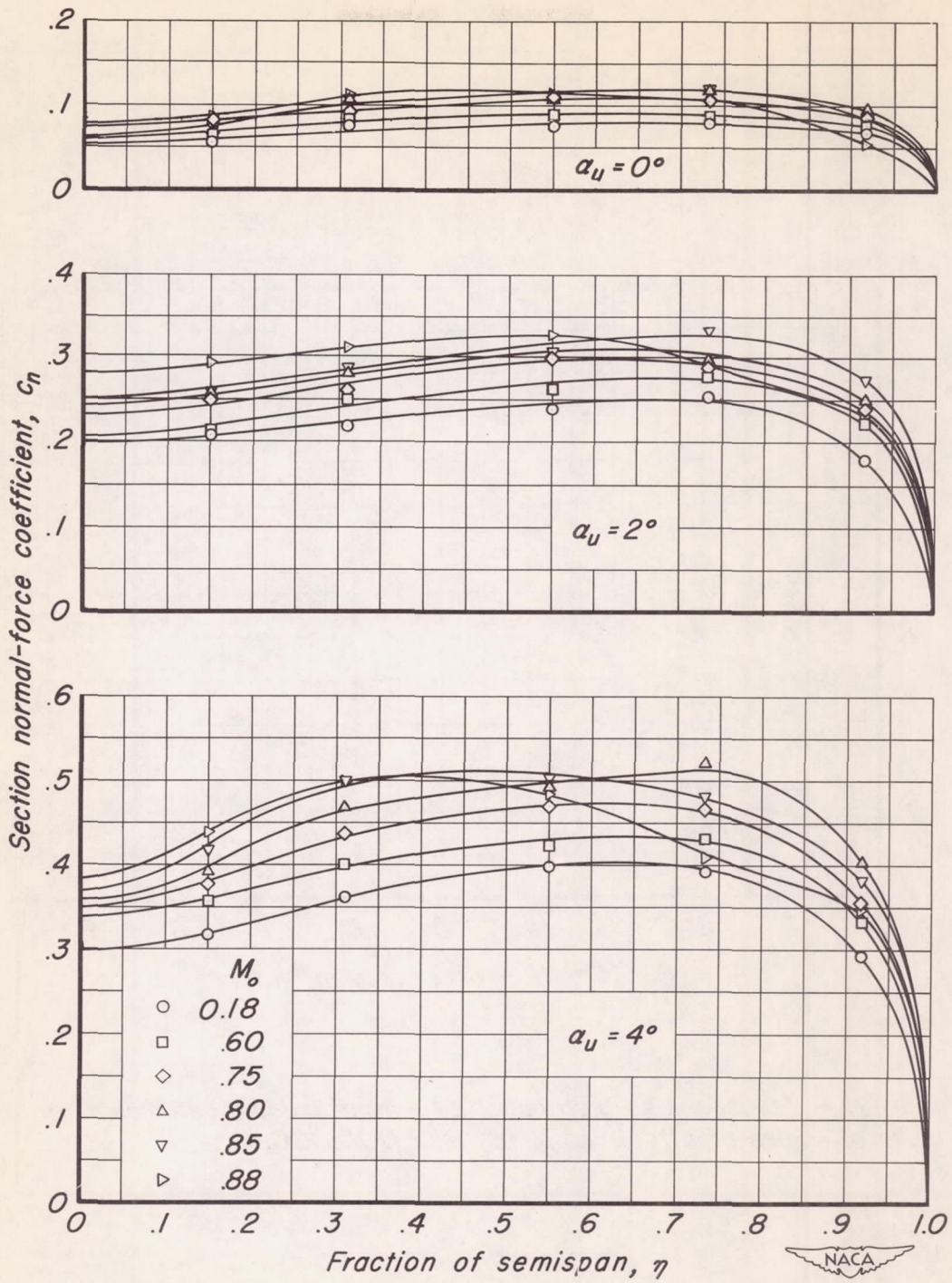

Figure 24.- The spanwise distribution of section normal-force coefficient at several Mach numbers for three angles of attack. R, 2,000,000.

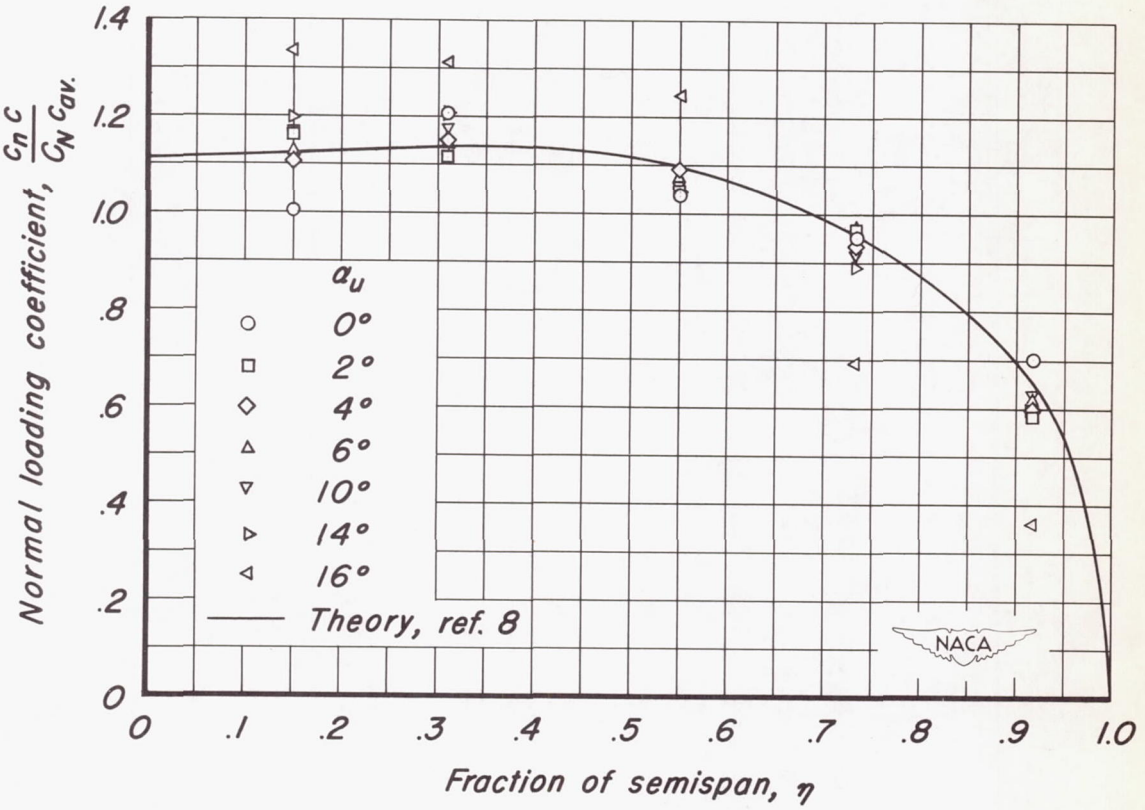

Figure 25.- The spanwise distribution of normal loading coefficient at several angles of attack. M_o, 0.18; R, 2,000,000.

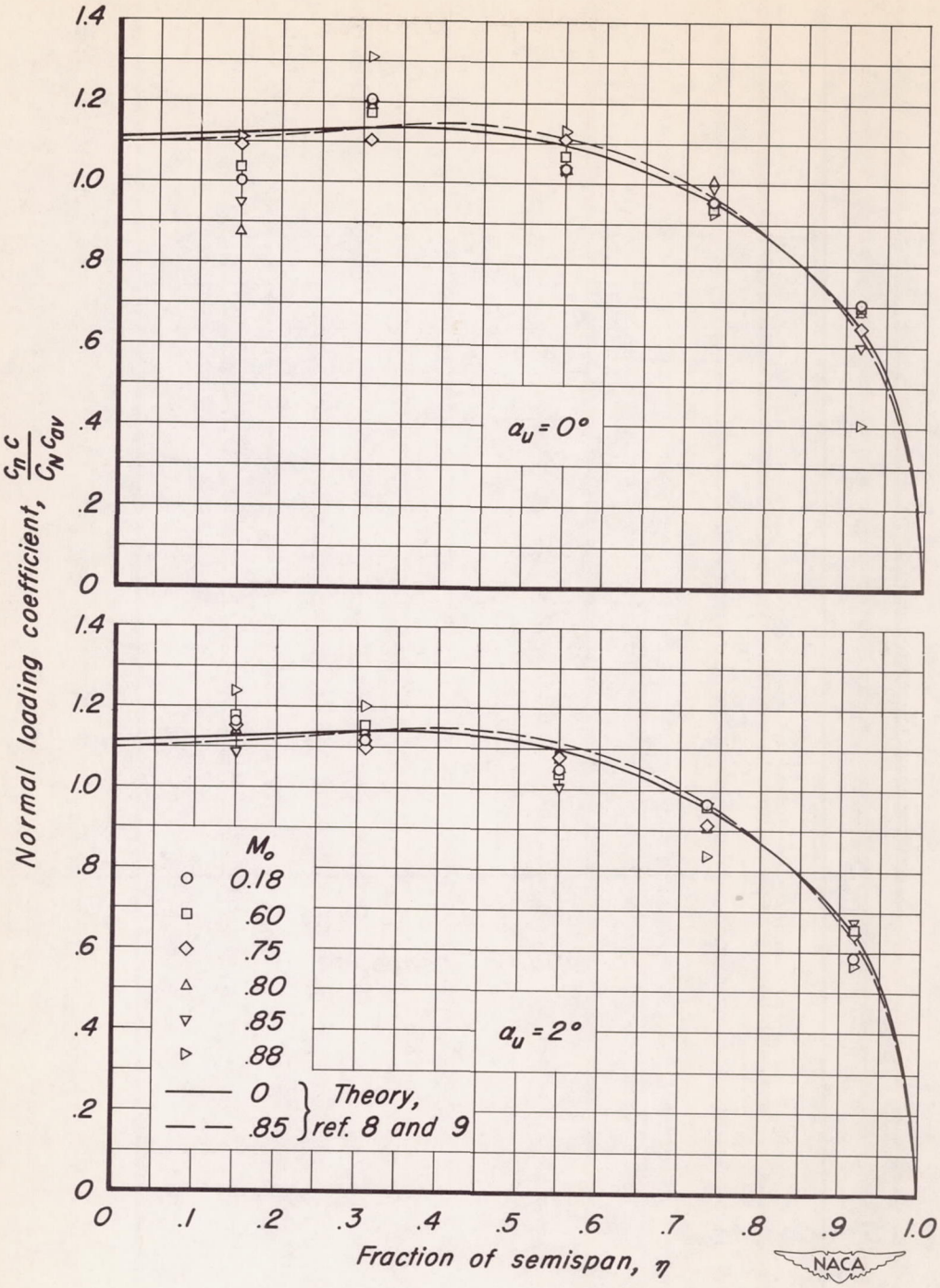

(a) α_u, 0°, 2°.

Figure 26.- The spanwise distribution of normal loading coefficient at several Mach numbers for three angles of attack. R, 2,000,000.

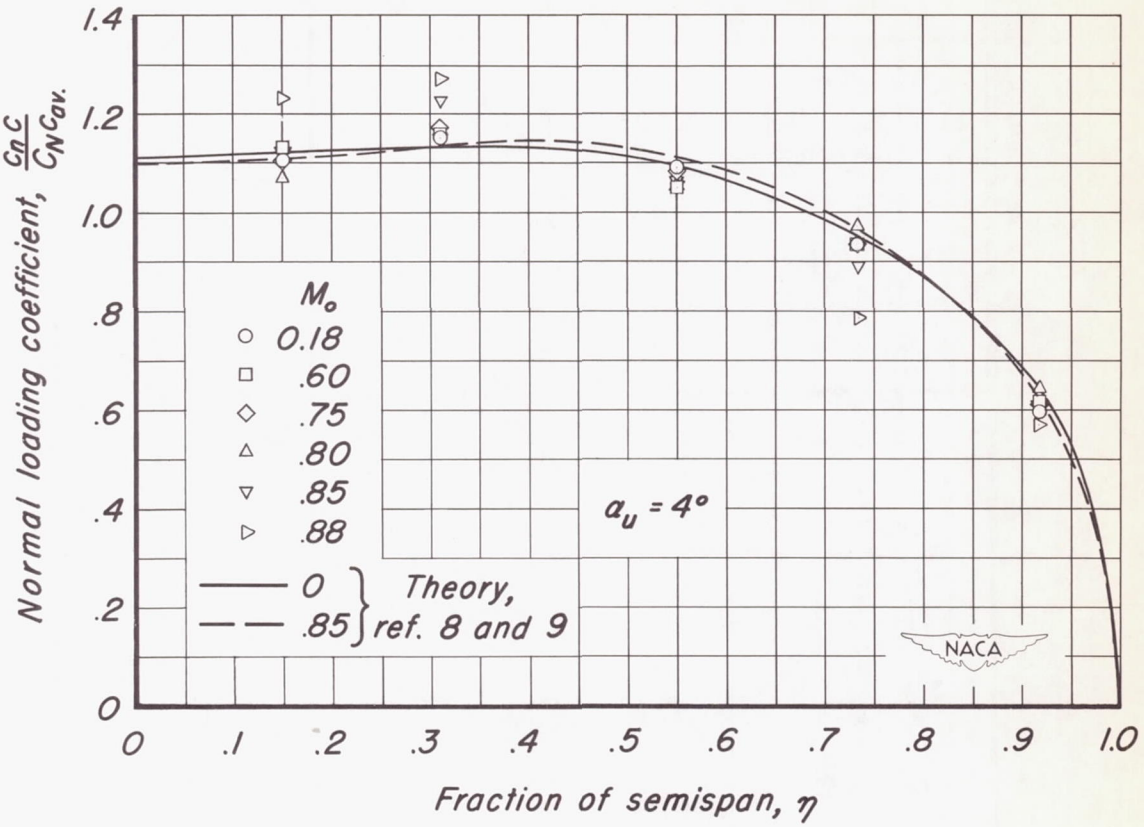

(b) a_u, 4°.

Figure 26. – Concluded.

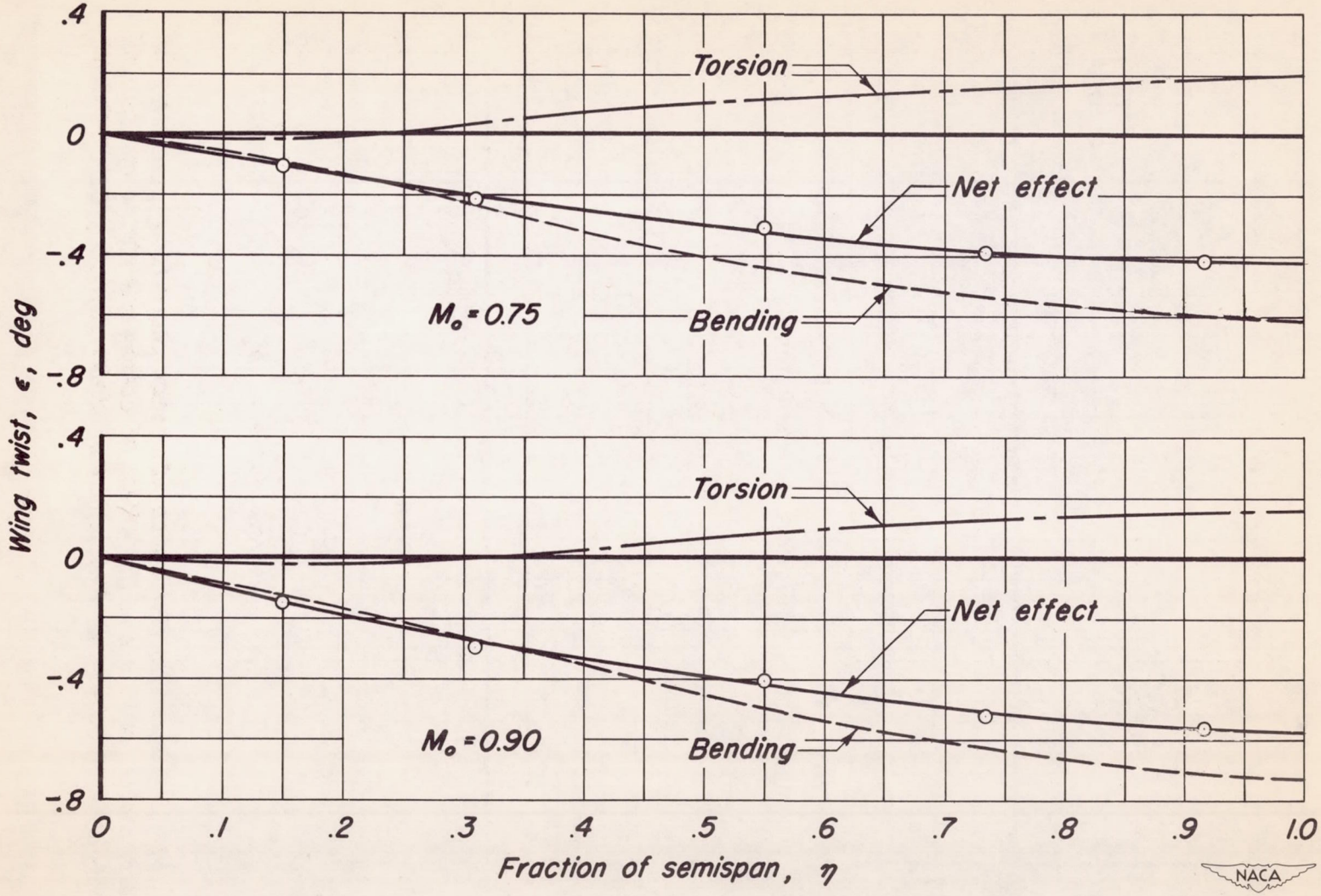

Figure 27.– The spanwise variation of wing twist determined from static tests simulating wing loadings at Mach numbers of 0.75 and 0.90. R, 2,000,000; a_u, 4°.

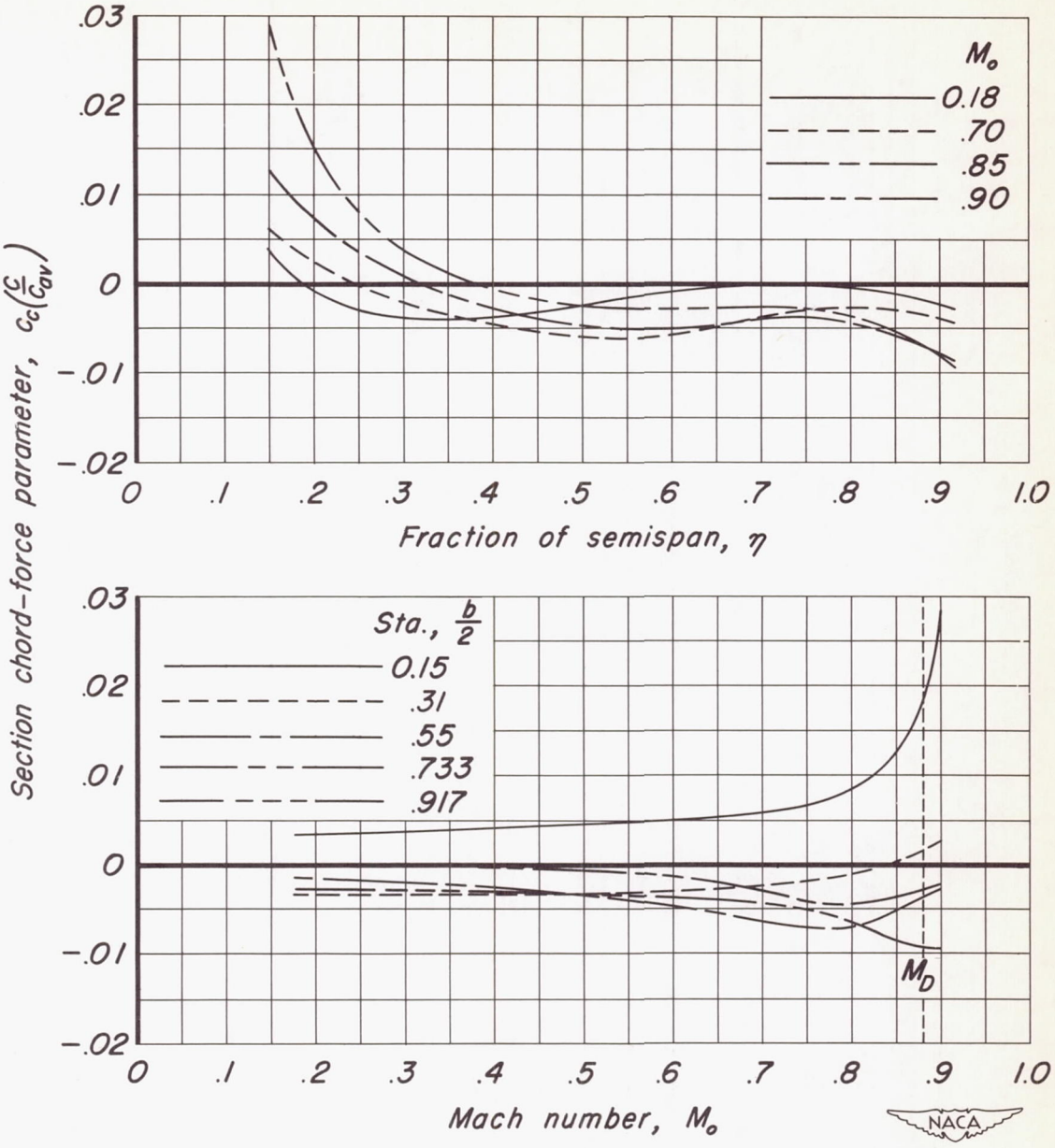

Figure 28.– The spanwise distribution of section chord-force parameter at several Mach numbers and the effect of compressibility on the section chord-force parameter at five semispan stations. α_u, 0°; R, 2,000,000.

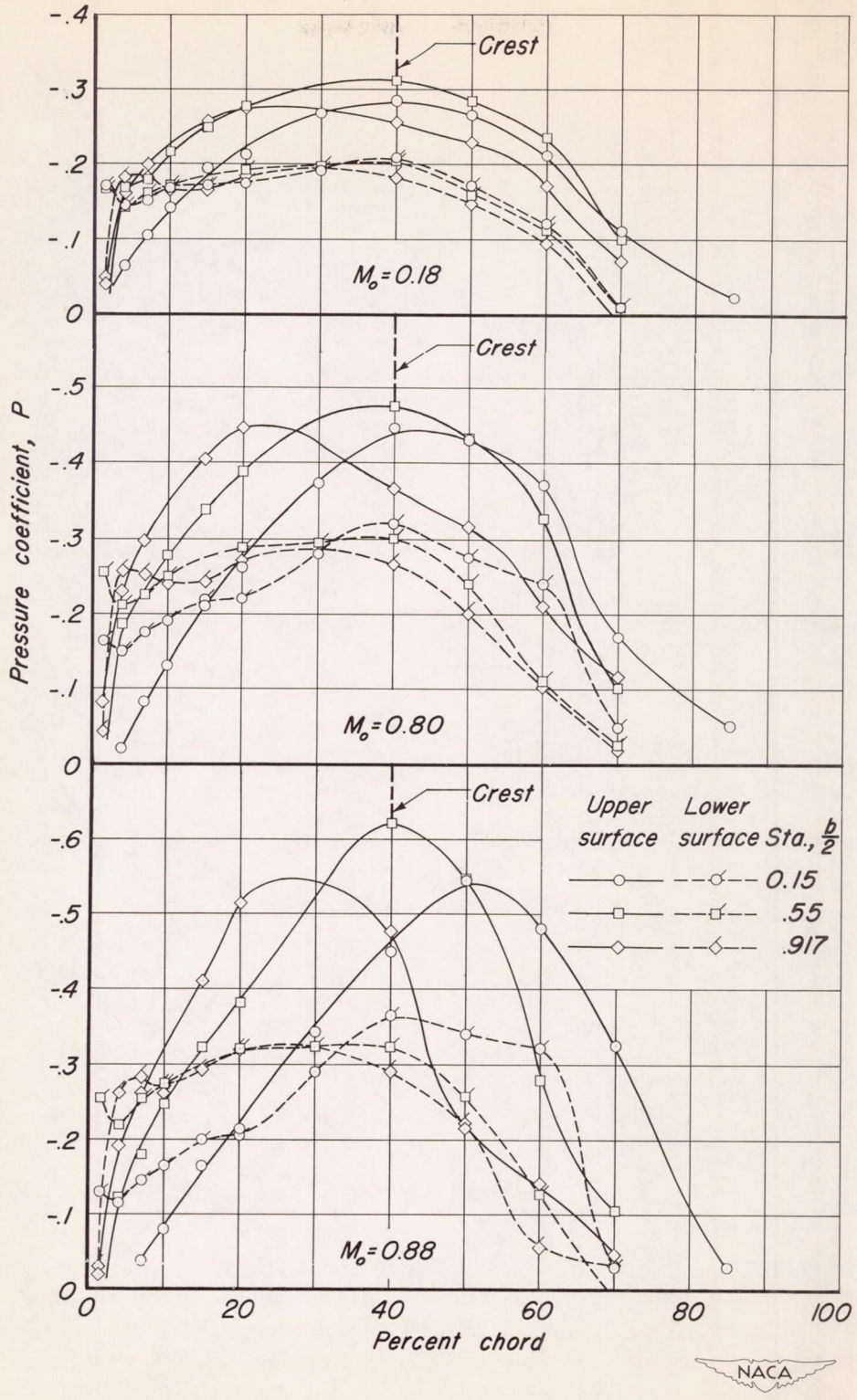

Figure 29.- The variation of chordwise distribution of pressure coefficient at three semispan stations for three Mach numbers. a_u, 0°; R, 2,000,000.

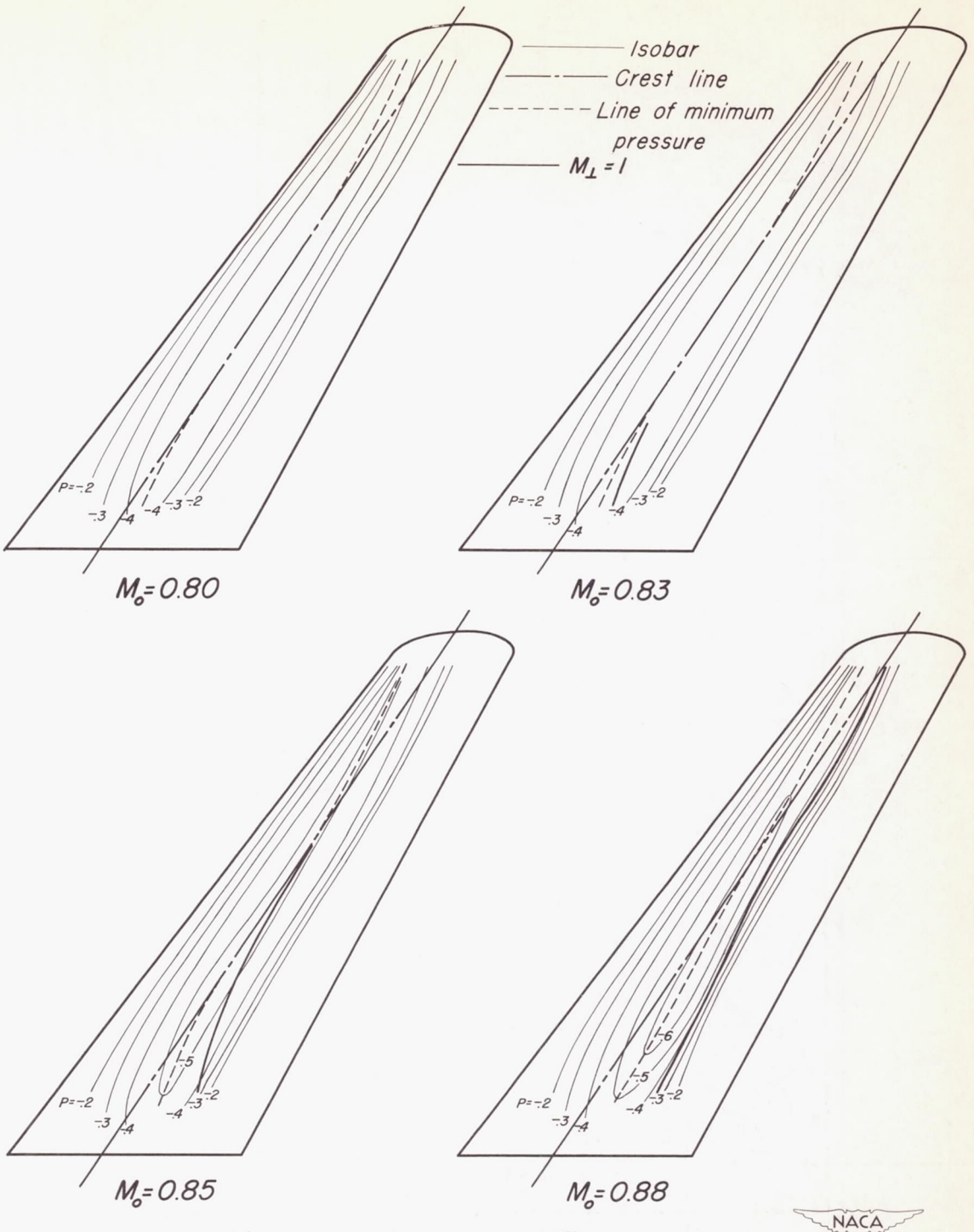

(a) α_u, 0°; crest at 0.40 x/c.

Figure 30.- The lines of constant pressure on the upper surface for several Mach numbers. R, 2,000,000.

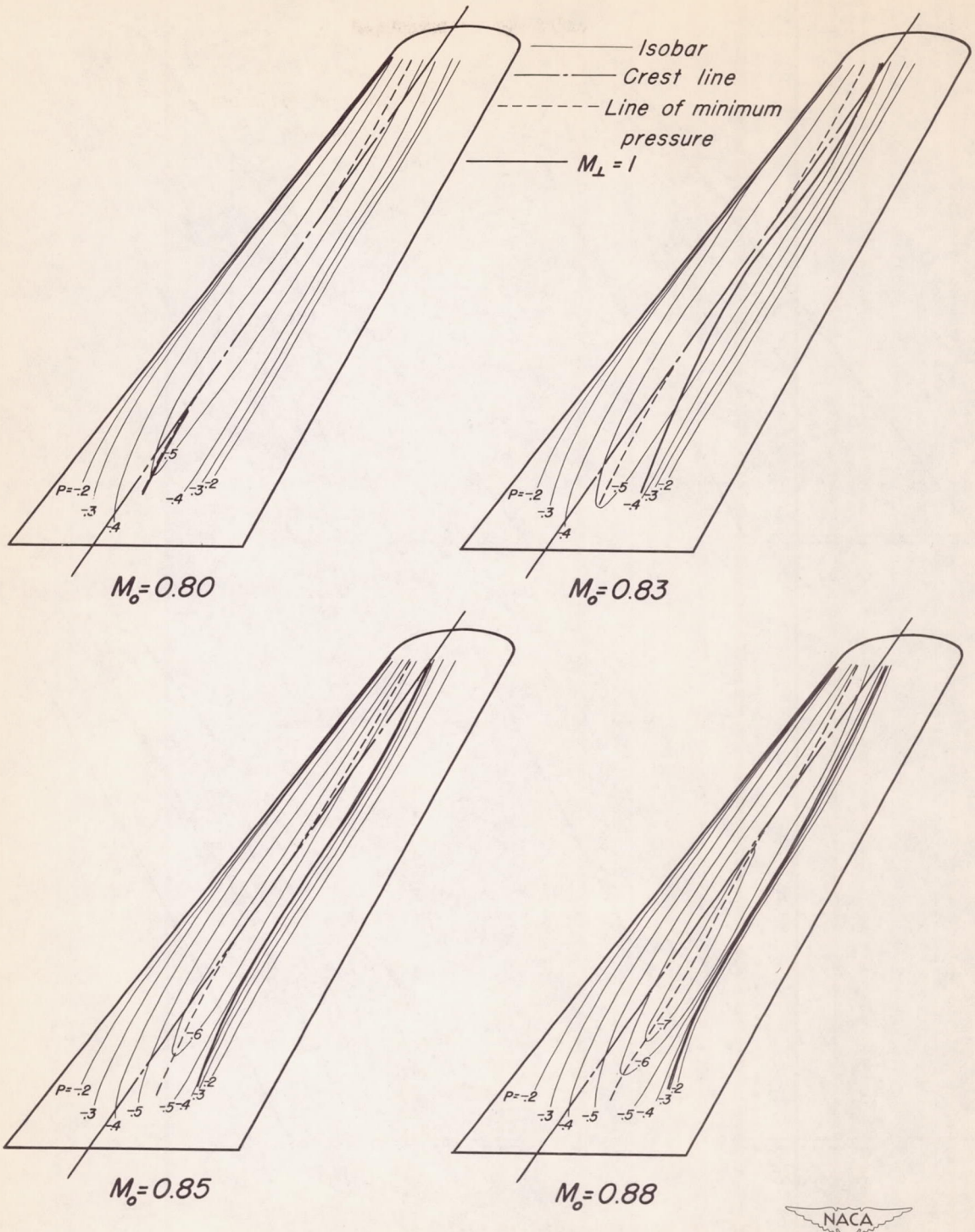

(b) α_u, 1°; crest at 0.36 x/c.

Figure 30. – Continued.

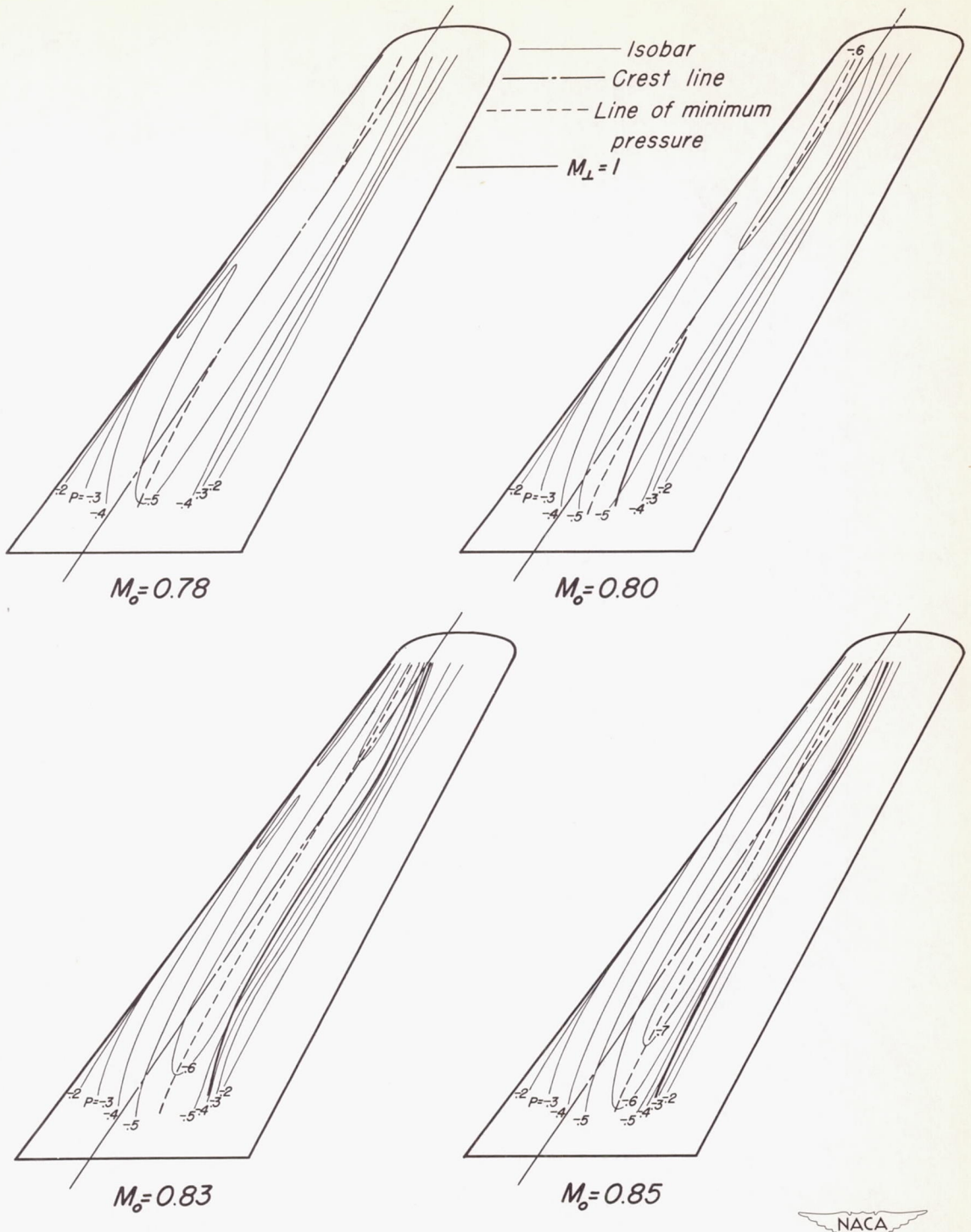

(c) α_u, 2°; crest at 0.315 x/c.

Figure 30.- Continued.

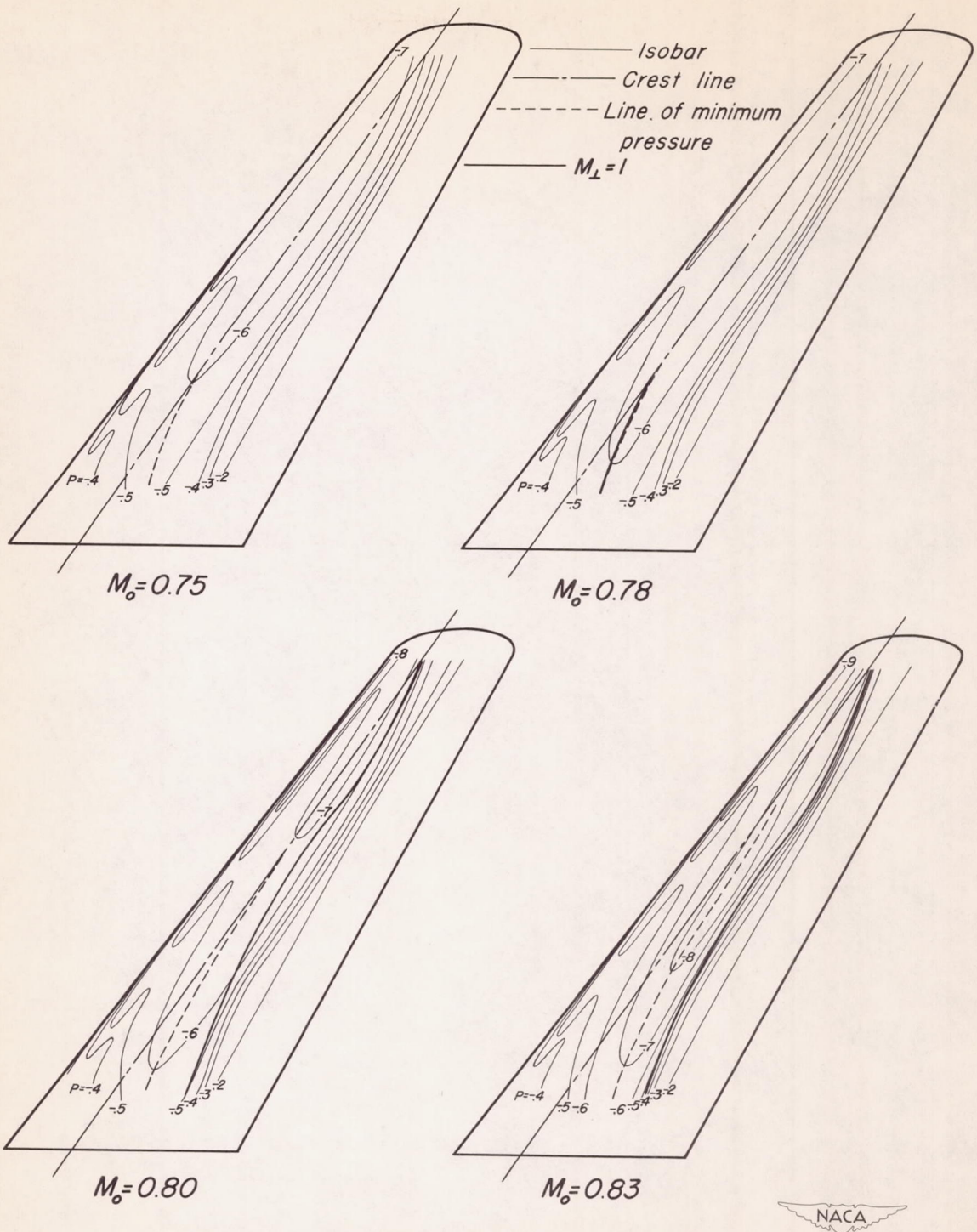

(d) α_u, 3°; crest at 0.29 x/c.

Figure 30.- Continued.

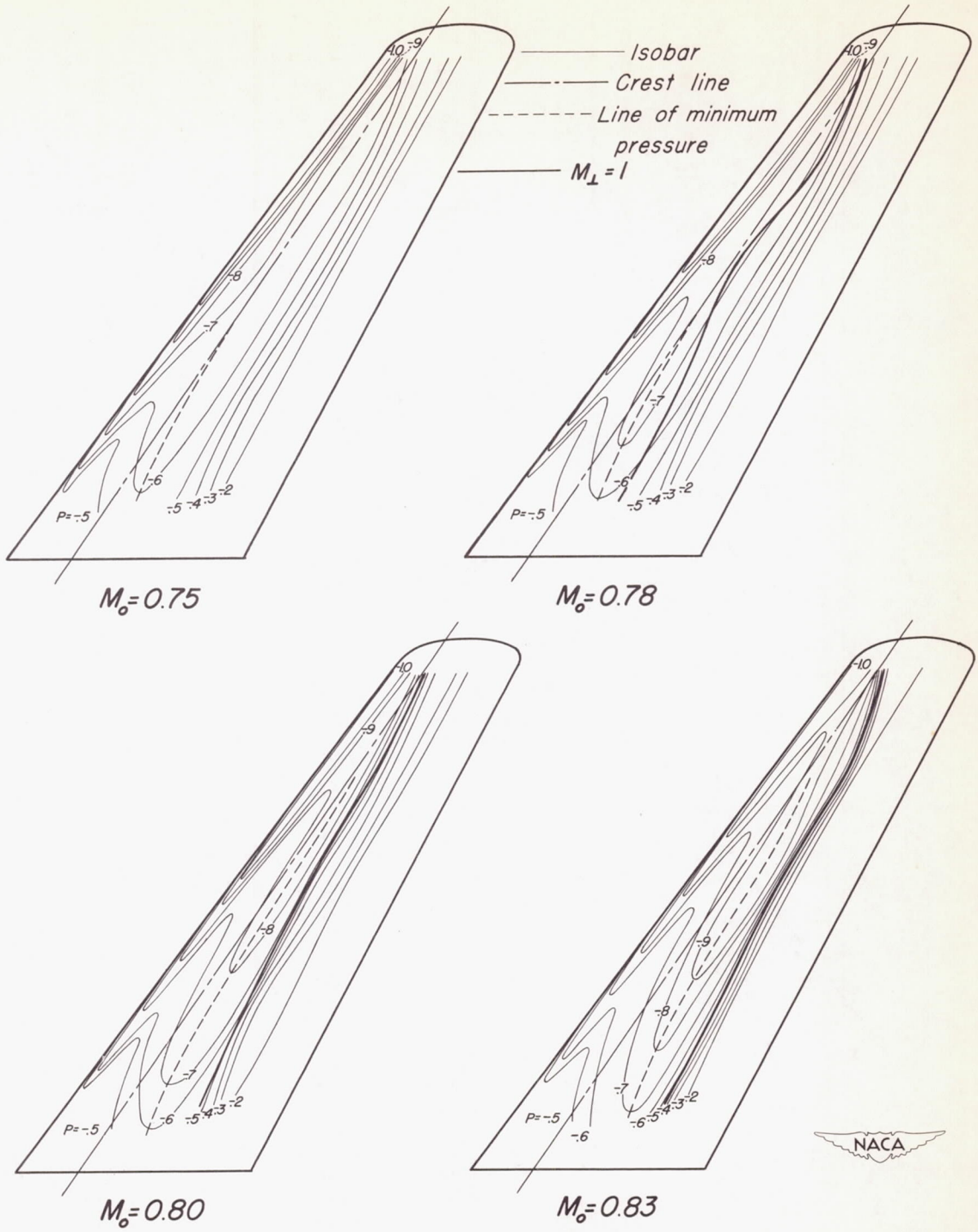

(e) α_u, 4°; crest at 0.265 x/c.

Figure 30.- Concluded.

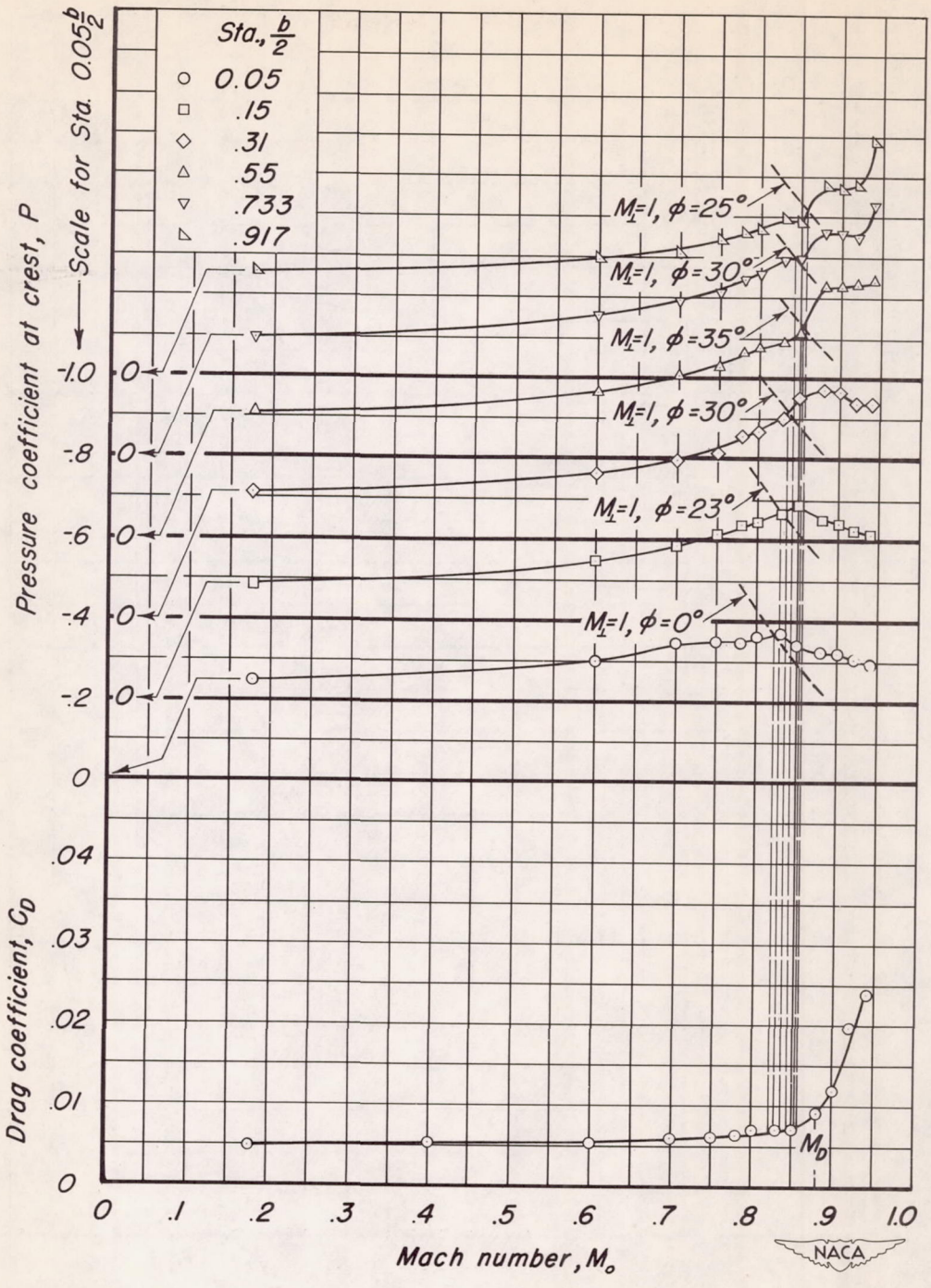

(a) α_u, 0°; crest at 0.40 x/c.

Figure 31. – The relation between the total drag increase and the attainment of critical flow conditions at the crest points of several semispan stations. R, 2,000,000.

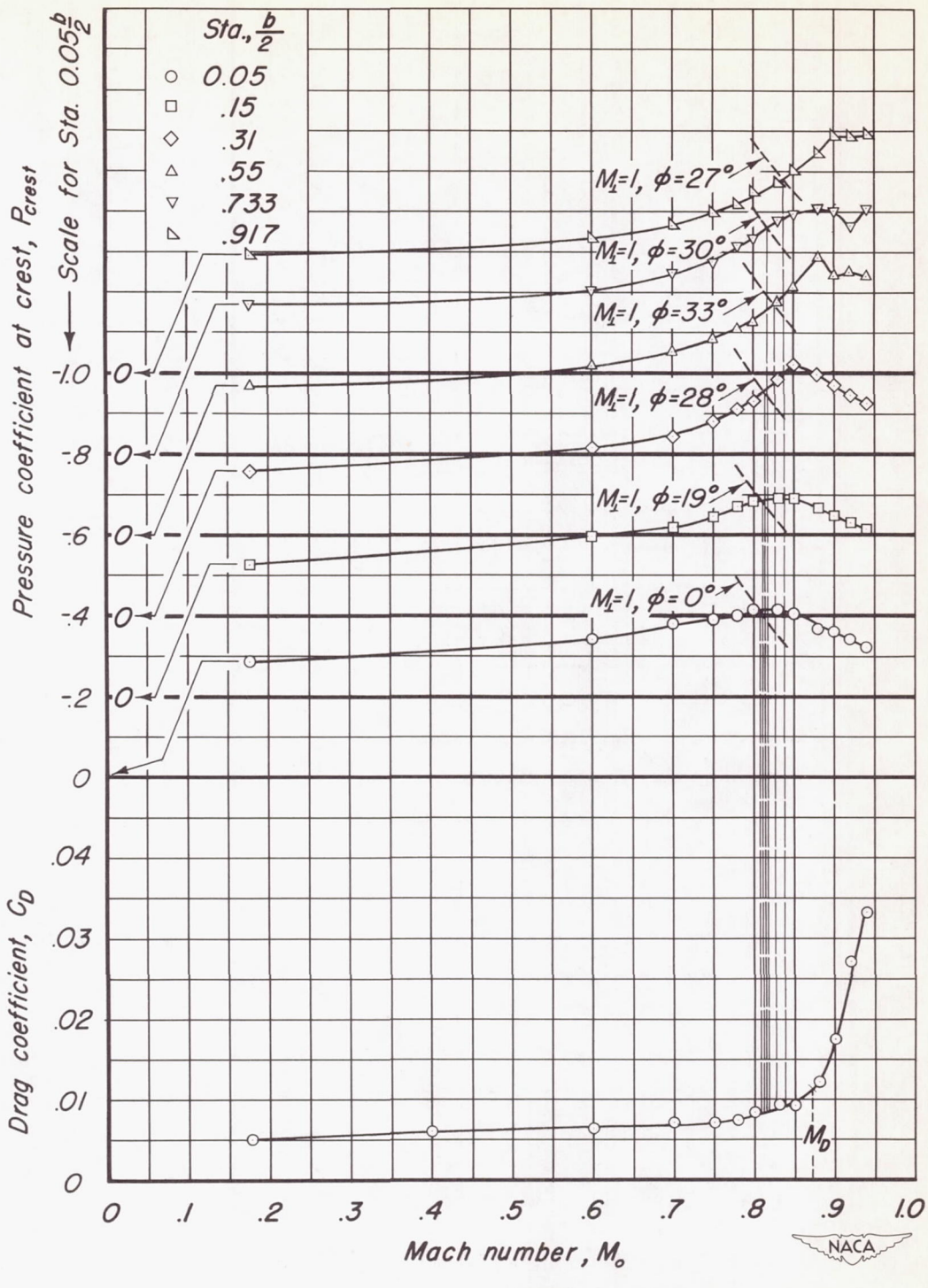

(b) a_u, 1°; crest at 0.36 x/c.

Figure 31. – Continued.

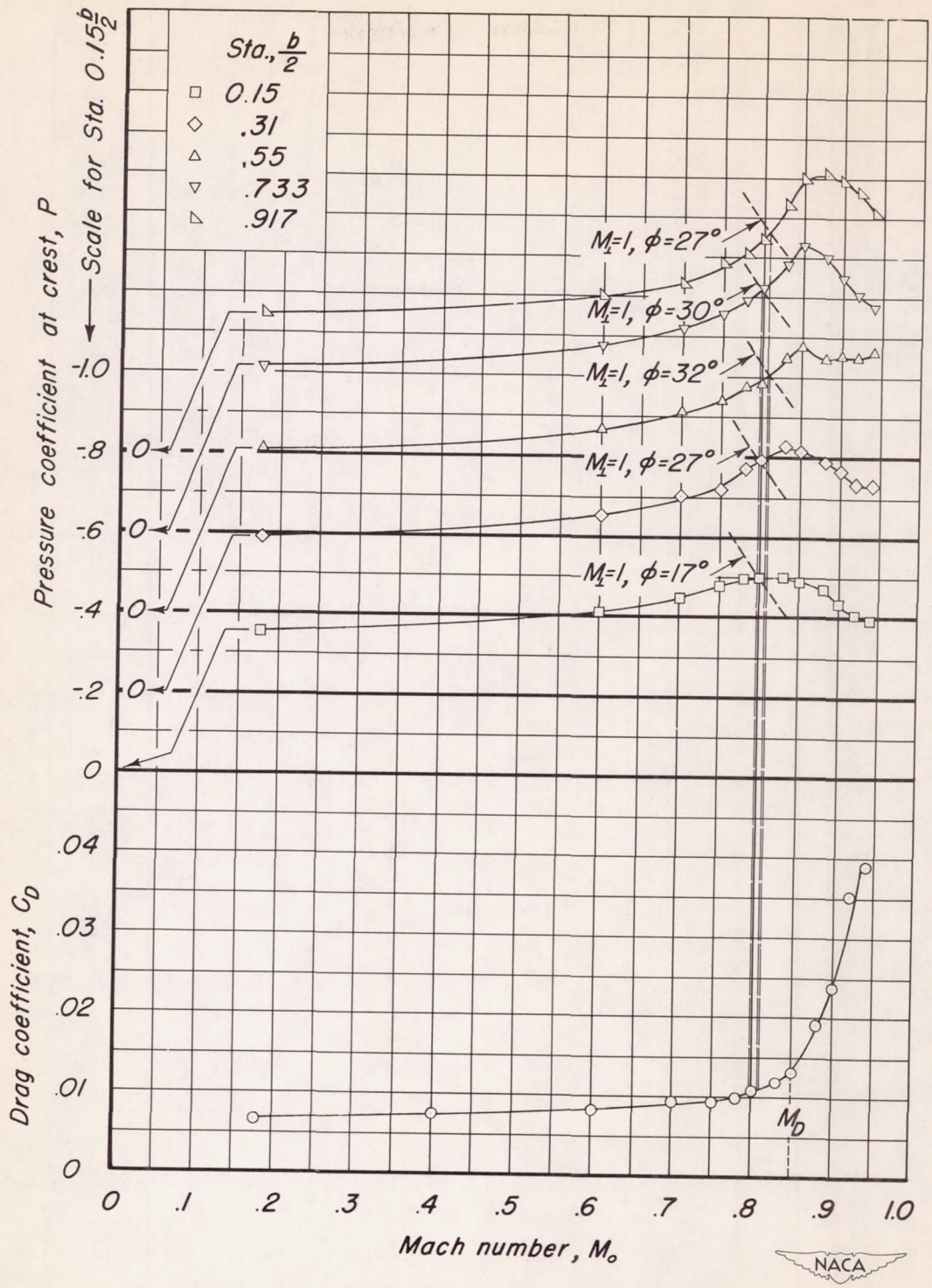

(c) α_u, 2°; crest at 0.315 x/c.

Figure 31. – Continued.

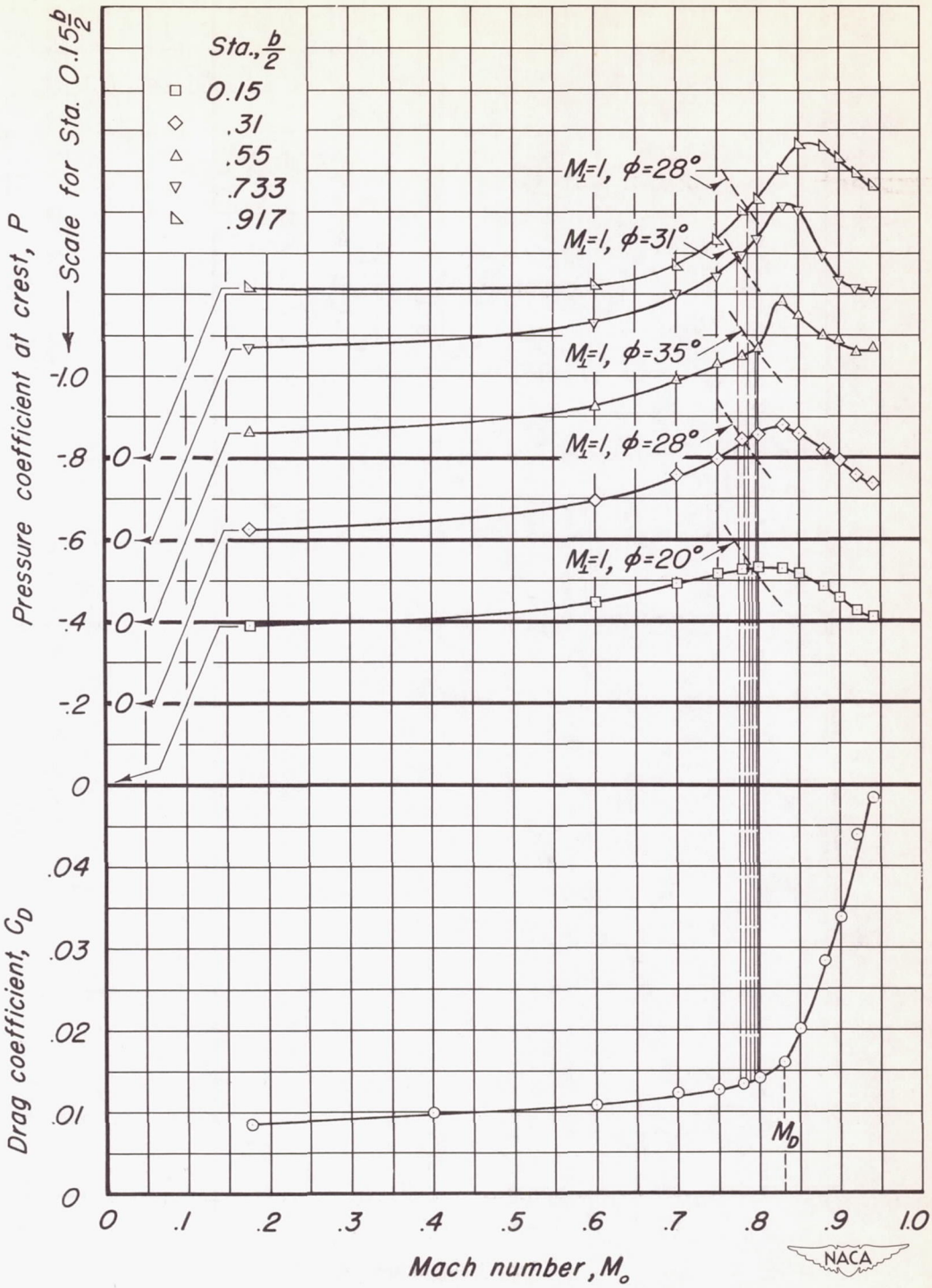

(d) α_U, 3°; crest at 0.29 x/c.

Figure 31. – Continued.

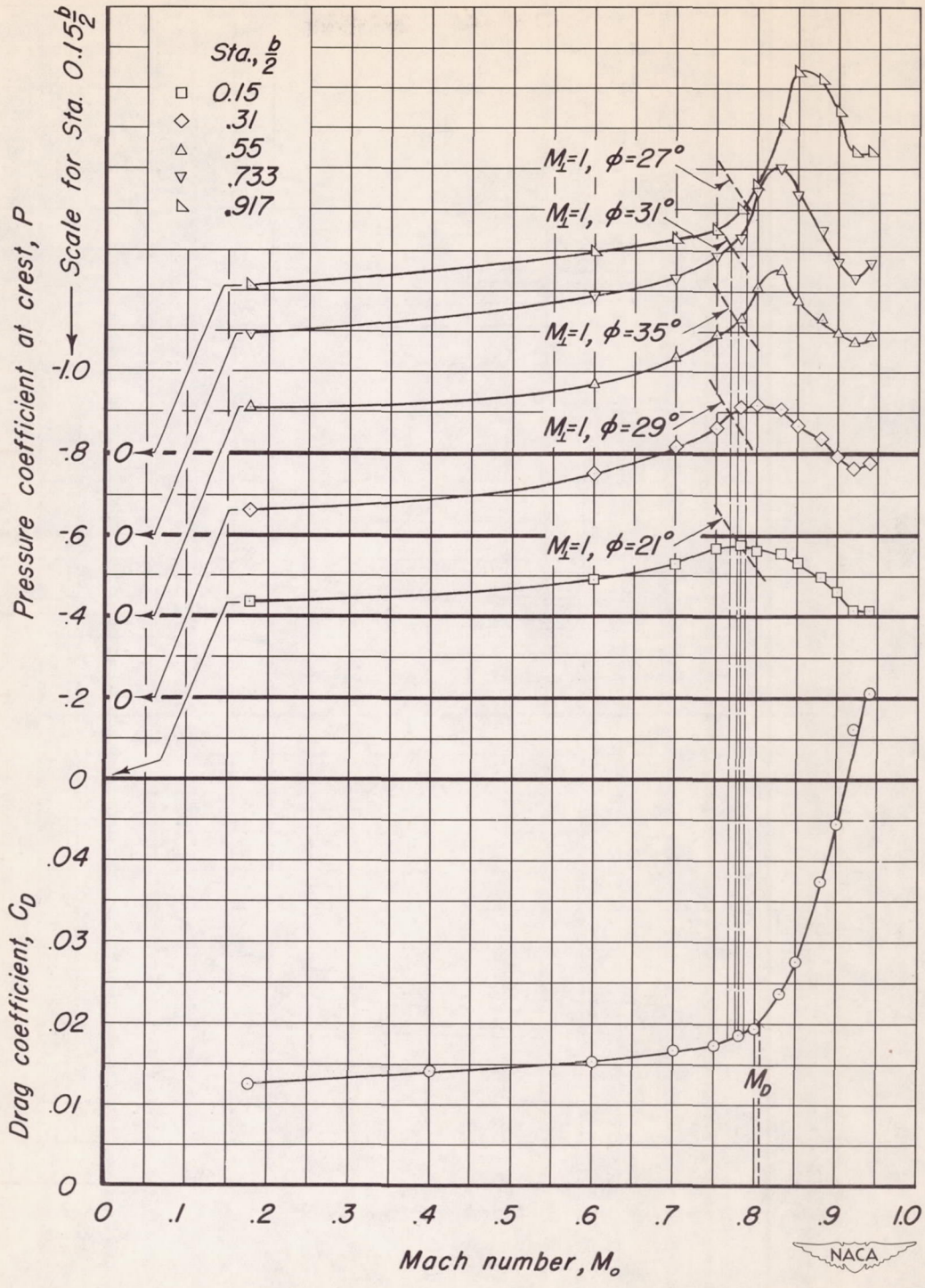

(e) a_U, 4°; crest at 0.265 x/c.

Figure 31. — Concluded.

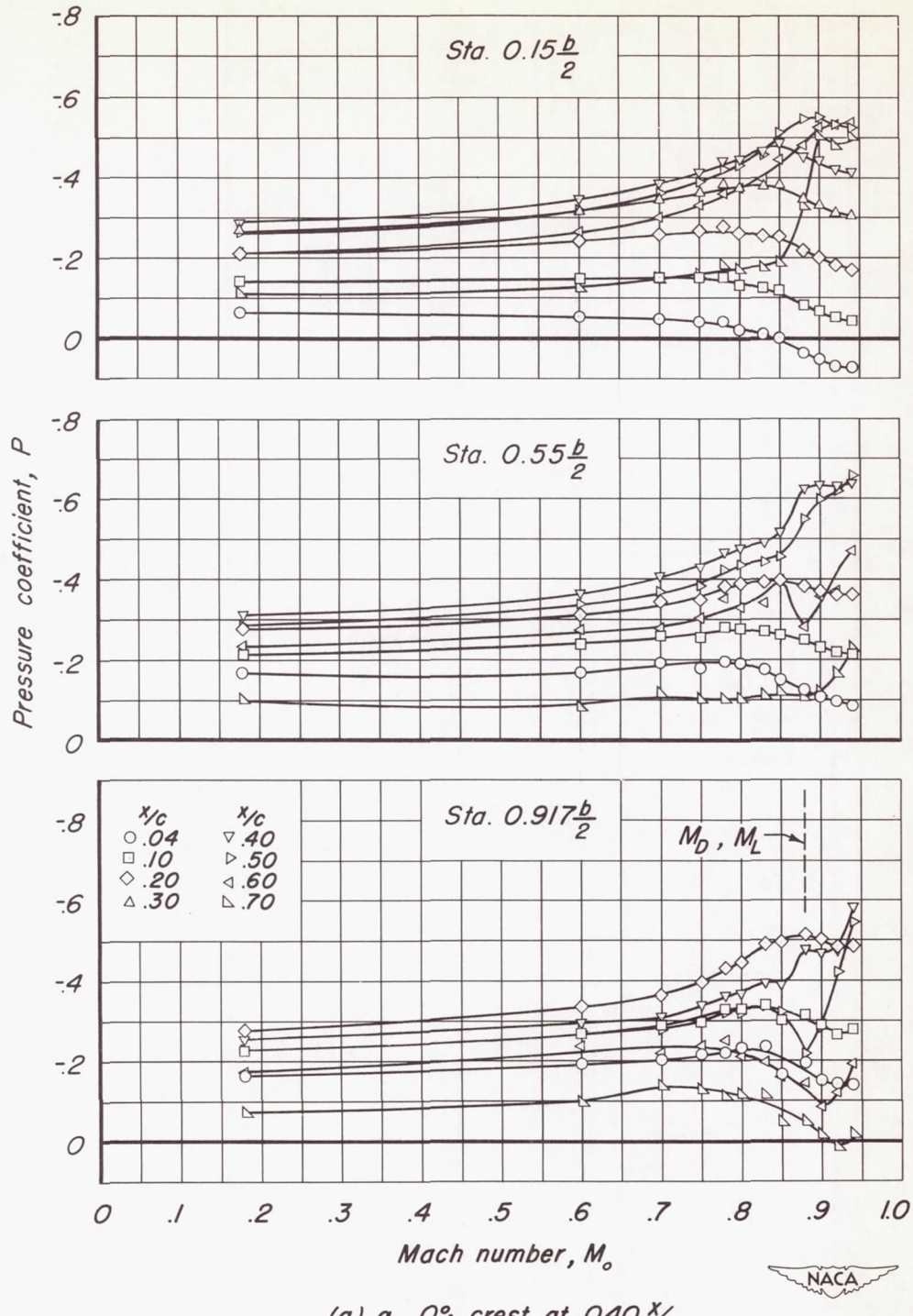

(a) a_U, 0°; crest at 0.40 x/c.

Figure 32.– The effect of compressibility on the pressure coefficients at several chordwise positions on the upper surface at three semispan stations. R, 2,000,000.

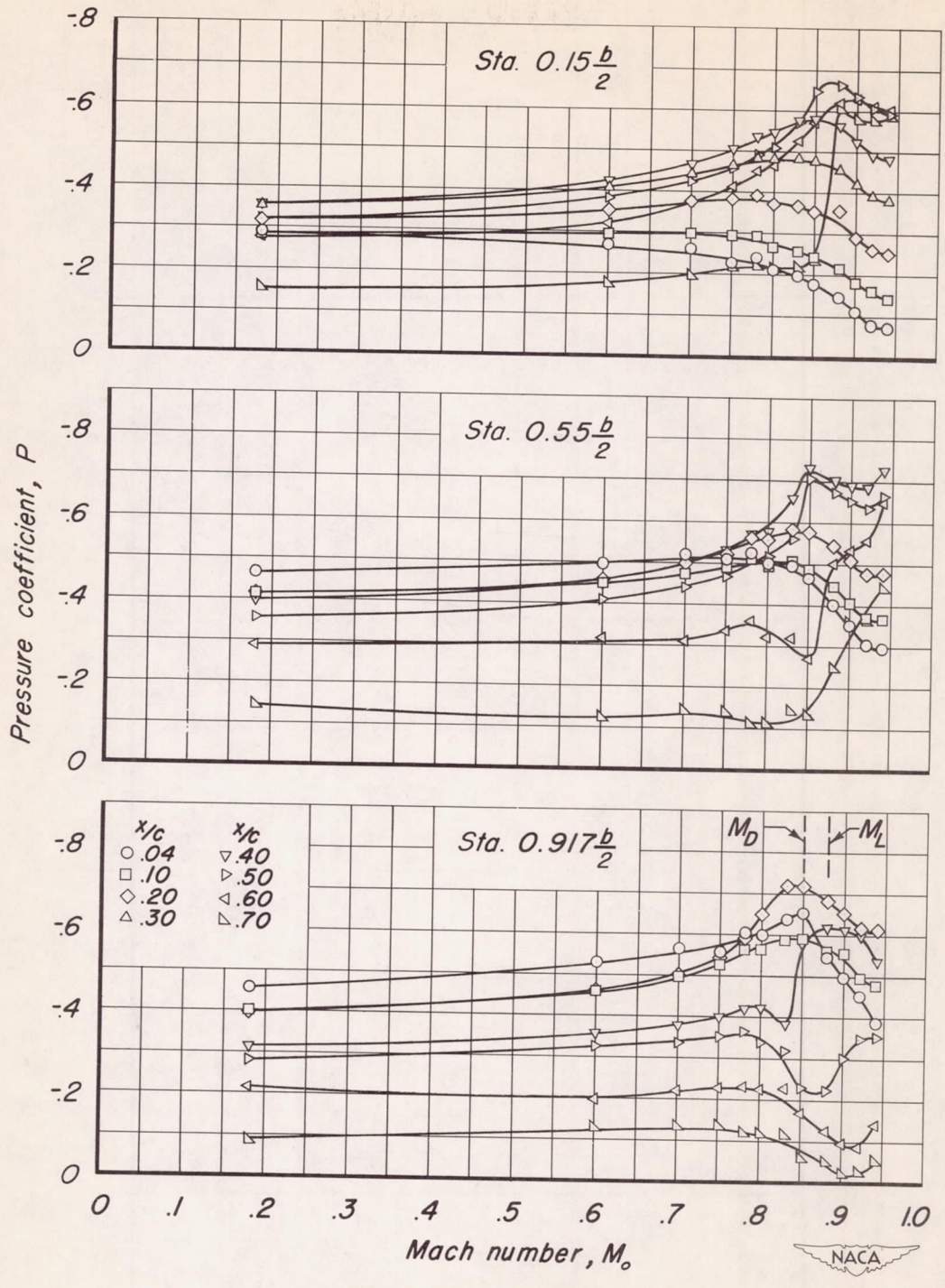

(b) a_u, 2°; crest at 0.315 x/c.

Figure 32. – Continued.

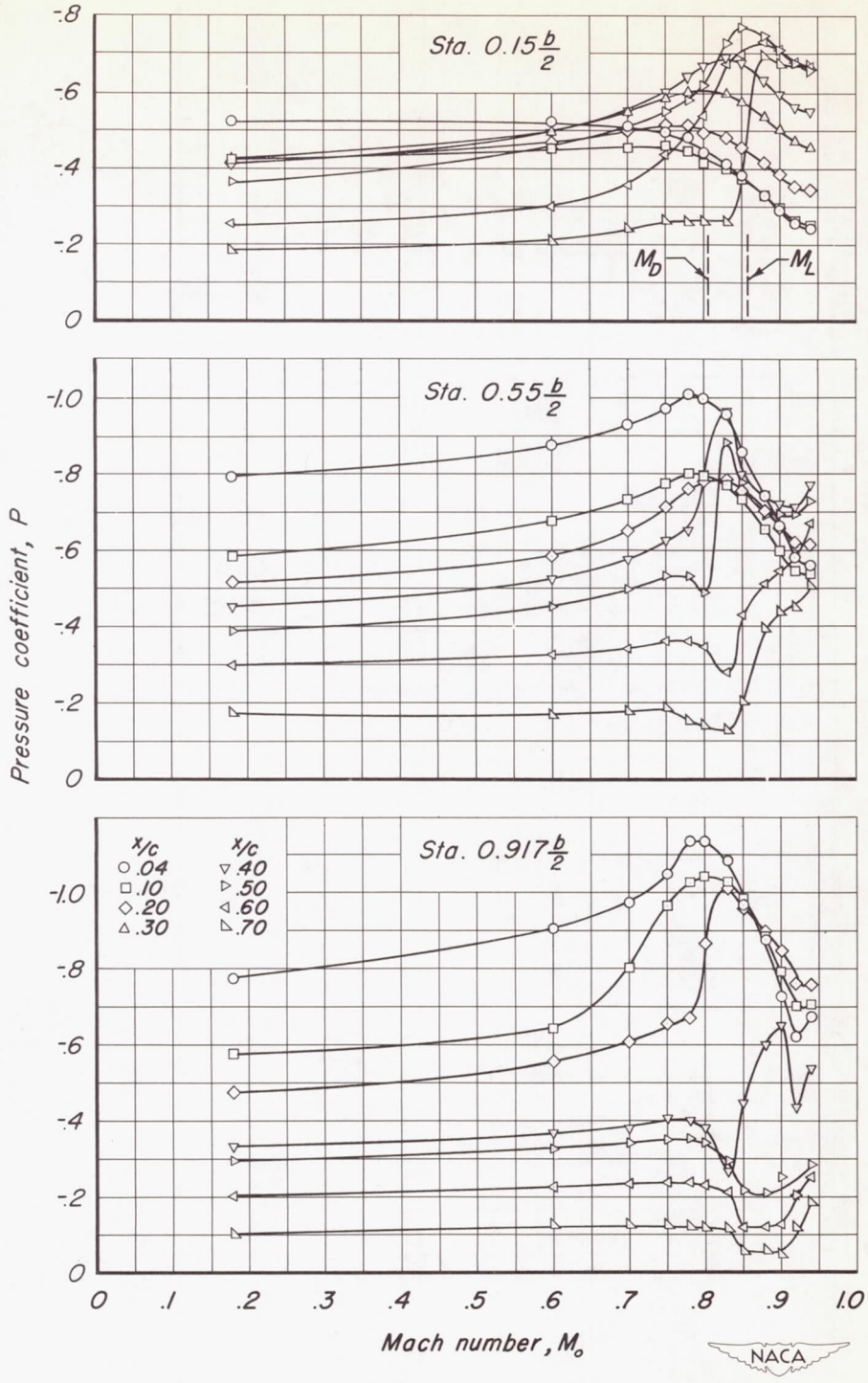

(c) α_u, 4°; crest at 0.265 x/c.

Figure 32.– Concluded.

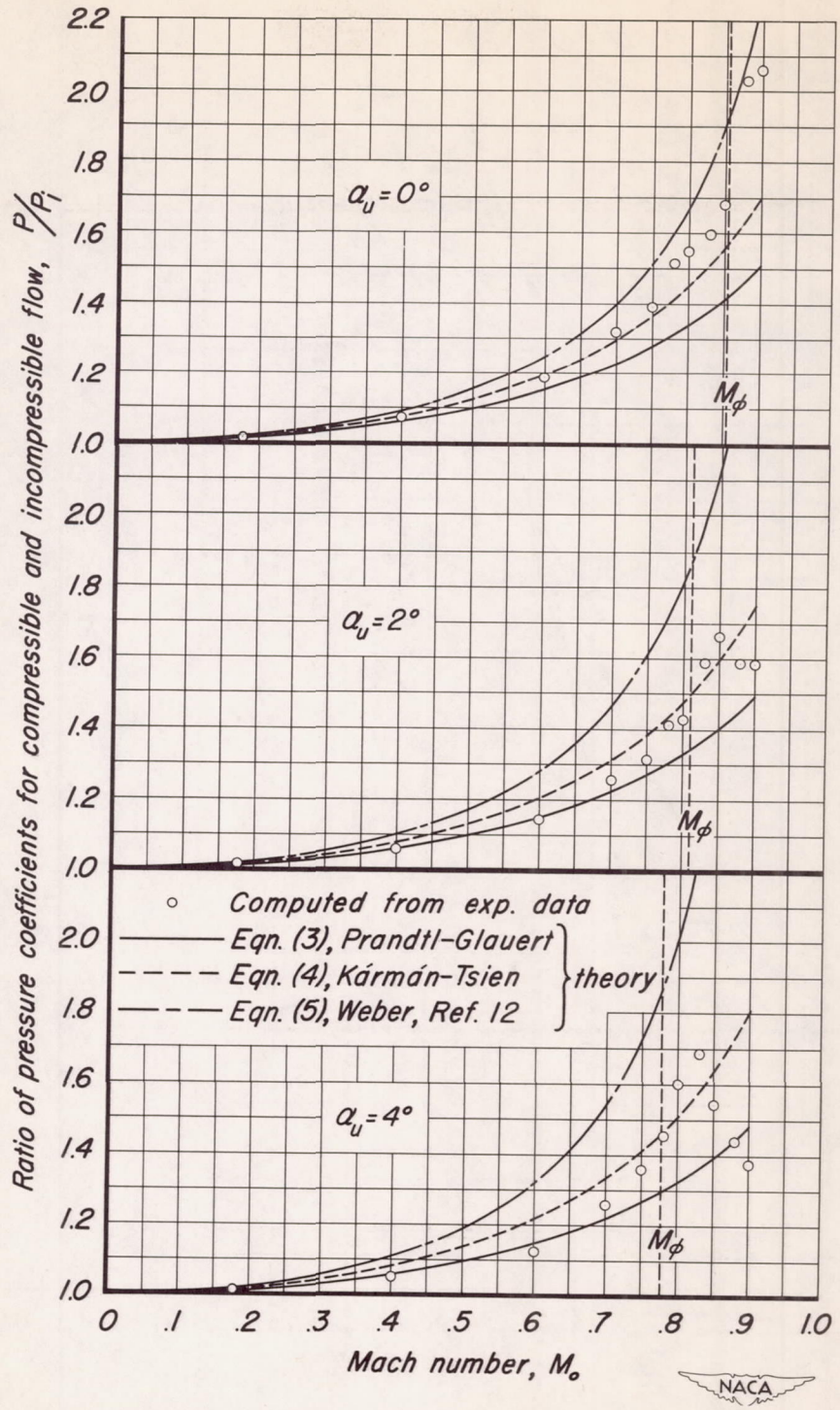

Figure 33.- A comparison of the theoretical and experimental effects of compressibility on the pressure coefficient at the crest point on the upper surface at station 0.55b/2 for three angles of attack. R, 2,000,000.

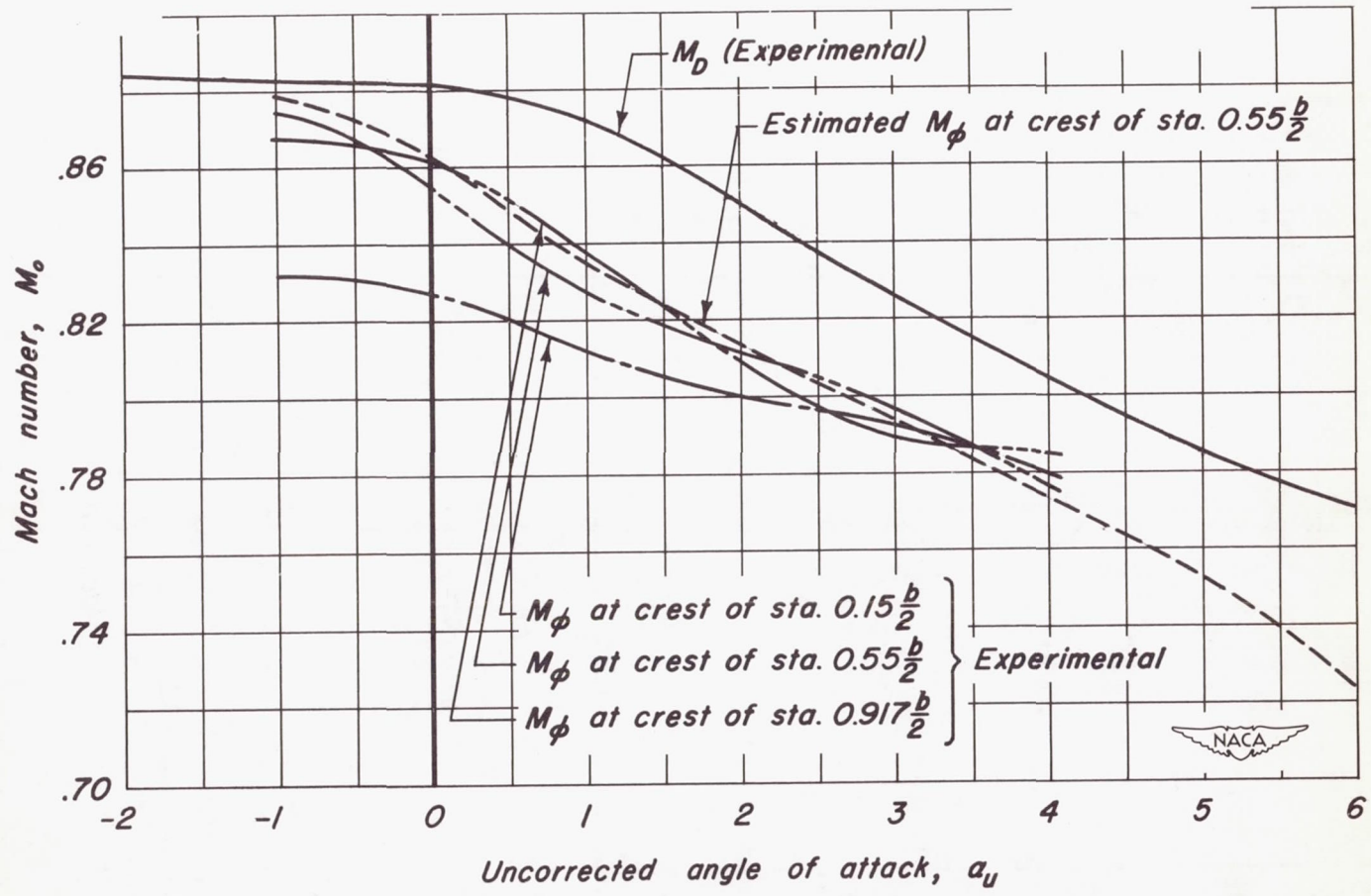

Figure 34.— The variation with angle of attack of the drag-divergence Mach number and the Mach numbers for the attainment of the critical flow condition at the crest points on the upper surface at three semispan stations. R, 2,000,000.

NACA-Langley - 2-10-54 - 75